ON THE COMPREHENSIVE OPTIMIZATION OF THE PROCESS AND QUALITY CONTROL FRAMEWORK IN PORTLAND CEMENT PRODUCTION TESTING USING QXRD-BASED ACCURACY CALIBRATION

A Thesis

by

RAMNATH MYLAPORE GANESH

Submitted to the Office of Graduate and Professional Studies of
Texas A&M University
in partial fulfillment of the requirements for the degree of

MASTER OF SCIENCE

Chair of Committee,	Zachary Grasley
Co-Chair of Committee,	Anol Mukhopadhyay
Committee Members,	Youjun Deng
Head of Department,	Robin Autenrieth

August 2018

Major Subject: Civil Engineering

ABSTRACT

The Bogue method is the current industrial standard for the compositional analysis of anhydrous and blended cements. However, this method is disadvantageous since the formulations were developed with archaic cement chemistry knowledge. This results in phase quantity estimation errors which can be as high as 9wt.% of the total cement. Quantification of cement phases through X-ray diffraction and Rietveld refinement is an effective alternative which determines the phase quantities directly rather than through estimation. Despite having several advantages over the Bogue method, the adoption rate of Quantitative X-ray Diffraction (QXRD) in industrial quality control is quite slow. Since industrial quality control demands a reproducible technique with high precision, QXRD falls short against the Bogue method with average performance in repeatability and reproducibility. Although cement chemists recognize round robin and proficiency testing as effective solutions for this shortcoming, none of the proposed solutions remain feasible in an online testing environment.

In this study, primary focus is allotted to promoting a viable solution to address the repeatability and reproducibility issue in QXRD. Improved QXRD protocols were developed, tested, and, optimized to be applicable in a manual as well as an automated testing environment. Techniques such as multispectral image analysis, point counting, heat of hydration measurements, and, phase decomposition tracing were harnessed to validate the resulting QXRD results with improved repeatability and reproducibility. Furthermore, a mathematical relationship between the Bogue method and the improved QXRD quantification was generated to qualify the improvements from a familiar perspective.

DEDICATION

To God

To my mother and brother for their enduring efforts to help me succeed in life.

ACKNOWLEDGMENTS

I would like to thank Dr. Anol Mukhopadhyay, Research Scientist, Texas A&M Transportation Institute (TTI) for guiding me through this research and for employing me as a Graduate Assistant Research for the project “Direct determination of cement composition by X-ray diffraction”. His continuous encouragement and financial support throughout my employment at TTI was a significant contributor towards the prompt completion of the Master’s thesis and my graduation requirements. I should also appreciate him for making my career in cement chemistry as I know of it.

I would like to thank Dr. Zachary Grasley, Professor, Zachry Department of Civil Engineering and Department of Materials Science and Engineering, Texas A&M University for his guidance and support in countless instances throughout my academic career at A&M. Particularly, I am thankful for his rich advice regarding the direction of my career after MS. Moreover, I would like to register my utmost appreciation for his class “Properties of Concrete” being one of the best taught courses that I had ever been part of. He was the one who first put me in touch with Dr. Anol, the product of which is this thesis and probably my career in the US.

I would like to thank Dr. Youjun Deng, Professor, Department of Soil & Agricultural Sciences, Texas A&M University - College Station for his support in helping me start out in the field of X-ray diffraction. His lab course and lab facilities turned out to be a perfect founding ground for understanding the fundamentals of mineralogy and diffraction studies.

I am thankful for the fruitful discussions on X-ray diffraction and preferred orientation with Dr. Nattamai Bhuvanesh, XRD Lab Manager, Texas A&M University. I would like to thank Peter Lausser (Bruker AXS), Paul Stutzman (National Institute of Standards and Technology), and, Jeff

Hook (Lehigh Hanson North America) for providing valuable advice regarding the nature of Quantitative X-ray Diffraction in the industrial situation.

I want to thank my friends and colleagues, Srikrishnan Sethuraman, Haresh Karnan, Kai-Wei Liu, Joshua Hogancamp, Narain Hariharan, Pavan Akula, Xijun Shi, Mostafa Jalal, Yash Menaria, Prashanth Reddy, Richa Bhardwaj, Alireza Joshagani, Pravin Saraswatula, and many more who helped me enrich my life at Texas A&M University.

Appreciation is due for several cement companies including, Lehigh Hanson Cement Company/Heidelberg (North America), Lafarge (North America), Holcim (North America & Europe), Supremo Cemento (Brazil), for directly or indirectly assisting with samples and information that was used in this research.

Perhaps, the most important appreciation is due for Texas Department of Transportation (TxDOT) for funding this research and providing cement samples for testing. Andy Naranjo, Clifton Coward Jr., Darrin Jensen, and, Masoud Moradian are individually appreciated for their continued involvement in this project and for supporting graduate students like myself.

I would like to thank the Texas A&M Transportation Institute for having me on their employment payroll and for providing the office services that helped me to concentrate freely and effectively on my research.

CONTRIBUTORS AND FUNDING SOURCES

Faculty Committee Recognition

This work was supervised by a dissertation committee consisting of Prof. Zachary Grasley (advisor) and Dr. Anol Mukhopadhyay (co-advisor) of the Zachry Department of Civil Engineering and Prof. Youjun Deng (member) of the Department of Soil and Agricultural Sciences.

Student/Advisor Contributions

All work for the dissertation was completed by the student under the advise of Prof. Zachary Grasley and Dr. Anol Mukhopadhyay of the Zachry Department of Civil Engineering.

Funding Sources

The work was made possible by the Texas Department of Transportation under the project number 0-6941 with Dr. Anol Mukhopadhyay as the Principal Investigator.

The contents of this work are solely the responsibility of the author and do not necessarily represent the official views of the sponsors.

TABLE OF CONTENTS

Page

LIST OF FIGURES

Page

LIST OF TABLES

Page

1. INTRODUCTION

1.1. Background

Cement as a construction material has been in employment since pre-Roman times, as a lime-cement variant. At present, cement is the most common construction material in the world, which is evident from its carbon footprint. Burning of limestone in the kiln at elevated temperatures releases carbon dioxide and results in the generation of clinker compounds that vary widely in their phase compositions. Addition of gypsum to this compound mixture produces Portland cement which in combination with aggregates and water gains gradual strength to form concrete. ASTM C150M-17 [1] lists commercial Portland cements to be of five types based on their compositional variety as, Types I/II, III, IV, V. Aside from the five major cement types, several blended cement types incorporating supplementary cementitious materials (SCMs) are enshrined in ASTM C595. Common SCMs include, fly ash, blast furnace slag, silica fume, metakaolin, to name a few. Limestone can also be added retrospectively to cement to engender high early strength.

1.2. Portland cement phase constituents

The first step in cement manufacturing is the production of cement clinkers from natural raw materials. Cement clinker is a product of limestone, clay/shale, stone, and sand calcined and sintered at extreme temperatures to a maximum of 1600°C. The raw materials pass through a rotary kiln, where the calcined limestone is converted to a melt. Dicalcium silicate (Ca_2SiO_4) phase precipitates around 1250°C. Often, this phase formation accompanies the incorporation of substitutional Mg^{2+} ions (or, Al^{3+} depending on the type of clay) instead of Ca^{2+} [2]. Hence, the product so obtained is not stabilized as pure dicalcium silicate, but as the impure belite (due to substitutional ions). The belite phase converts to impure alite (pure form: tricalcium silicate, Ca_3SiO_5, or C3S) at around 1550°C. Depending on the type of impurity substitution and the amount

of SO_3 ions in the system, the alite may precipitate as the M3 and/or M1 polymorphic configurations [3, 4]. The interstitial phases, tricalcium aluminate or aluminate phase ($Ca_3Al_2O_6$ or C3A) and tetracalcium aluminoferrite or ferrite phase ($Ca_4Al_2Fe_2O_{10}$ or C4AF), are formed on rapid cooling from 1500°C. Aluminate may stabilize in cubic or orthorhombic morphologies depending on the amount of alkali oxides present in the kiln during rapid cooling. Ferrite phase stabilizes alongside the aluminate phase where some Al^{3+} (in the C3A structure) is substituted by Mg^{2+}, thereby forming a more stable structure with a lower reactivity than the aluminate phase. Depending on the alkali content, and the prevailing ion-rich atmosphere in the kiln, the periclase phase may occur in varying quantities in the clinker. Usually, a high quantity of the periclase phase (>4 wt.%) in the final Type I/II clinker is an indication of poor kiln controllability with respect to chemistry of the clinker [5, 6].

1.3. Problem description

Current protocols (ASTM C150) dictate that the Bogue method for quantifying cement compounds is used to calculate clinker and cement composition. The Bogue methodology utilizes oxide compositional values obtained from X-ray Fluorescence (XRF) to generate phase fraction estimates of alite, belite, aluminate, and ferrite - the major cement phases.

Several investigators had observed that the Bogue method incorporates various errors in its formulation which lead to the generation of incomplete and inaccurate chemical composition information [2, 7-9]. Furthermore, the Bogue method is incapable of describing the actual information about amorphous contents, limestone phases (calcite and dolomite), calcium sulfates, and other additives.

Sometimes, changes to the chemistry of the melt inside the kiln can arise due to the variations in raw materials or burning conditions. These changes can lead to the clinker phases stabilizing in variant crystal structures that diverge from the actual or anticipated morphology. Such variants are called phase polymorphs. The polymorphic forms of the major clinker phases influence the hydration characteristics of the cement paste to a considerable extent [10-14]. This phenomenon was not well understood during the formulation of the Bogue method [15], which led to the method being developed discrediting such vital information.

The failure of the Bogue method to properly track such changes mean that the overwhelming control over cement performance properties is lost by the manufacturer. For instance, the accurate phase fraction determination of limestone phases can tell the difference between overuse or underuse of burning high-quality limestone to get the desired phases. In addition, the presence of sulfate phases, predominantly from the gypsum phase, poses as another challenge where the cement setting properties are directly affected. Furthermore, the complications involved with the different polymorphs of sulfate and their influence on ettringite formation (reaction with the aluminate phase) cannot be understood from the Bogue method.

Now, quantification through X-ray Diffraction (XRD) is a direct method of measurement that can overcome the disadvantages of the Bogue method. Quantitative X-ray Diffraction (QXRD) can directly identify and measure the limestone, sulfates, and the polymorphic variants in cement, thereby presenting as a natural solution to many problems with the Bogue method. Still, certain disagreements remain in the cement fraternity regarding the potential of the QXRD to generate consistent and accurate results. Chiefly, there exists a mismatch between QXRD results of the same cement analyzed in instruments that vary widely in their X-ray generation voltage and optical setup, which is manifest in the repeatability and reproducibility of the results.

1.4. Scope of the research

In this study, the problems in QXRD are described in detail. A deep study of the existing QXRD framework was performed to discover areas for improvement and to lay the groundwork for comprehensive testing. The suggested improvements to certain shortcomings in the existing protocols were tested and analyzed intensively using QXRD, supported by secondary characterization. User-friendly solutions were generated for direct applicability in cement production testing.

1.5. Thesis Outline

Chapter 1 deals with the introduction to the disadvantages of the Bogue method and introduces the potential of QXRD.

Chapter 2 details the analytical methods used in this research and identifies the problems in current chemical analysis protocols.

Chapter 3 addresses the QXRD problems discussed in Chapter 2 by congregating ideas from current literature and performing experimental investigations to validate the proposed ideas.

Chapter 4 comprises case studies where the employment of QXRD in quality control can help improve the process control framework in cement manufacturing.

Chapter 5 summarizes the observations and findings of this study and catalogues the conclusions derived from each chapter.

Fig.1 presents a general outline of this study.

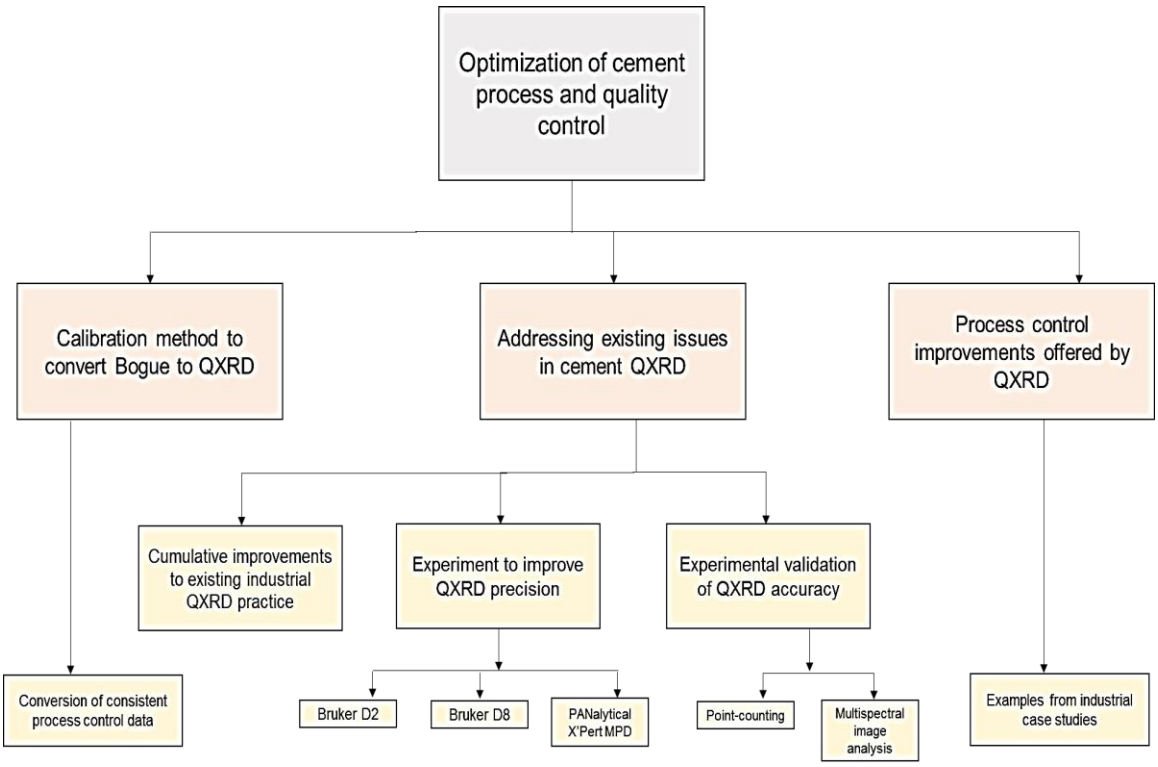

Fig. 1. Tree diagram describing the areas of focus of this research

2. ANALYTICAL METHODS - AN OVERVIEW

2.1. Existing techniques for cement analysis

2.1.1. Bogue and Modified Bogue methods

The Bogue method is the current industrial standard for the determination of chemical composition of cement. This method uses oxide compositional estimates to compute the major cementitious phase fractions through a series of simultaneous equations. It is a statistical quantification technique that was developed (in 1929) by casting matrix inversion of the stoichiometric quantification of clinkers as the known variables, and the oxides and phases as the unknown variables. Based on the quantity of oxides, the phase fraction determination can be calculated using a set of simultaneous equations derived therewith. Since the number of phases and oxides was limited to 5 respectively, only four clinker compositions were taken to be representative of all clinker types. The original Bogue formulated matrix is reproduced in the following equations,

$$\begin{pmatrix} CaO \\ Al_2O_3 \\ SiO_2 \\ Fe_2O_3 \\ SO_3 \end{pmatrix} = \begin{pmatrix} 0.7368 & 0.6512 & 0.6226 & 0.4610 & 0.4119 \\ 0.2632 & 0.3488 & 0.0000 & 0.0000 & 0.0000 \\ 0.0000 & 0.0000 & 0.3774 & 0.2100 & 0.0000 \\ 0.0000 & 0.0000 & 0.0000 & 0.3290 & 0.0000 \\ 0.0000 & 0.0000 & 0.0000 & 0.0000 & 0.5881 \end{pmatrix} \begin{pmatrix} C3S \\ C2S \\ C3A \\ C4AF \\ C\$ \end{pmatrix} \quad \text{Eq. (1)}$$

In the rightmost matrix, C represents CaO, S represents SiO_2, A represents Al_2O_3, F represents Fe_2O_3, and $ represents SO_3.

C3S= 4.071 x %CaO - 7.600 x %SiO2 - 6.718 x %Al2O3 - 1.430 x %Fe2O3 - 2.852 x %SO3 ⋯⋯▶ Eq. (2)

$C2S = 2.867 \times \%SiO_2 - 0.7544 \times \%C3S$ ⟶ Eq. (3)

$C3A = 2.650 \times \%Al_2O_3 - 1.692 \times \%Fe_2O_3$ ⟶ Eq. (4)

$C4AF = 3.043 \times \%Fe_2O_3$ ⟶ Eq. (5)

This situation restricted the stoichiometric quantification matrix of the Bogue composition to essentially a 5x5 matrix, which is a hardly sufficient representation for an equation with encompassing applicability. Also, the quantification is limited to only 4 clinker phases as the representative constituents of a clinker. The Modified Bogue method, proposed by Taylor [7], took the quantification of the sulfate and other minor phases into account for the cement coming from a finish mill. This meant that the method was suitably prepared for industrial applicability since almost all phases in the cement were considered.

However, the equations of Modified Bogue were formulated in much the same way as the Bogue method which meant that there was still not a large enough dataset to be considered "statistically reliable". Although the polymorphic variations were discussed by Taylor, their incorporation in the Modified Bogue method was absent. Hence, the Modified Bogue did not offer a significant improvement to the Bogue technique. The impact of the shortcomings of both quantification techniques is prominent in the standard deviation uncertainties in their phase estimations. For the alite phase, the Bogue method contributes to ±9 wt.% uncertainty in its determination, which was lowered slightly by the Modified Bogue.

2.1.2. Corrections to the Bogue method

While formulating the Modified Bogue, Taylor hypothesized that the Bogue method was found to consistently under predict the alite content in cement. He owed it to the absence of the maintenance of equilibrium during the clinker cooling stage, which paves the way for unregulated

interstitial substitution in the major cement phases. As a correction, Taylor proposed that the following situations need to be followed studiously to ascertain the actual chemical composition of the cement/clinker. First, the oxide calculation needs to be extremely accurate and need to be calculated through wet chemical methods to satisfy the accuracy requirement. Secondly, the oxide quantification must match the physical form of oxides attached to specific phases (CaO in sulfates, insoluble residue, alkali oxides and sulfates, etc.) in the clinker. Third, the derived phase quantification data need to be statistically meaningful and any distinction between polymorphs shall be neglected.

The final condition should serve as a reminder to the imperfect understanding of cement chemistry when the corrections were formulated and is a good example of why the Bogue or the Modified Bogue should not still be in practice. Furthermore, the proposed modifications failed to illustrate the polymorphic differences in phases nor provided any information about the limestone phases (calcite, aragonite, dolomite) and minor phases such as alkali sulfates, portlandite, periclase, brucite, etc. within the ambit of the methodology. Particularly, the nature of the polymorphs of the major cement phases can alter the performance characteristics of the cement in a macroscopic way. Their identification, and quantification becomes very important to exact increased control over cement performance predictability, and valorize the input given in the form of fuel and raw materials.

2.1.3. Extent of errors in Bogue and Modified Bogue

The errors of the Bogue and Modified Bogue stem from the hypothesis that the cement phases are prevalent in their ideal state of molecular representation, which facilitates the Bogue constant calculation for the predominant oxides. In reality, the case is far from ideal as the clinker phases incorporate several substitutional impurities in their crystal structures. The combined

protocols received a modification by L. A. Dahl [16] in 1939 to factor in the addition of the calcium sulfate phase, but it remains unchanged to this date. Taylor in 1989 [7] purported that the Bogue calculation underestimates the alite and overestimates the belite, with a mean discrepancy of 8 wt.% calculated from Quantitative X-ray Diffraction (QXRD) of rapidly-cooled clinkers. Relatively recent research by Stutzman et al. [9] lead to the observance of a quantification variation of ±9.6 wt.% for alite and belite, ±2.2 wt.% for aluminate, and ±1.6 wt.% for ferrite, respectively from the actual stoichiometric composition of a commercial clinker.

2.2. Quantitative X-ray Diffraction (QXRD)

X-ray diffraction-based quantification technique determines the phase fraction estimates directly through the quantification of the orderliness of the crystal structures. X-rays are incident on a fine powder of a cement sample and the diffracted X-rays from the sample are collected in the detector. The diffracted X-rays symbolize the reflections obtained from the spacings between the crystalline symmetry of the phases. The spacings between rows of crystalline grains (or, crystallites) represents directly as the spectral identifier of an explicit crystalline phase. Least-squares refinement of a crystalline phase using the Rietveld method [17] against its real structure provides the quantification of that phase. Hence, QXRD is a fingerprint technique for the identification of crystalline phases, and the phase quantity is mirrored in the intensity of diffraction.

Preliminary analysis of cement through QXRD was performed on bulk and chemically pre-treated cement by Hjorth [18], Aldridge [19] and Gutteridge [20], through the single-peak fitting method. After the introduction of the reference-intensity-measurement by Hubbard and Snyder [21], several investigations followed [22-24] but most of the XRD evaluations were assisted by peripheral chemical analysis, or pre-treatment methods. Some of the sample pre-treatment methods

include dissolution of the interstitial phases (aluminate and ferrite) using salicylic acid-methanol combinatorial solution [25], dissolution of the silicate phases using a KOH-Sucrose solution [18], grinding the cement to less than 5 μm followed by spray-drying [26, 27], and different sample loading schemes [26, 28-30]. Such pre-treatment methods, although crucial for an accurate quantification, made the replication of QXRD impractical in industrial quality control. Further exacerbating the situation was the operating power of the computers of the 1970s, which found it difficult to accurately compute least-squares refinement of multiple peaks simultaneously.

With the arrival of micro-processor units, improved software programs for cement QXRD were developed which engendered quantification through the Rietveld method and whole-pattern fitting [31-33]. However, the QXRD methodology was not practiced the same universally and the requirement of a guide for performing accurate and rapid QXRD was highly warranted. Stutzman [24] in 1996 devised a QXRD methodology as a precursor for the employment of a standard QXRD protocol for quantitative cement analysis. Following Stutzman's pioneering efforts, several researchers around the world [34-42] updated their best practices followed for cement QXRD. Focus was shifted towards ascertaining a common and standardized protocol to provide for a rapid analysis with higher accuracy than the ASTM C150. This led to the development of an ASTM standard procedure for QXRD, ASTM C1365 [43], which opened up its adoption in industrial offline quality control. Automated cement analysis followed [44-48], with QXRD being projected as the best practice for the holistic automation of industrial quality control, right from sample collection till analysis of results.

2.2.1 Issues in QXRD

In spite of decades of research in the development of a universal QXRD protocol, ASTM still fails to recognize cement QXRD with a standard that is practicable in online quality control.

The underlying reasons can be segmented into two major divisions: (i) the systematic and random errors during sample preparation and measurement, and (ii) the non-reproducible nature of powder diffraction that generates the systematic and random errors. The following sections discuss these barriers in greater detail.

2.2.1.1. Systematic and Random errors

Cement QXRD suffers from a variety of systematic and random errors which are induced throughout the process. But the majority contribution of systematic errors is effected during the sample preparation stage only. The reason for this discrepancy is that QXRD sample preparation is an extremely subjective technique and is highly sensitive to small alterations or mistakes in every stage of preparation. Chief of them being the inducement of preferred orientation which causes a systematic deviation from the actual composition. Other effects such as absorption contrast effect, flat specimen error, sample transparency, porosity effects, etc. can either be controlled before sample loading or do not affect the quantification to a large magnitude. Among the random errors, personnel-dependent random errors in sample preparation can skew the exact quantification but can be overcome with the help of replicative testing. Hence, the preferred orientation effect was assigned the most deliberation in this work and its reduction was processed through established correction techniques.

Preferred or preferential orientation is usually seen when the cleavage or growth mechanisms of some crystals (especially platy ones) may lead them to orient in a particular crystallographic direction, when the powder is compacted in the sample holder. Preferred orientation is most often seen in anisotrophic morphologies, for example plate-like morphologies. This is caused due to a single unit cell parameter (say, c) being longer than the face plane of the crystal (in this case, the xy-plane) which causes the crystallite to fall in a specific orientation onto

the specimen holder. Since the Rietveld method works by measuring the relative peak intensities, this can lead to an overestimation of the phase in question. The problem is further intensified in large plate-like crystals (e.g. Portlandite, an oft seen case) and when the sample is pressed to form a flat surface [49]). Preferred orientation can occur in alite, gypsum, hemihydrate, portlandite, dolomite, and calcite phases in the OPC as seen in **Fig. 2**.

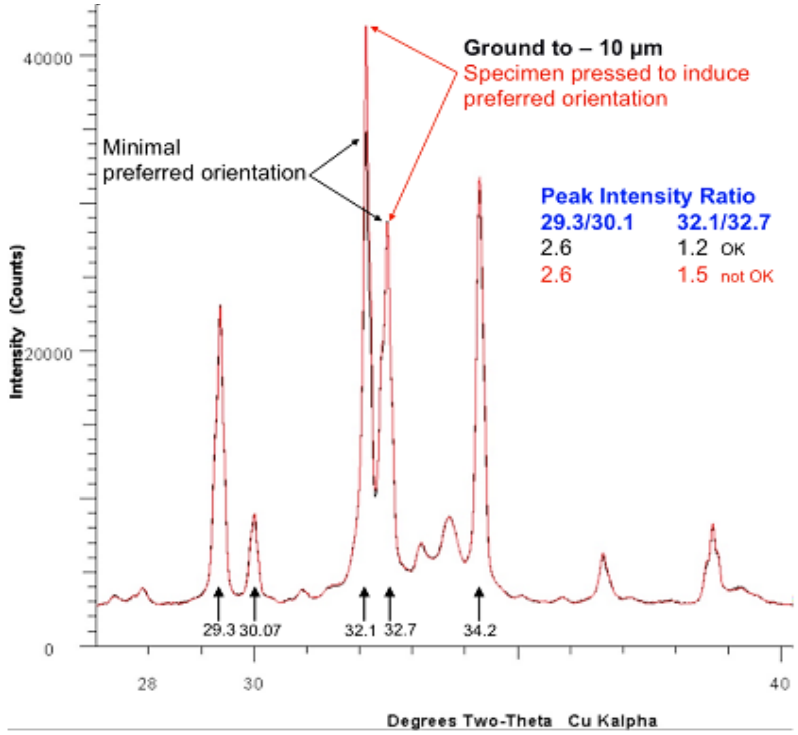

Fig. 2. Differential peak intensities contributed by alite preferred orientation (Reprinted from [50]). The peak intensity ratios (inset) denote visual representation of preferred orientation.

Morphological anisotropy can have a major impact on preferred orientation similar to broadening. Two such morphologies are readily seen in cement as in plate-like (orthorhombic) and needle-shaped morphologies (monoclinic) [49, 51]). The plates or needles lie parallel to the surface and an increasing number of such structures are packed in a highly regular manner. The direction

or planar axis that is perpendicular to the surface is called as the preferred orientation axis. This direction coincides with the direction of the reciprocal lattice vector that is normal to the flat face i.e. this direction represents the reciprocal lattice vector of the flat face. Hence, the intensity from the parallel reciprocal lattice will be higher than any other intensity due to the anisotropic distribution of axis lengths. Depending on the axis lengths, the preferred orientation axis can be based on the shortest or the longest axes. In alite, the preferred orientation axis is the longest axis whereas in Portlandite it is the shortest axis. In both cases, the intensity of the constructive interference of the plane perpendicular to the preferred orientation axis is greatly increased due to the anisotropy.

Two approaches are often performed to minimize the effect of preferential orientation: modified backloading [52] and micronizing to form smaller crystallites [53]. The formation of smaller, highly spherical grains of cement is a well-established method of reducing the preferential orientation. But care should be taken that no phases or grains are lost or modified due to the friction generated during particle size reduction through milling. Micronizing was practiced as a means to reduce the particle size without a drastic loss of phases [38, 50, 54-57]). But, the backloading method is sufficiently advantageous over the formation of spherical aggregates by spray-drying because of the swiftness of sample preparation and loading. Detailed information on the backloading methodology is described in the current protocols segment under Section 2.5.

2.2.1.2. Reproducibility and Repeatability

The presence of the systematic and random errors breeds uncertainty in the quantification estimates of the final phase fractions. This is a major shortcoming in QXRD and is a leading factor preventing its industrial adoption. Even with the well-known errors in the Bogue method, the precision and reproducibility of the end results was unquestionable. This situation was stimulated

after the introduction of the pelletization and fused bead sample preparation techniques [58]. Moreover, ASTM E177-86 [59] introduced standard averaging techniques to provide consistently repeatable results within 95% confidence limits which are applied to Bogue results. Although, the repeatability can be taken care of using the latest version of ASTM E177, the reproducibility poses a problem owing to differences in sample preparation, instrument capabilities, and extraneous corrections.

As a solution to address the problem of reproducibility in QXRD, researchers from NIST and PCA proposed collaborative testing as an effort to resolve this issue at the analysis stage. Historically, such collaborative testing lead to round robin and/or proficiency tests on cement which further lead to the development of consensus mean estimates to generate a highly reproducible and accurate quantification. The earliest of such methods was performed by Aldridge on a series of samples numbering around 200 [8]. This two-part series [8, 60] compared the inter-laboratory precision and bias of the X-ray Diffraction and Bogue methods and qualified a methodology to obtain maximum obtainable precision with the prevalent technology. Youden, Crandall and Blaine [61, 62] formulated the proficiency testing protocol for the comparative calibration of the accuracy of cement testing procedures between different labs based on the large-scale classification of the available test results plotted in a two-dimensional regime. The pioneering effort by Aldridge was followed by a series of efforts in later decades [57, 63, 64] to improve upon the inter-laboratory variations in QXRD through round-robin consistency analysis.

Later, ASTM denoted the standard practice for performing round robin testing and analysis [65] in addition to evaluating precision and bias statements [59, 66]. Round-robin tests involve the participation of several labs with locally-optimized QXRD protocols to perform phase fraction quantification on the same cement sent out in different batches. In all those procedures, emphasis

is laid on the measurement and analysis portion of the protocols whereas the sample preparation was left quite flexible. This resulted in such procedures acting as a retrospective calibration or correction on the errors induced way before measurement and analysis. The fault was apparent when Petersen and Weber-Wisman [67] theorized that sampling and sample preparation errors account for more than 80% of the total errors in QXRD. **Fig. 3** is similar to that representation. The outlying differences contributed by measurement and analysis are left to 10-15% of the total errors which are often negligible when quantified in phase fractional terms normalized to 100 wt.%. With replicative testing effectively taking care of the sampling variations (due to random errors alone), the evolution of a very precise quantification scheme demanded focus on sample preparation consistency. Hence at the turn of the last decade, with increasing automation in cement quality control, pressing the cement in the form of a pellet was considered as a feasible protocol that can significantly improve the precision of QXRD [46, 47, 67]. Moreover, the performance of the round robin analyses is a rare, and irregular occurrence and does not follow the time constraints demanded for the quick and precise calibration in an industrial lab. The pelletization method can directly overcome such difficulties and can incorporate local requirements into its fold to evolve a rapid analysis protocol. An example of a similarly successful venture lies in the well-known role played by pelletization in achieving highly reproducible results for calculating elemental oxide percentages in XRF.

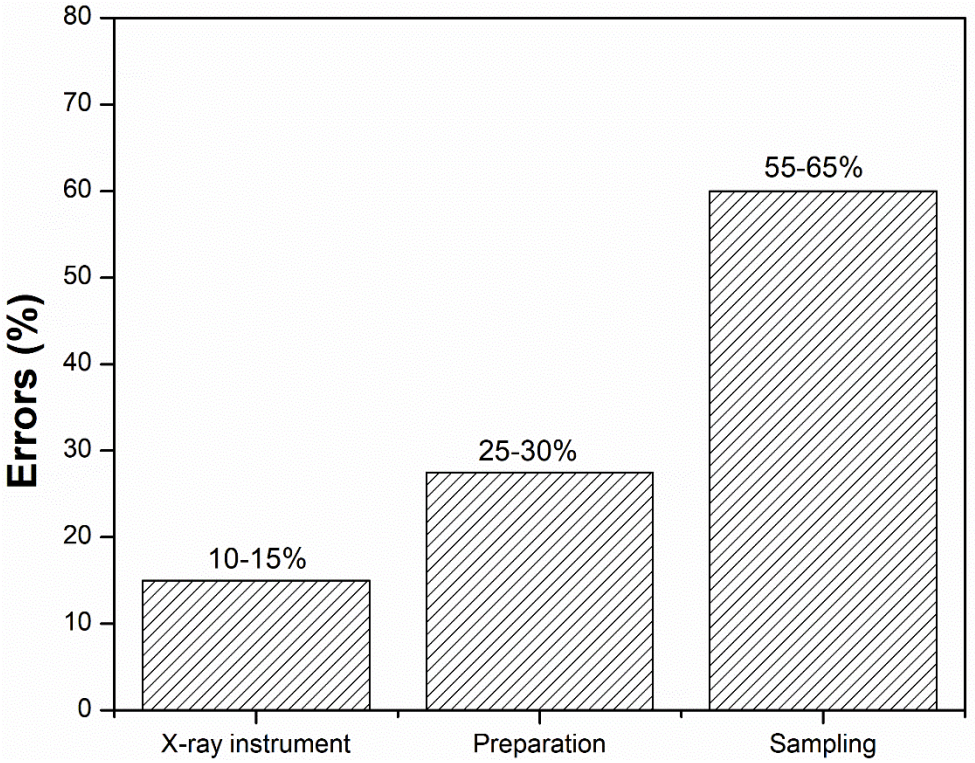

Fig. 3. Distribution of errors in a typical X-ray diffraction analysis

2.2.2. Techniques for QXRD sample preparation

In order to promote a precise and accurate QXRD quantification, several sample pre-treatment techniques are in employment in the wake of decades of research. Exact perusal of these techniques forms the foundation for the current QXRD protocols enshrined in ASTM C1365. For this work, the most popular sample pre-treatment techniques were performed to develop an understanding of the advantages and shortcomings behind the historical QXRD framework.

2.2.2.1 Grinding

Grinding or Micronizing is a proven technique to reduce particle size of cement and mitigate detrimental effects such as preferred orientation and the absorption contrast. One of the pioneering efforts in classifying the influence of particle size affecting the accuracy of X-ray

powders was performed by Gordon and Harris [68] in 1955, who quantified the existence of a 12% error in QXRD single phase quantification when the particle size is above 20 μm. The existence of coarse size fractions impacting the statistics of the reflected intensities was expounded in 1974 by Klug and Alexander [69]. It was commonly understood during the following period that for an accurate analysis, the particle size requirement must be less than 10 μm. Major contributions occurred in the later works of D. K. Smith [70] and Whitfield & Mitchell [71] regarding the understanding of how particle statistics can influence the intensity of reflected radiations. Smith [70] established that the influence on preferred orientation and absorption contrast effects was highly advantageous when the particle size was reduced from 40 to 10 to 1 μm. Whitfield and Mitchell [69] observed that reducing the particle size to less than 2 μm can engender precise diffraction patterns and eliminate spottiness to a considerable extent. They promoted wet micronizing using isopropyl alcohol in a McCrone micronizer as a sample preparation technique for an excellent X-ray diffraction pattern. Successive research illustrated the error associated with such particle size reduction with commercial cements.

Enders in 2003 [47] explained about the loss of a sizeable proportion of the gypsum phases in cement during micronizing owing to the differential in hardness between phases. During grinding, the gypsum crystallites (with Moh's hardness of 2) get ground first as the strain imparted by the grinding elements is higher on the softer gypsum phase than the harder silicate phases. The major cementitious phases have their Moh's hardness in the range 5-6, with the exception of calcite (Moh's hardness = 3) which gets acted upon after gypsum. Le Saout et al. [38] found that the complete loss or conversion of the gypsum phase to its dehydrated transforms can occur as early as 60 seconds to 2 minutes into grinding. This development directly challenged the historical perception for accurate quantification: wet grinding must be proceeded for 10 minutes to produce

cement size fractions in the 2 μm range. Hence, significant particle size reduction in commercial cements cannot be considered a viable solution for improving particle statistics as it can affect the mineral contents. Novel methods need to be promoted to address the issue of preferred orientation, and absorption contrast individually. In this context, backloading to reduce preferred orientation and careful clinker pre-grinding before gypsum addition to reduce absorption contrast were looked at as more feasible alternatives. An example of a wet ground sample with a reduced preferred orientation can be seen in **Section 4.2**.

2.2.2.2. Backloading

XRD sample preparation demands the preservation of a flat powder sample surface, devoid of porosity. This is realized when after packing the powder, the surface of the sample is lightly pressed with a smooth glass slide. Preferred orientation is manifest on the powder sample preparation when the surface of the powder is pressed, as the crystallites get oriented in a parallel direction [51]. As a work around, the sample surface can be pressed lightly with a rough textured entity such as frosted glass or sand paper such that random orientation can be induced. Or simply exposing the other side of the sample (backloading) can be performed so that the collection of reflections from parallel orientated grains can be minimized.

In backloading, the powder is poured in a special sample holder as described by Moderl [52]. The backloading technique, obscures the hind surface where the sample was pressed using a glass disc for flatness. Since the front face is backed against a frosted glass slide, the pressing generates random oriented crystallites when the front face is exposed to X-rays. Over the years, this technique has proven to reduce preferred orientation of a small magnitude found in cement phases. However, the potential for automating this technique is to be pondered upon owing to the difficulty in preparing the sample during backloading. Another drawback of the backloading

method is the inducement of specimen displacement bias. This can occur if the quantity of powder to fill the backloaded mount is insufficient, or if too much pressure is applied on the pressed side. The specimen displacement parameter is refinable in most QXRD programs. Hence, the use of sufficient powder is paramount to harness accurate results for backloaded samples. Moreover, backloading is not a highly reproducible technique by itself and several trials are required even for a trained user to prepare a good sample. Hence, a modified technique is required that is reproducible and easy to follow for automated sample preparation.

2.2.2.3. Selective Dissolution

The usual method of identifying and quantifying accurately the polymorphs of the major silicate phases (alite and belite), interstitial phases (aluminate and ferrite), and minor phases (periclase, alkali sulfates, etc.) is through wet chemical methods. Dissolution and reprecipitation of the major cement phase groups to enrich the other phase groups is a very accurate mode of stoichiometric quantification. Luke and Glasser [72] explained that even binary and ternary blends of cement, fly ash, slag, and silica fume can all be quantified to less than ±1 wt.% accuracy using selective dissolution. Individual methodologies exist for the dissolution of silicate phases (the KOSH method, exemplified in **Fig. 4**) [18], the interstitial phases (the SAM method, exemplified in **Fig. 5**) [20], and all crystalline phases (HNO_3 method) [73] in cement and the supplementary cementing materials.

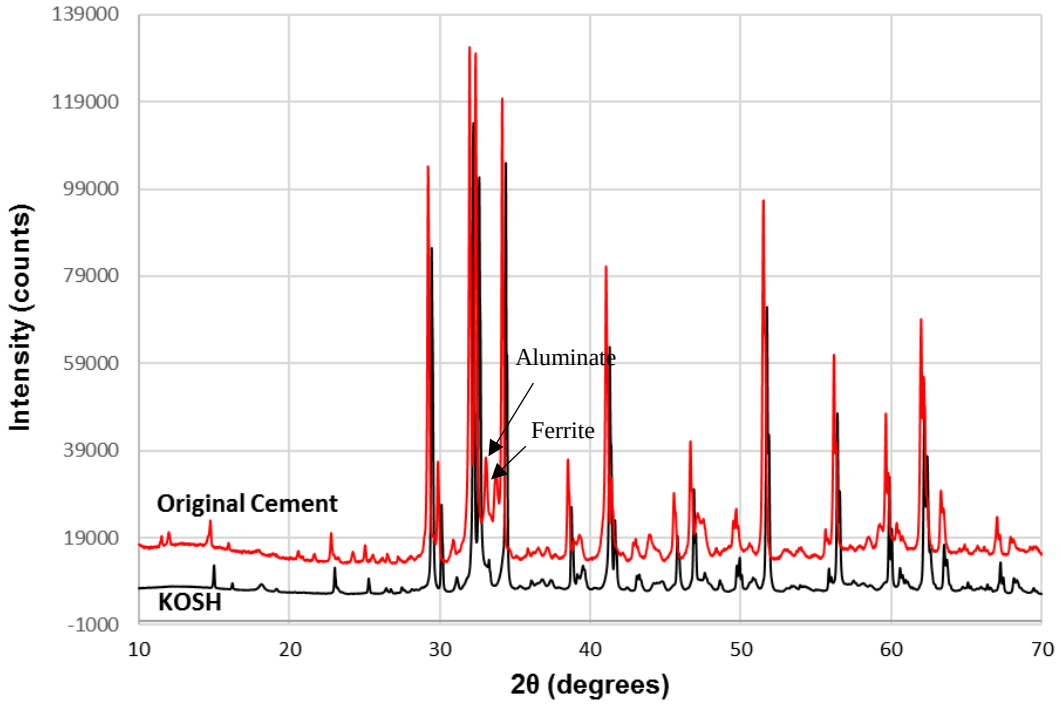

Fig. 4. Example of the KOSH method of selective dissolution of interstitial phases

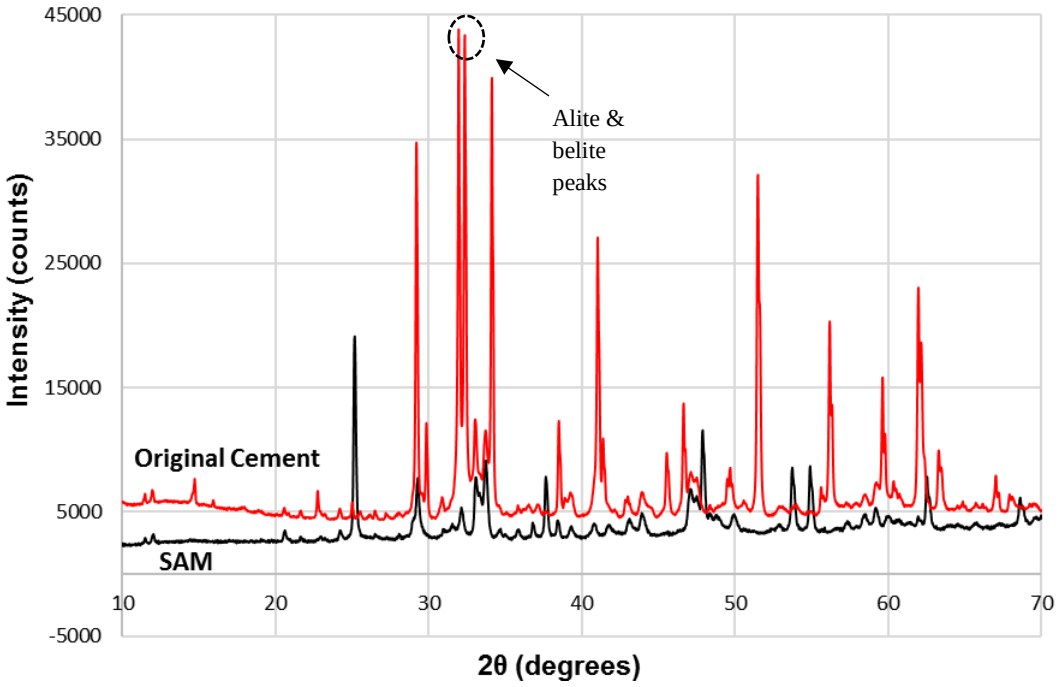

Fig. 5. Example of the SAM method of selective dissolution of alite and belite phases

2.3. Supportive characterization tools

Accuracy in quantification is a perennial issue with the QXRD and demands the usage of supplementary information for extracting the actual information about the phases. In addition to wet chemical methods, tools such as optical microscopy, isothermal calorimetry, and differential thermal analysis were identified to be effective aids for an accurate quantitative analysis. Microscopic quantification using traditional point-counting methods were incorporated in the round robin testing procedure for cement quantification [63]. In fact, microscopy is utilized in the morphological examination of the cementitious phases after clinker formation in offline quality control. Furthermore, microscopy-based phase quantification provides an indisputable accuracy in estimations surpassed only by the stoichiometric phase quantification. Investigations into the application of optical microscopy results to QXRD analyses was touched upon previously by several researchers [8, 35, 38, 39].

The pioneering work performed by Scrivener and Pratt [74] in imaging and quantifying the cement phases through back-scattered scanning electron microscopy demands special mention. It paved the way for incremental development in the image analysis procedure equating the level of accuracy achieved from traditional point-counting. Currently, the quantification of the major cementitious phase fractions is performed to a particularly high accuracy through a combination of backscattered electron (BSE) microscopy (reinforced through X-ray imaging) and quantification through multi-spectral image analysis. Stutzman [50] first described the methodology in quantifying the cement phase fractions through a practice of demarcating the phase boundaries of a BSE image through their spectral identifiers.

In an analogous manner, calorimetric analysis of cement is used to predict the performance behavior of the cement after hydration. Calcium sulfate and calcium hydroxide information

obtained from DTA/TGA analysis is quite useful as a validation technique owing to the accuracy in tracing decomposition reactions.

2.3.1. Optical Microscopy (OM)

The utilization of optical microscopy for the characterization of cementitious materials dates back to over 100 years. Henri Le Ch'atelier [75] investigated the phase constituents of Portland cement clinker on a polarizing microscopy. This pioneering investigation produced the now familiar facet that tricalcium silicate dominates the clinker microstructure. Subsequent work by Tornebohm [50], Bates and Klein [76], and other investigators provided a detailed description of the phases and textures of clinker minerals. These techniques later became well-developed with time and further advancements were provided to apply to routinely study the clinker microstructure.

Recent resources for quantitative microanalysis of clinkers include the encompassing works of Campbell [77] and Hofmanner [78]. These works take the influence of the method developed by Delesse [79] to convert 2D area fractions in 3D volume fractions, to subsequently obtain the weight fractions.

Point-counting procedure to quantify the phase constituents is enshrined in two ASTM standard protocols, the C562 [80] and C1365 [81]. This technique accesses the field of view obtained from optical microscopy and the number of crystals of the different clinker phases are counted manually. Counting is accomplished through the clear phase distinctions of the different phases, which are known to have widely variant morphologies. It is crucial to have several fields of view for the quantification to be statistically reasonable since this technique involves a manual operator.

2.3.2. Scanning Electron Microscopy (SEM)

Backscattered electron (BSE) imaging of cement polished sections has demonstrated immense potential in studying cement and fly ash systems [74, 82]. Flat, polished sections prepared by following standard petrographic procedures are representative of the contents of the whole cement or clinker. The phase distinctions are garnered by observing the features in greater detail than optical microscopy measurements of similar polished sections. Moreover, deeper magnification ranges and the advantage of obtaining elemental information for mass balance calculations (for Modified Bogue analysis) added strength to this technique. However, the BSE images are restricted to two-dimensions and suffer from limited spatial resolution which means direct connectivity to the actual three-dimensional microstructure cannot be obtained [83].

The major cement phase distinctions under BSE are a function of their backscatter electron (BE) coefficients. This coefficient is depending on the atomic numbers of the elemental constituents of the phase and is different for each phase. Although primarily employed in the morphological detection of the different cement phases, the BSE can be a very useful tool when coupled with image analysis [84-87]. The BE coefficients distinguish between phases and help in calculating the phase fraction distribution as performed by Goldstein et al. [88]. The following table lists the BE coefficients of the common cement phases.

Table 1. BE coefficients of common clinker phases (Referenced from [87, 88])

Phase	BSE coefficient
Alite	0.1716
Belite	0.1662
Aluminate	0.1639
Ferrite	0.186
Periclase	0.1213
Free Lime	0.1882
Arcanite	0.1652

2.3.2.1. Multispectral Image Analysis (MSIA)

Multispectral image analysis is a tool used for the phase segmentation of the clinker phases in this study. It was developed by researchers from Purdue University [89] to demarcate boundaries in remote sensing images. The micro-application of MSIA was introduced by Lydon in determining the mineralogy of rocks with the help of ImageJ [90], a free image analysis program. It was followed by the application of multispectral image analysis to characterize fly ash phases in 2010 [86]. The method utilized the delineation of different fly ash phases through the elemental information gained from EDS mapping images. Depending on the abundance of a particular element in a phase, the X-ray micro-analysis assigned specific pixels to the material. Convergence

of the most important elemental mapping lead to a clear distinction between the varied phases. The same procedure was followed in a successive research on tracing the hydration of blended cements [85].

Stutzman in 2015 [87] designed a step-by-step procedure to characterize and quantify the clinker phase constituents through MSIA. Direct and accurate quantification through MSIA can now be made possible by the careful preparation of clinker polished sections. However, the qualification of multispectral image analysis with accepted high accuracy methods such as optical microscopic point-counting, or QXRD is lacking. This study aims to correct this situation by correlating the quantification of BSE-multispectral image analysis with optical microscopic point counting and QXRD. Accuracy comparison of pellet QXRD is also facilitated as an outcome of this correlation.

2.3.3. Thermogravimetric Analysis (TGA)

Thermogravimetric analysis (TGA) is used to calculate the accurate percentage of calcite composition in cement and associated materials through evaporative dissociation of CO_2 from calcite. The TGA is an instrument that continuously measures the mass loss accompanying the expulsion of evaporative phases such as water & CO_2 at a steady increase in temperature. This technique requires no external sample preparation step as the bulk cement powder is poured into a TGA standard 90µL alumina sample pan and another empty alumina pan is used as the reference [91]. 30 mg of cement sample is heated from room temperature to 1000 °C at a ramp rate of 20 °C per minute in a non-reactive nitrogen atmosphere to fully capture the carbonate dissociation. On heating, the expulsion/evaporation of unbound water at around 100 °C is followed by the evaporation of the bound water present in common cement phases such as gypsum ($CaSO_4.2H_2O$) first and portlandite ($Ca(OH)_2$) second till 500 °C. From 500 to 950 °C, the expulsion of CO_2 from

the cement brings about a mass loss that provides evidence of the presence of carbonate phases in the cement, especially calcite and dolomite. Researchers are yet to agree on the exact peak position range of the carbonate peak [92], but the 750-900°C is widely accepted as the temperature range associated with CO2 expulsion from calcite [92, 93]. Among other factors, it is known that crystallite size of the calcite can play a role in lowering the dissociation temperature such that the corresponding endotherm is shifted to a slightly lower range [94, 95]. Also, longer heating times can lead to the decomposition happening at lower a temperature range which means that a faster ramp rate than usual can contribute to a slight shift of the peak towards the right [91]. Nevertheless, the peak intensity should not be considerably affected as the destructive nature of the technique coupled with the small sample size makes sure that the sample is completely incinerated.

The amount of CO_2 lost during the heating of the cement from 500-900 °C is the popular practice to estimate the calcite in the cement [93, 96, 97]. This is because the calcite is assumed to contain both the poorly-crystalline part (TGA decomposition range from 500-700 °C) and the well-crystalline part (TGA decomposition range from 700-900 °C) in the cement [96]. Although the existence of poorly-crystalline calcite in commercial cement is low (due to carbonation of portlandite) and questionable [92, 93, 98, 99], for reasons of consistency with reference investigations the standard practice was followed here. A 15% standard deviation regime was imposed on the TGA calcite quantification to account for the drift of the weighing scale measurement inside the TGA. **Table 2** illustrates the important phase decomposition temperature ranges in cement TGA analysis.

Table 2. Important phase decomposition temperature ranges in cement

Temperature Range	Phases
0 °C to 70 °C, 70 °C to 130 °C	Gypsum to hemihydrate transition, hemihydrate to anhydrite transition [100]
Till 300 °C	Bound water release [101]
400-500 °C	Bound water release from portlandite [92, 102, 103]
750 - 900 °C	CO_2 release due to calcite [92, 93]

2.3.4. Isothermal Calorimetry (IC)

The addition of the calcium sulfate phase (as gypsum) to the cement helps in reducing the rapid conversion of C3A to hydrogarnet, instead forming ettringite [2]. This reaction is influenced by a variety of factors, chief of them being the type of the calcium sulfate and C3A polymorphs. [104] recognized that the inter-grinding of gypsum with the clinker in a finish mill can promote better control over C3A reactivity than extraneous gypsum addition (inter-blending). Inter-grinding of gypsum with clinker can lead to polymorphic transitions in gypsum which can affect the cement's performance characteristics. Gypsum-to-Anhydrite conversion can occur as early 2 minutes into grinding, due to the rapid dehydration produced by the attrition heat. Anhydrite (solubility: 2.6 g/L) dissolves slower than the gypsum (solubility 2.4 g/L) with the C3A leading to

a much slower formation of ettringite [105]. Isothermal calorimetry measurements can accurately highlight the extent of reactivity differences between gypsum and anhydrite.

A cursory look at the solubilities of the two phases reveals that the rate of dissolution of anhydrite is much slower than the gypsum in an Al-rich environment [106]. Sometimes, the formation of calcium sulfate hemihydrate (CaSO4.0.5H20) from gypsum can lead to the increased rate of formation of ettringite owing to the quicker solubility of hemihydrate [14]. Winnefeld et al. [107] observed through calorimetry that two cements with equal amounts of hemihydrate and gypsum contents generated ettringite within 5 minutes and 4 hours respectively. Such a rapid reaction can sometimes lead to false setting. Hence, the grinding process in a finish mill must be carefully regulated so that the phase conversion of gypsum shall be avoided. Another vital aspect is the reactivity differences of cubic and orthorhombic C3A in a sulfate-rich environment [13].

Comparative analysis of gypsum vs. anhydrite reactivity in cement typically uses a combination of isothermal calorimetry, QXRD, and sometimes the TGA to properly delineate the conversion of the reactants at every stage of the process. Investigations with incremental amounts of calcium sulfate addition to cement, from 2 wt.% to 40 wt.% [108-110], incorporating all 3 polymorphs in varying abundances describe the process in good detail. Starting from the initial amount of ettringite formed [11] to the conversion of hemihydrate to secondary gypsum [107] to the reduced total heat produced by a pure anhydrite phase reaction with clinker [108], the quantum of related information gained from isothermal calorimetry is quite rich. An interesting information was gained recently where isothermal calorimetry measurements could identify enhanced alite formation due to calcium sulfate present as gypsum compared to anhydrite [110].

2.4. Discussion on the gaps in existing research

It will be clear from the descriptions of the analysis methodology of the various cement chemical analysis methods that no single method can comprehensively provide all significant information without serious shortcomings. This calls for a situation where the drawbacks of one method are compensated by the advantages of the other. For instance, the accuracy calibration of QXRD through point-counting results or the validating the stability of MSIA through pellet QXRD or combinations of these. This is facilitated since the accuracies of the aforementioned methods are quite close to each other.

However, the Bogue quantification was neglected from the analyses since the errors contributed by the Bogue method are relatively large. Further, the Bogue method is an estimating technique while the other discussed methods are determining in nature. A like-for-like comparison is difficult to be achieved through the correlation of the Bogue method with the direct methods and any relationship manufactured thence will be purely mathematical.

In view of this situation, there exists a scarcity of research in correlating the Bogue method to other direct analytical methods. A statistical correlation is possible which may not necessarily have a physical significance. This problem was allotted special focus in this study.

Concurrently, the problems with QXRD sample preparation need a revision of their known solutions for industrial application. This can lead to further improvements in future and pave the way for the creation of a single accurate chemical analysis method for cement production testing. Improved solutions for some of these barriers are discussed exhaustively in the forthcoming chapter.

3. CASE STUDIES OF QXRD ADOPTION IN CEMENT PRODUCTION TESTING

An extension of the literature survey for this study is the industrial perspective of the effectiveness of QXRD. Although QXRD is considered as an upgrade to C150, the areas where the employment of QXRD can make an impact on process valorization is not fully understood. The following sections contain qualitative and quantitative information on cement production domains where QXRD adoption in online process control can lead to significant advantages.

3.1. Effect of alite polymorphic information on cement performance

Alite phase in industrial clinker undergoes polymorphic transformations through the process of clinkerization at different temperatures. Bigare et al. in 1967 [111] established the presence of six polymorphs, the rhombohedral R polymorph (above 1050 °C), three monoclinic M polymorphs (950-1000 °C), and three triclinic T polymorphs (600-900 °C °C). The polymorph that is stabilized at the highest temperature of formation at above 1050 °C is the R polymorph. Incidentally, this polymorph is the most stable of all alite polymorphs. However, due to impurity considerations in the substitutional lattice spaces, the alite is sometimes stabilized in the form of M or the T polymorph. Following the pioneering research, Maki et.al., established the prevalence of only three polymorphs in commercial alites in successive papers [112, 113] with a conjunctive microscopy-XRD study. Depending on the SO_3 and MgO composition in the hot meal, the alite phase can stabilize in the form of the monoclinic M1 and M3 polymorphs, or in rare cases, the T3 polymorph. The pseudo-hexagonal phases of M1a (the R polymorph) and M1b polymorphs were re-designated as the M1 and M3 polymorphs, which extended the count of polymorphic transforms to 7. Further, Maki et.al. generated a precursor method to identify the difference between the two polymorphs through their X-ray diffraction profiles. The M3 polymorph displayed characteristic doublet peaks between 32-33° 2θ and 51-52° 2θ.

A more realistic method of differentiating between M3 and M1 was succinctly outlined in a recent paper by Li et al. [4], depending on the MgO and SO_3 ratio which extended on Maki's observations. Increasing MgO favored the stabilization of the C_3S as the M3 polymorph whereas, an SO_3-rich atmosphere in the kiln favored the stabilization of the M1 polymorph, and an increased belite content than an MgO-rich environment (**Fig. 6**). However, it is known that in a commercial clinker both the M1 and M3 polymorphs are often seen in a defined ratio based on the SO_3/MgO ratio in the kiln. As a result, there needs to be a cap on the ratio of the M3 polymorph to the M1 polymorph to promote better control over cement strength development behavior. Kiln burning temperature, and substitutional ions are the major variables that can lead to effective control over the stabilization of the M3 polymorph within a required limit. **Figs. 6 and 7** represent the relationship between SO_3 addition and strength development through the formation of the M1 polymorph.

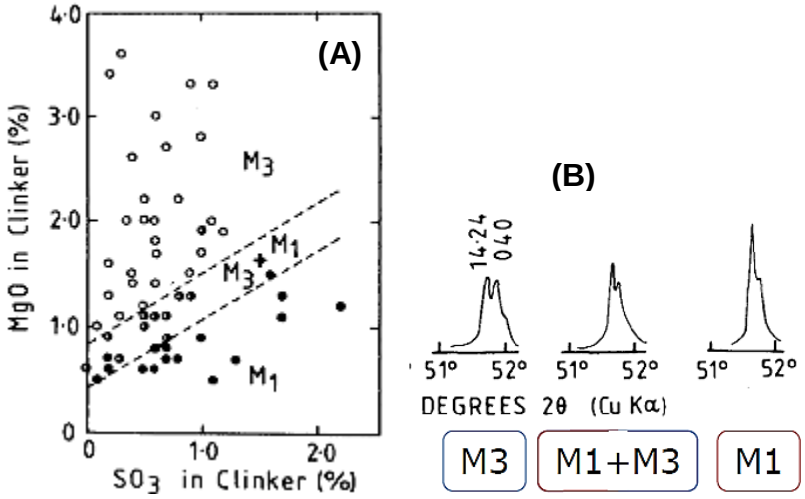

Fig. 6. (A) Regions of formation of the two proliferous alite polymorphs based on kiln chemistry, and (B) Difference between M3 and M1 polymorphic variations found in commercial clinkers (Reprinted from [112])

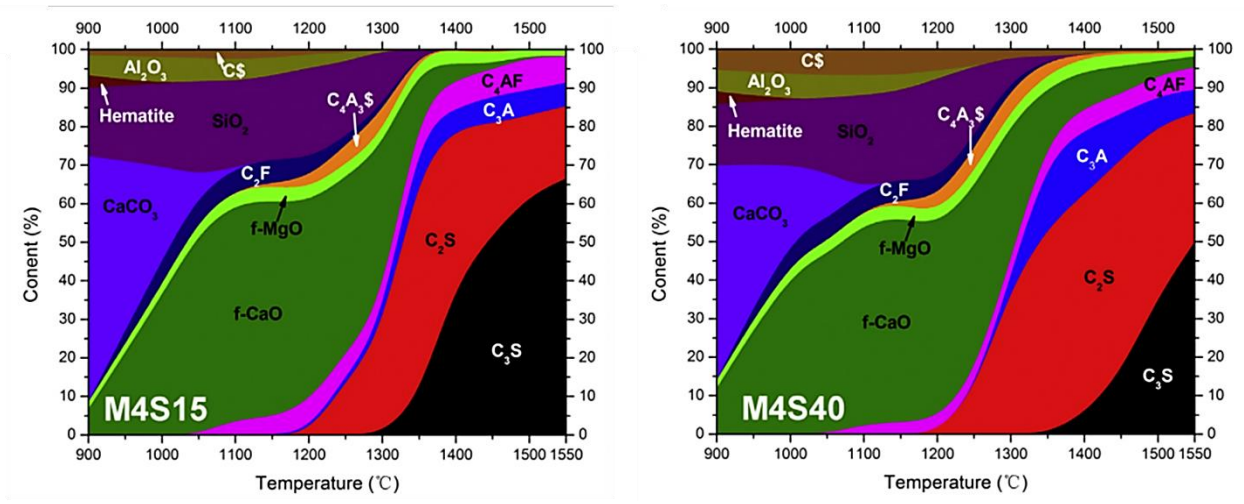

Fig. 7. Images illustrating the increase in C2S and reduction in C3S with SO3 addition (Reprinted from [4])

The ideas generated from Maki et al. to Li et al. were extremely useful in advancing the cement chemistry understanding in a kiln applicability scenario. It allowed cement plants to perform case studies to clearly delineate the extent of the accuracy of our current understanding of cement chemistry. Preliminary work on this regard was performed by Supreme Cemento (Brazil) (**Fig. 8**), where the advantageous characteristics of the M1 polymorph was clearly seen. Subsequent research by Dyckerhoff (Switzerland) (**Fig. 9**) showed a slight increase in the 3-day strength of the cements with increasing M1 ratio in the alite. The compositional accuracy was realized by reducing the particle size of the raw meal so that increased M1 can be obtained. Another method of producing M1-rich alites is to use a fuel combination of natural coal and petroleum coke, which can give rise to an increased SO_3 environment than other conventional fuels [114].

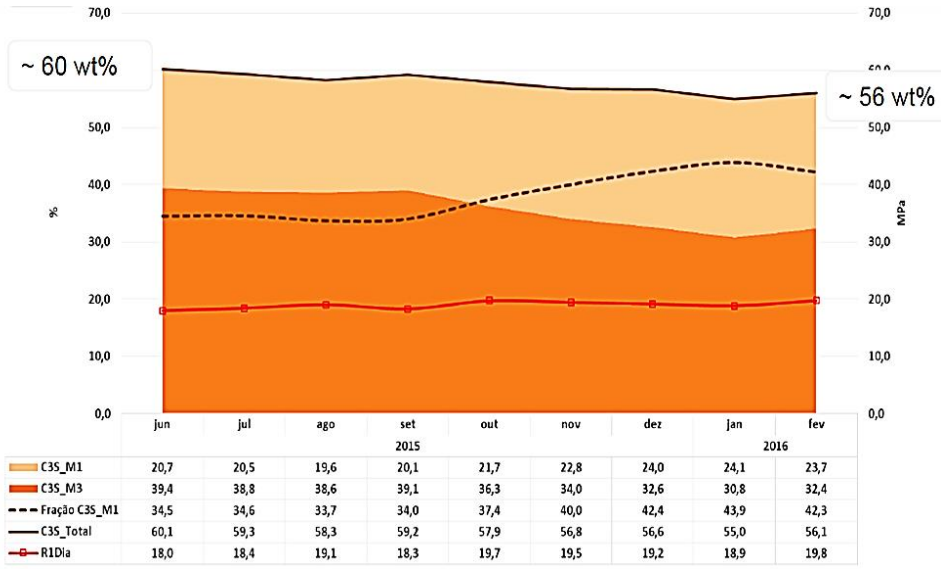

Fig. 8. Case study performed by Supreme Cemento (Brazil) describing the increase in M1 polymorph with SO_3 content in clinkers most closely representing the Types I/II, V

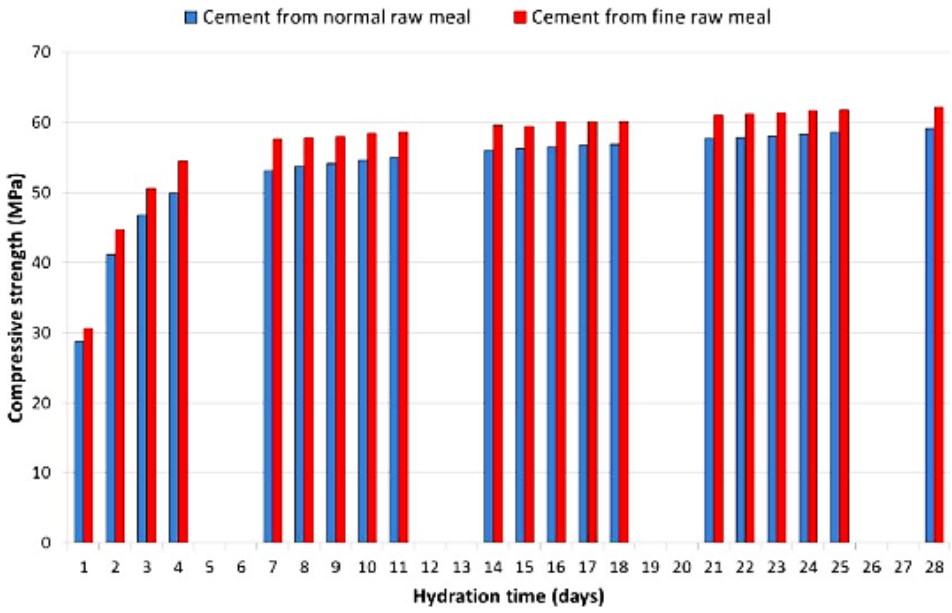

Fig. 9. Case study performed by Dyckerhoff Cement illustrating the observance of increased strength with increased M1 polymorph brought about by using a finer raw meal

3.2. Effect of sulfate and aluminate polymorphs

C3A is a very important phase in cement as its dissolution in water is rapid and proceeds through initial precipitation to C3AH6 (hydrogarnet) and calcium hydroaluminate (AFm phases) [115-118]. C3A stabilizes as different polymorphs depending on the prevailing conditions in the kiln. During the cooling stage in the kiln, the C3A is present in the form $M_{3x}\ Ca_{3-x}\ Al_2O_3$, where the M represents the type of the prevalent alkali ion in the kiln, and x can be anywhere between 0 to 0.25 [2, 119]. If the alkali-ion content (usually Na) is quite low, x will be between 0-0.1 and leads to the formation of the cubic aluminate polymorph. If the alkali content is higher, orthorhombic aluminate will be stabilized with the x between 0.1-0.2 [2, 120-122]. Often, the alkali-ion concentration in a kiln is not highly enriched beyond the limit x = 0.1 (cubic) which makes the monoclinic polymorph of C3A (x = 0.2-0.25) extremely rare. Furthermore, alkali enrichment in the kiln is often an indicator of poorly-maintained furnace conditions, so is the monoclinic polymorph.

Alkali or Orthorhombic aluminate dissolves faster in water saturated with gypsum than the cubic aluminate owing to a fundamental difference in the morphology, which is apparent on their reactivities [13]. As a result, cubic aluminate is most preferred owing to the control it offers in deciding the quantity of sulfate addition. Hence, the control of the alkali-ion rich atmosphere in the kiln is very important to obtain a cubic aluminate ratio greater than 95% of the orthorhombic aluminate [114] to better predict of hydration behavior.

In order to prevent the rapid reaction of C3A phase with water, calcium sulfate phases are added to the clinker at varying compositions based on the dissolution chemistry of sulfate and aluminate phases. In addition to the C3A polymorphs, the reactivity of the different polymorphs of the sulfates play a crucial role in the hydration behavior of C3A and the formation of ettringite.

Benstead in 1982 [14] proposed that hemihydrate has a higher solubility than gypsum, which promotes faster supersaturation of the pore solution with sulfate ions, thereby increasing the early strength by quicker reaction with aluminate to form ettringite. This behavior was exhibited so long as the gypsum/hemihydrate quantity was within 30 wt.% of the aluminate phase, wherein above that limit the trend was reversed. Hemihydrate increases the rate of precipitation of the ettringite (67% greater than gypsum) since the reaction is disposed of the precipitation of the transitional AFm phases, thereby favoring strength development during the first 2 hours. However, the presence of anhydrite will destabilize the aluminate-gypsum reaction, owing to its significantly low solubility, and is not favored in the cement.

Prominent work performed by Pourchet et al. [11] on C3A-gypsum reactivity by a combinatorial analysis of Minard's procedure and calorimetry analysis describes the exact difference between the reactivities of gypsum-hemihydrate (illustrated in **Fig. 10**). In commercial cements, 30% of the added aluminate reacts with pure gypsum instantaneously to provide the AFm phases while the rest of the aluminate converts to ettringite gradually. When hemihydrate is added, no AFm production takes place which in fact offers better control over the reaction as the ettringite reaction can be monitored more effectively. Although hemihydrate has a reactivity advantage over gypsum and anhydrite, the presence of hemihydrate leads to rapid setting which is undesirable in field conditions.

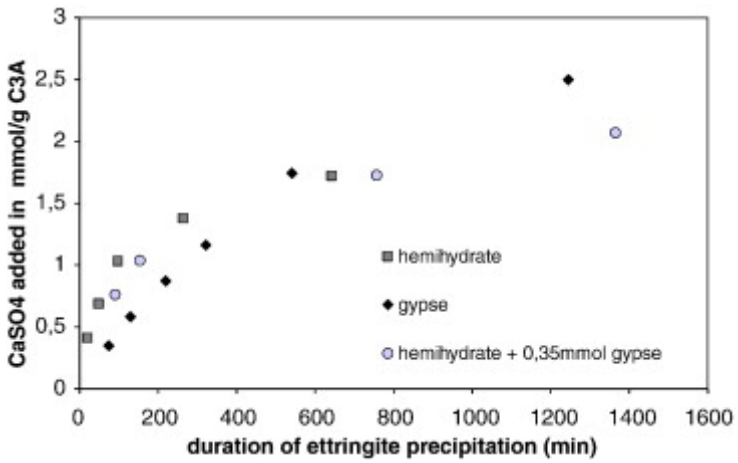

Fig. 10. Difference in reactivities between aluminate-hemihydrate and aluminate-gypsum in presence of water (Reprinted from [11])

3.3. Phases introduced due to alternative fuel substitution

Increasing usage of secondary/alternative fuels is employed in the clinkerization and grinding processes to reduce the carbon footprint. With the prospect of modifications to the burnability with increasing substitution of conventional fuels, distinct phases emerge during clinker production. Ferruginous materials in alternative fuels such as glauconite, chlorite, etc. can lead to ferrous iron formation in the clinker, while also providing mineralizing effects [123]. Generally, combustible organic wastes contain a lot of energy and increase the atmosphere of major oxides such as CaO, Al_2O_3, MgO, etc. Especially, increasing alumina environment can increase the generation of tricalcium aluminate in the clinker as well as the introduction of the amorphous aluminate phase which is more reactive than the crystalline form [13]. Alternative fuel utilization can also manipulate the clinker phase chemistry of alite and belite. As seen in **Fig. 11** with the substitution of sewage sludge to increase belite formation [124], the introduction of various alternative fuels can cause a marked shift in the performance characteristics. It is highly

important to track such and similar changes in clinker process control using QXRD to improve the predictability of the final cement performance.

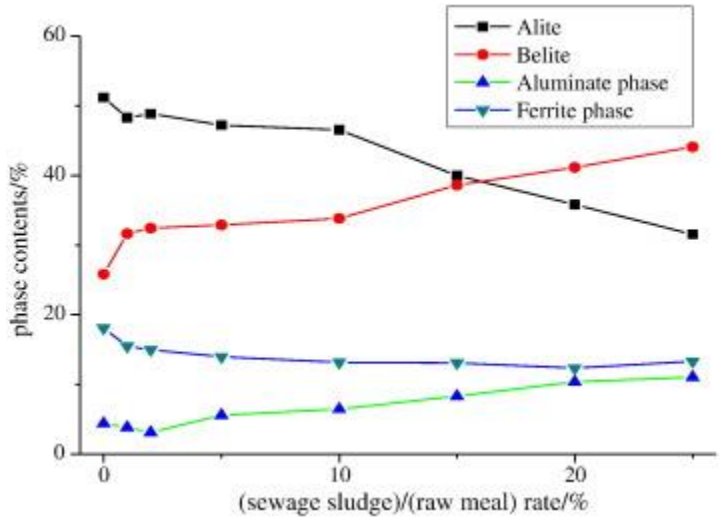

Fig. 11. Change in the clinker phase constituents with increasing (sewage sludge)/(raw meal) ratio (Reprinted from [125])

Here, online QXRD can play a leading role in tracking the modifications to the clinker chemistry from the well-known cement chemistry perspectives. For instance, standalone analysis by Dyckerhoff Cement showed that online QXRD analyses of rubber tires - a cheap alternative to coal - imparts phases as divergent as metallic iron, wax, and, sucrose to the cement. Using an online QXRD setup, the dehydration of gypsum after grinding can be monitored as well as the quality of gypsum added before grinding [126]. A significant increase in the amount of organic waste/sewage sludge substitution can reduce the viscosity of the molten meal, increasing the size of the alite crystals owing to increased ion mobility [127]. This can lead to the stabilization of the M1 morphology (as seen in **Fig. 12** (right)) as the predominant alite polymorph since M1 alite forms larger crystals than M3 alite [4]. Similar grain growth behavior for alite was observed with increased phosphorus content found in most bio-fuels [124, 127-129].

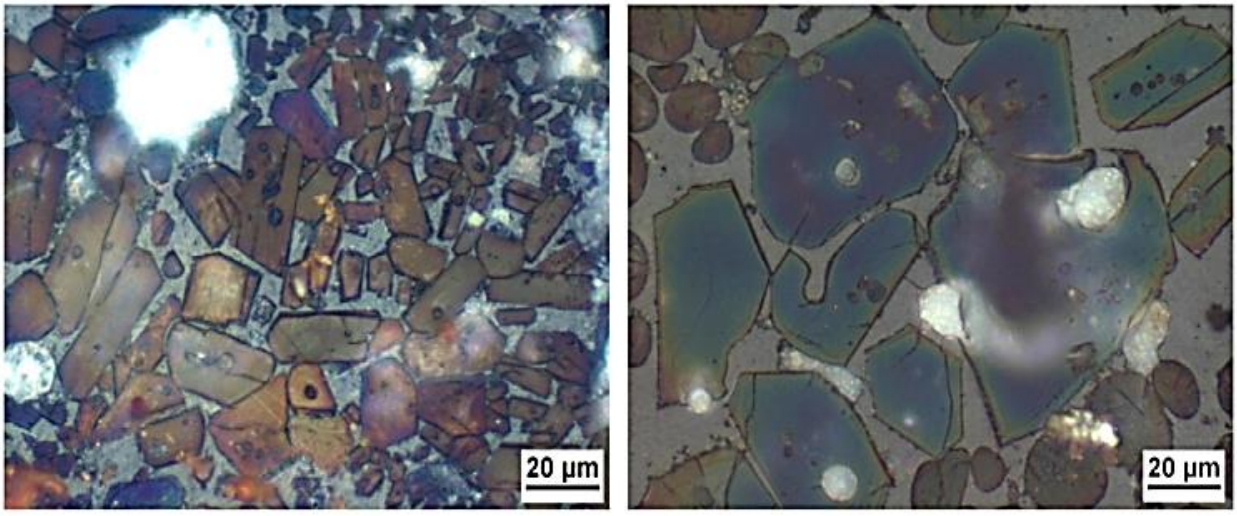

Fig. 12. Increase in alite crystal size due to alternative fuel usage (Reprinted from [127])

Apart from bio fuels, alternative fuel usage can also impart increased heavy metal ion fraction in the kiln, which can cause health hazards such as Zn, Sn, and Cu [130, 131]. Most importantly, heavy metals can isomorphically substitute the interstitial Al^{3+} and Fe^{2+} ions to significant property alterations. When in abundance, the heavy metals can react with major clinker oxides to produce new phases. Sn^{2+} can react with lime to form calcium stannate ($CaSnO_4$) inhibiting carbonation reaction [132]. Moreover, increased Sn can promote the formation of Aft and Afm phases without impacting the performance of the hydrated paste [133]. In another case [134], the trapped Cu ions in the clinker phases can be detrimental to the formation of C3S since they favor decomposition of C3S to C2S and free lime. Increased Zn ion concentration can in turn affect the formation of the aluminate phase favoring ferrite [130]. Since the existing online quality control protocols cannot identify such markers of inferior performance, the current situation (without QXRD) poses as a handicap towards the increasing substitution of conventional fuels.

3.4. Impurities in limestone, polymorphs, and associated phases

Retrospective addition of limestone to Type I cement to promote the early strength is characterized as Type I-L cement [108, 135]. ASTM C595 allows the incorporation of 15% limestone by weight of the blended cement. Alternatively, limestone aggregates are added to concrete for high early strength as coarse or fine fractions. The positive aspects of the fine limestone aggregates impacting the concrete early strength have been investigated extensively by Bentz in [136, 137]. However, in order to predict the performance characteristics of I-L cements, the various polymorphs of limestone should be characterized. Calcite, aragonite, and, vaterite are the 3 polymorphs commonly seen in conventional limestones. A multi-scale investigation by Bentz et al. in 2013 [137] revealed that the trigonal calcite is preferred in concrete because, (i) it promotes nucleation and growth of calcium silicate hydrate gel at early ages, (ii) it accelerates and amplifies silicate hydration, and, (iii) provides a source of carbonate ions to participate in reactions with the aluminate phases present in the cement (and fly ash). Conversely, the orthorhombic crystal structure of aragonite withdraws the hastening effect on silicate hydration at a similar particle size as calcite. However, because these two forms have similar solubilities in water, the aragonite does contribute to an enhancement in the reactivity of the aluminate phases in the investigated systems, chiefly via carboaluminate formation [138]. The carboaluminate makes for the reduction of sulfate addition and stabilizes the ettringite [139, 140]. Moreover, it is more voluminous [139, 141] and stiffer [142] than sulfoaluminates after hydration, thereby reducing porosity and increasing early strength. QXRD can help promote the formation of carboaluminate by clearly identifying between aragonite and calcite in the additive limestone.

The quantification of the purity of the added limestone as calcite is an important contributor to the desired performance enhancement. Online QXRD can help with the identification and

quantification of the exact nature of the undesirable phases and their polymorphs, leading to their subsequent removal. Critical phases such as pyrite (usually found near limestone quarries), the different calcite polymorphs, dolomitic impurities in limestone, ankerite, siderite, etc. are the commonly observed impurities with natural limestone. A joint effort by Schwenk Zement KG (Germany) and Bruker AXS showed the presence of the aforementioned impurities (and a few more) in natural limestone that was considered to be highly pure. This is illustrated in **Fig. 13** with the observance of feldspathic, siliceous, and, clayey impurities in limestone.

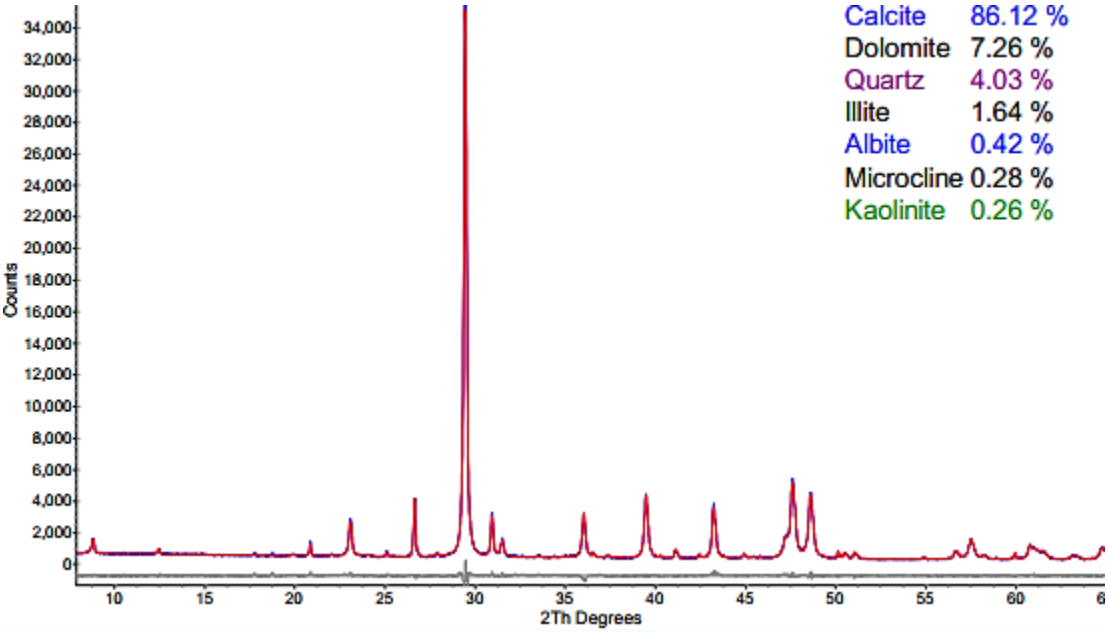

Fig. 13. XRD pattern from Bruker AXS representing the presence of quartz, feldspar, and kaolinitic impurities in natural limestone

3.5. Hotmeal and raw meal analyses

The analysis of the feed raw meal sent into the kiln can be examined first before the manufacture process is initiated. In the raw meal, both favorable and unfavorable phases can co-exist depending on the quality and synthesis/extraction of the raw materials. Usual examples that

pertain to the raw meal QXRD lie in analyzing the purity of gypsum and limestone added to the kiln, with the latter added either retrospectively or with the batch.

The raw meal after calcination undergoes de-carbonation and loss of bound water and is hauled out through the conveyor belt as the hot meal. In the hot meal, the degree of de-carbonation of limestone can be evaluated by the quantification of the free lime phase using QXRD. In another case, the presence of the alite phase at the intermediate stage of clinker processing is an indication of the excessive production of clinker dust in the kiln. Clinker kiln dust (CKD) is a mass of fine-grained materials rich in SiO_2 and can form a layer on the molten melt reducing the thermal efficiency of the kiln. The regular removal of the CKD is vital which leads to their presence being unsolicited in the kiln. QXRD analysis of the hot meal can pinpoint this deviation from the process control routine to make timely adjustments.

In addition, the buildup of alkali sulfates or silicates in the kiln can lead to the blockage of preheaters or precalciners of raw materials which can affect the overall thermal efficiency of the kiln. Case studies conducted by the Holcim plant at Siggenthal, Switzerland (**Fig. 14**) revealed that the presence of alkali phases such as Spurrite and Langebeinite in the hot meal caused the obstruction of three preheater tubes leading to a monetary loss equivalent to around 36000 tons per year of cement as per 2009 inflation levels (equivalent to $1.6 million per year). The problem was resolved once the raw feed was adjusted to reduce the SO_3/Cl ratio such that crusting and lumping of the alkali phases was unseen afterwards.

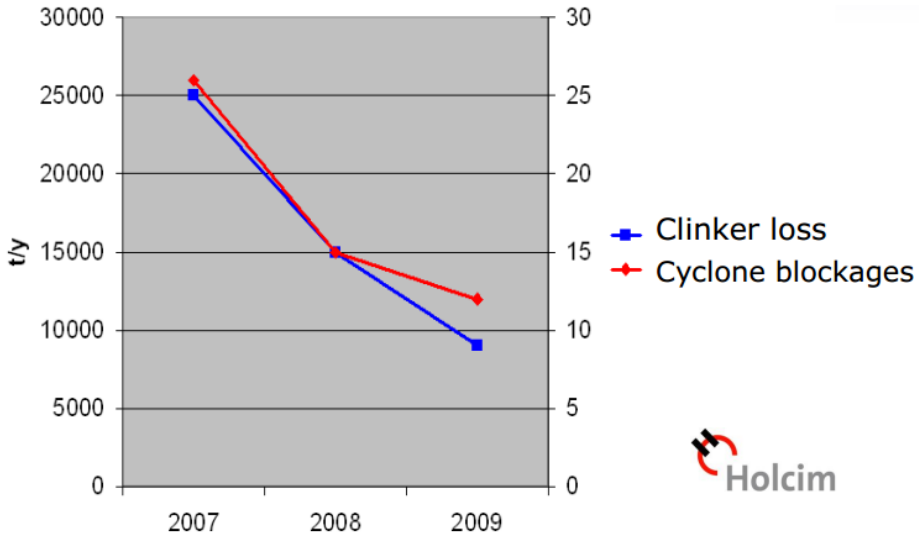

Fig. 14. Graph from Holcim cement describing the improvement on financial results after addressing the cyclone blockages

3.6. Effect of alkali phases in cement

The presence of alkali sulfates in cement is often unstoppable owing to the prominence of alkali oxides in the raw meal. The alkali ions usually get substituted in the major cement phases however a tiny fraction of the alkali ions can react with the sulfate or can get oxidized to form alkali oxides and sulfates. The existence of both compound groups is undesirable in cement, owing to the problems with excessive cement/mortar expansion on hydration. ASTM C191 specifies a test for the measurement of the expansion of cement using an autoclave apparatus, which are increasingly being under the scanner due to safety concerns. Commonly seen phases which lead to such expansions include, the periclase, free CaO, and a variety of alkali sulfates (Arcanite, Spurrite, Aphthitalite, Langebeinite, Thenardite, etc.). The arcanite phase can lead to the formation of the syngenite phase whereas the MgO and CaO can lead to the formation of brucite and portlandite respectively, leading to increased expansion. However, it is well-understood that the presence of such phases below a universal fraction of 2wt.% for all phases individually is

acceptable provided that quite a few of such phases don’t occur in the same clinker [50, 143]. Although the alkali oxide phases are limited to the expansion drawback, the alkali sulfate phases pre-hydrate the cement by just absorbing atmospheric moisture leading to clumping and encrustation in sample conveyors. The customary practice to counter clumping of cement is to add a small fraction of limestone to the cement such that it is workable for baggage and shipping. However, clumping due to alkali sulfate hydration cannot be solved that way as it is independent of limestone reaction. A workable solution would be to identify the alkali sulfate during the hot meal/sample batching analysis and retrospectively correct for the next batch. This solution is possible only with the use of the routine QXRD as the exact nature of the alkali sulfate can be identified through direct measurement.

4. IMPROVEMENTS TO EXISTING CHEMICAL ANALYSIS FRAMEWORK

4.1. Statistical correlation between Bogue and QXRD

A direct comparison of Bogue and QXRD can facilitate the understanding of the QXRD protocols from the viewpoint of the historical perspective of cement analysis. A pilot study of Bogue to QXRD conversion performed by Stutzman [144] in 2010 developing QXRD specifications by extrapolating Bogue specifications. This work involved comparing QXRD results derived from a variety of methods such as single-peak fitting, internal standard, RIR method, and the Rietveld method against the corresponding Bogue quantification data. Since the QXRD dataset wasn't method-specific, the estimated QXRD results from the correlation showed large deviations from actual QXRD when it was reproduced for this work. Moreover, the estimated QXRD was not validated with actual QXRD information of separate cement samples.

In this study, efforts were made to address such shortcomings. Direct comparisons between Bogue and Rietveld quantification for a clinker dataset repository numbering above 300 was performed. The samples were predominantly Type I clinkers and their quantification was sourced from the Lehigh Hanson cement plant in Maryland. A linear regression model was generated to derive estimated QXRD information from a given Bogue data.

Data processing to obtain the specification limits was performed by applying Working-Hotelling-Scheffe bands. Simple linear regression does not incorporate the distribution of the measured results. Often when an estimation is needed to be drawn, the intertwined relationship between slope and intercept is not accurately represented by linear confidence limits alone. Lark pointed out that this relationship can be significant in datasets derived from least-squares calculations leading to negative or physically unreasonable estimations [145].

Although the QXRD errors are relatively low compared to Bogue errors, they need to be properly accounted for in the uncertainty of phase determinations. Primary effort to apply simultaneous confidence limits for deriving the chemical composition of cements was made by Sieber et al. [146] to create a framework for the assignment of 1σ uncertainty ranges. This was extended by Stutzman in [144] with the use of Working-Hotelling-Scheffe (WHS) simultaneous confidence intervals based on statistical tests of significance [147]. Applying WHS processing creates tightened confidence limits around a linear regression correlation and naturally eliminates bad or underused data. It also extends the validity of correlation especially at lower Bogue quantification ranges.

4.1.1. QXRD estimation using Bogue data

Table 1 of ASTM C150 has several specification criteria based on a historical relationship between performance behavior of cement and the phase quantities. Extensive research is necessary to renegotiate the terminology of ASTM C150 into QXRD terms. Hence, a Linear regression of the 320 cements received from Lehigh Hanson yielded a general Bogue to QXRD correlation. This correlation was tested on 10 cements belonging to various ASTM C150 cement types. Mean QXRD quantification of the cements was observed to be within acceptable deviation (within ±1 wt.%) from the estimated QXRD. The Bogue to QXRD correlation, aided by WHS bands, is general in the sense that it covers the commercial range of phase quantities for the alite, belite, aluminate, and ferrite phases. Hence, its application over the gamut of the ASTM C150 types yielded highly accurate estimations. The code used to generate WHS plots in MATLAB is included in the Appendix.

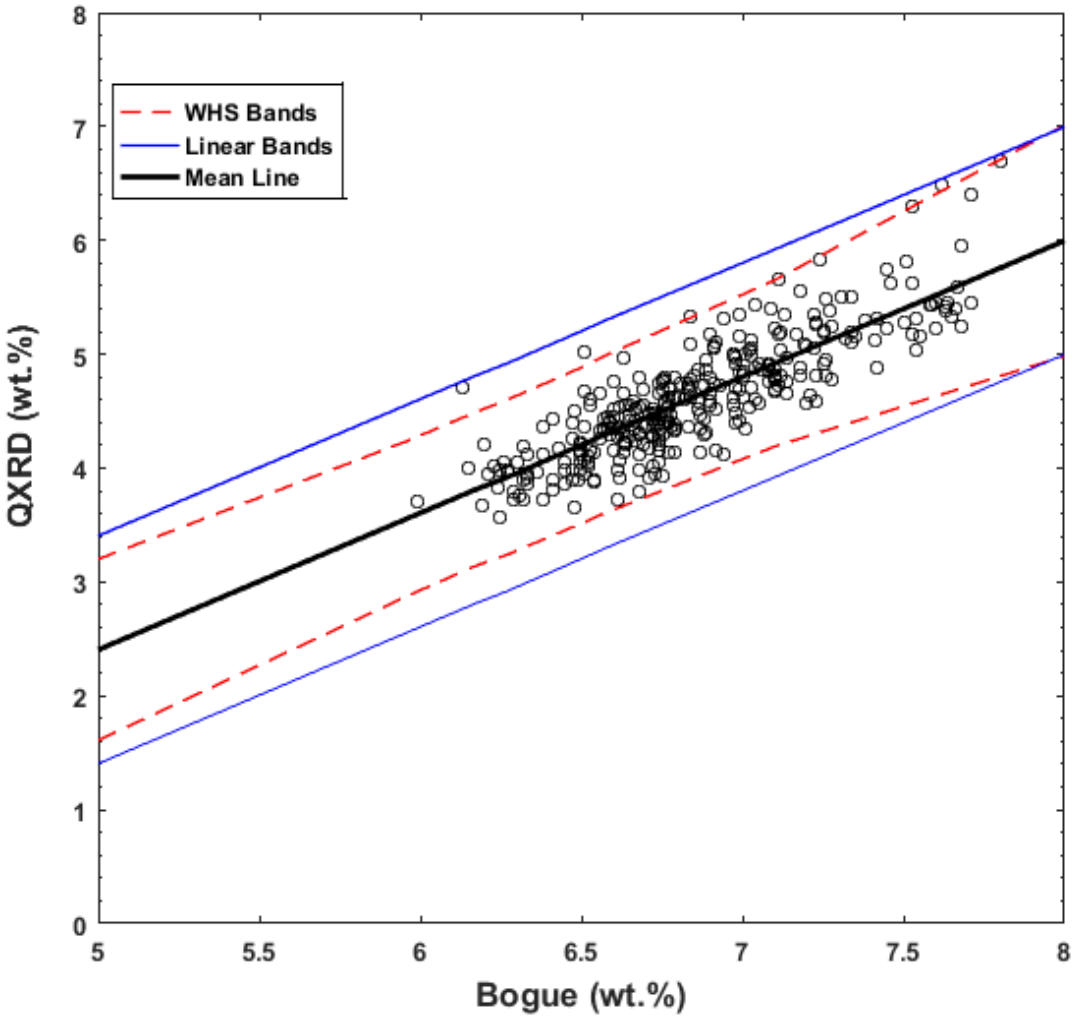

Fig. 15. C3A correlation between Bogue and QXRD for over 300 cements. The mean line represents the linear regression correlation, the solid blue lines represent ±1wt.% confidence limits, and the dashed red lines represent the WHS confidence limits. WHS confidence limits consider the distribution of the dataset, unlike the standard ±1 wt.% linear confidence limits. It is apparent from the widening of the WHS confidence bands towards greater Bogue values and constriction at smaller Bogue values.

Fig. 15 represents the Bogue to QXRD correlation for C3A correlation of 320 cements and **Figs. 16 & 17** represents the bias in quantification between estimated and quantified QXRD. The

WHS confidence bands condense the prediction to about 13% near the centroid of the dataset. The distance from the hyperbolic center of the WHS bands to the mean of the dataset is an indicator of the precision and accuracy of the measurement. Stutzman [144] described that in the comparison of the Bogue technique to any direct quantification method, the bias contributed by the Bogue method is carried over in the correlation. It means that although both techniques calculate the same quantity parameters (phase fractions), the bias incorporated by the Bogue method can lead to the result not being equal to zero in the absence of any phase. This is apparent when the Bogue quantity is made zero. The corresponding absolute value of QXRD estimation (3.6 wt.%) was found to be equivalent to the distance from the centroid of the dataset and the center of the hyperbola.

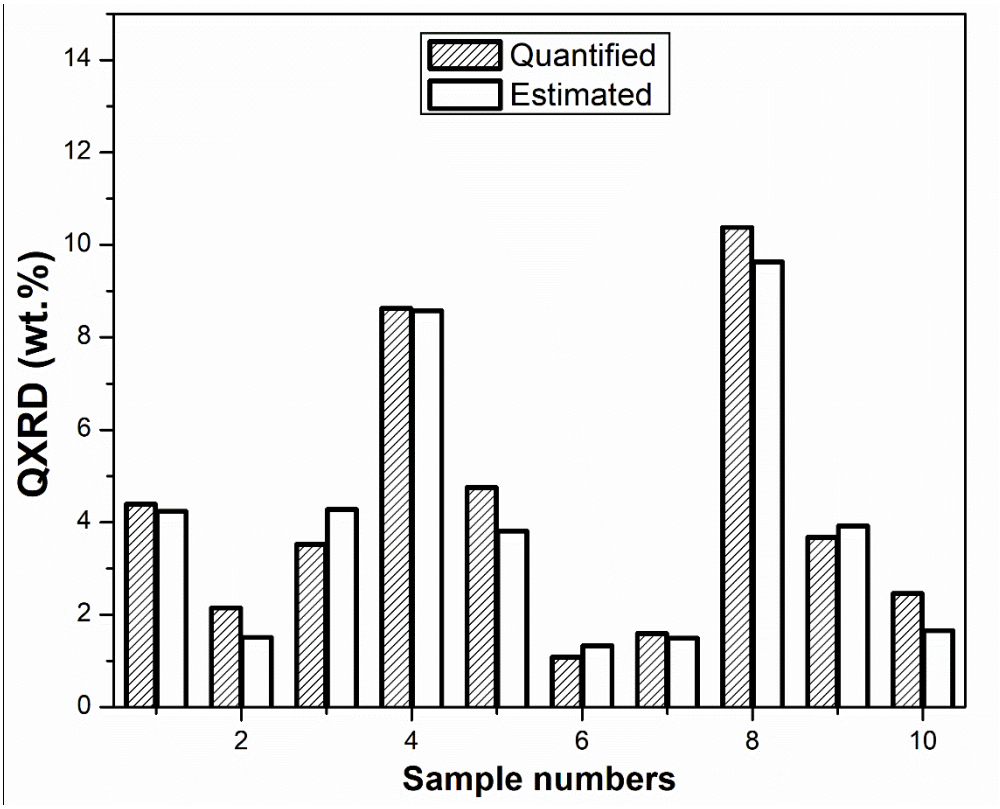

Fig. 16. Bar plot tracing the differences between estimated and quantified C3A for the 10 sample cements

4.1.2. Bias in estimated QXRD

Differences between estimated and quantified QXRD were represented in the form of the bias between the estimated and quantified results. The accuracy of the estimations was reinforced by the negligible bias in the quantification between estimated and actual QXRD. 9 out of the 10 cement samples (range of C3A estimations = 1.7 to 8.9 wt.%) passed the C3A correlation when the standard XRD variation of ±0.8 wt.% was imposed (this model will hereby be mentioned as current model). In comparison, the existing literature model only passed 4 out of 10 estimations. Factors such as the type of the cement, the quantity of Bogue estimations or the errors incorporated in Bogue did not play a significant role in affecting the estimations. The following plot illustrates this observation.

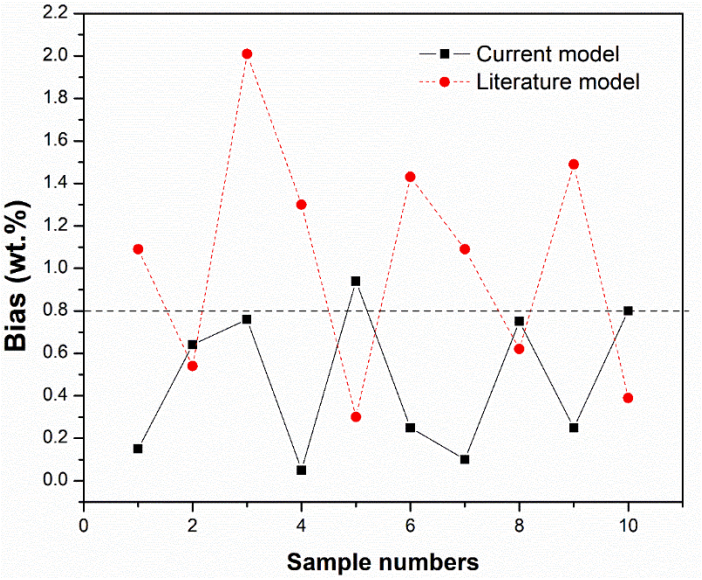

Fig. 17. Plot showing controlled bias between the means of the estimated and quantified QXRD for the C3A phase in the current model against the wide bias variations in the literature model.

For the C3A, the correlation ceased to be valid (QXRD estimation < 0 wt.%) below 3.5 wt.% (Bogue) without the application of the WHS limits. The validity of the correlation extended to 1 wt.% of Bogue C3A input after utilizing WHS confidence bands. In contrast, the application of linear bands restricted the correlation to 2.7 wt.% below which the QXRD estimation turned zero. The Bogue quantification can sometimes churn out C3A estimations lower than 2wt.% especially in IL cements. WHS correlations are advantageous in such cases since they incorporate the distribution of the dataset into their processing.

4.1.3. Extension to significant phase and relationships

When the correlation was extended to alite using the current model, the variation between the estimated and quantified QXRD increased owing to the higher abundance of alite in cement. Hence, the acceptance limit was extended to ±4 wt.% for alite. The validation was encouraging for all alite fractions with the exception of a few cases where the correlation was slightly incompatible. This difference from the excellent correlation for the C3A can be due to the abundance of alite in cement. It is logical to infer that the errors in determination or estimation increase as the occurrence of the phase increases. **Figs. 18 and 19** represent the C3S WHS correlation of 320 cements and the bias in the correlation respectively.

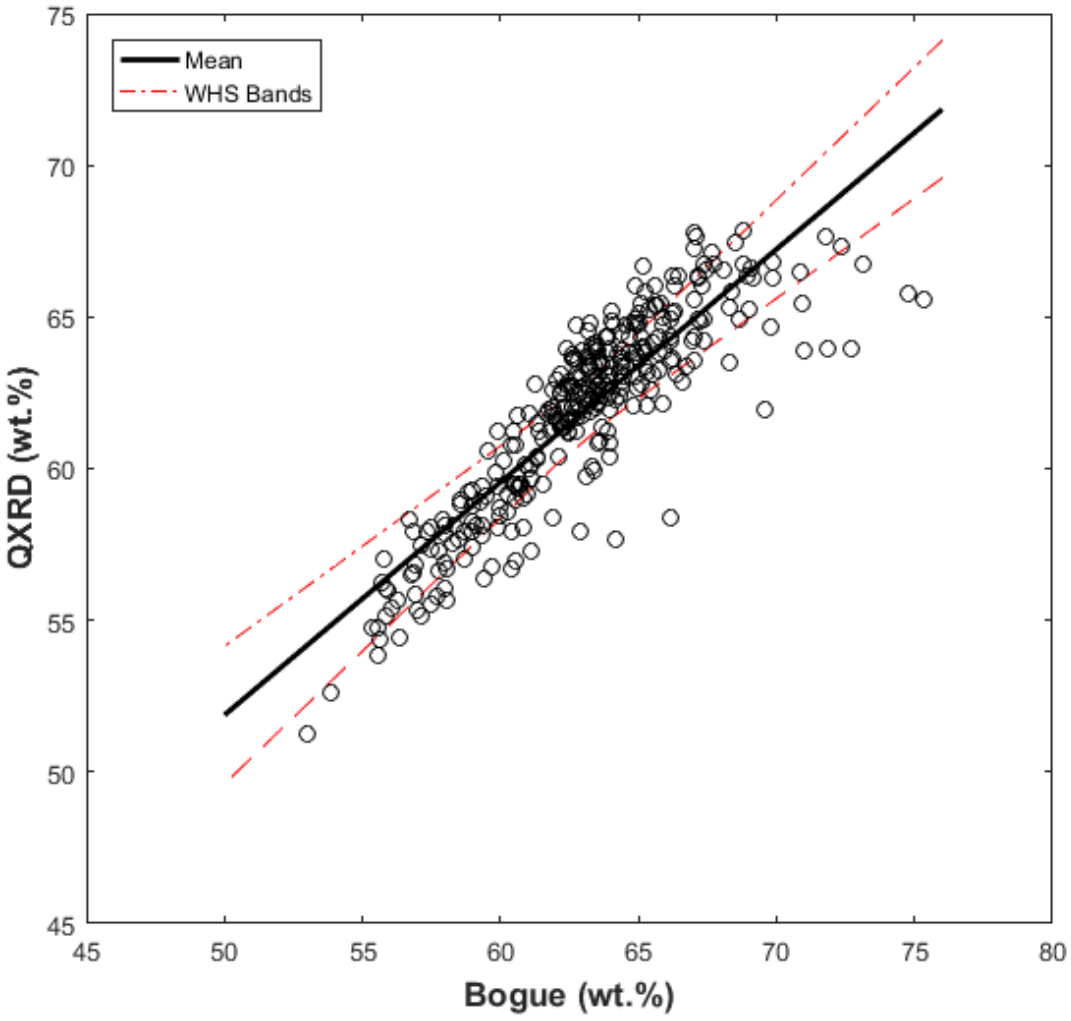

Fig. 18. Plot of the C3S Bogue to QXRD correlation of 320 cements with WHS limits

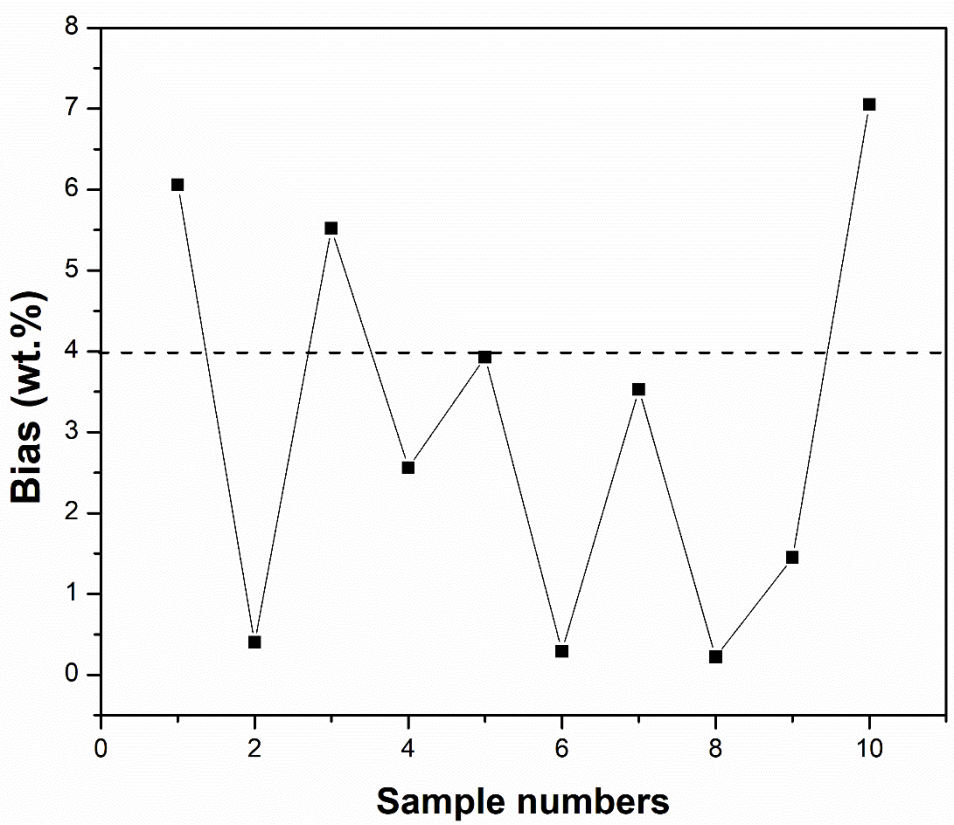

Fig. 19. Bias estimates of C3S Bogue to QXRD correlation (acceptance range for the relationship was fixed at ±4 wt.%)

The special relationships (C3S + 4.75.C3A) and (C4AF+2.C3A) were calibrated next where the Bogue quantification specification should be closer to 100 and 25 respectively. These combinations are used as practical markers for heat of hydration and sulfate resistance phase quantity limits, respectively. Detection of the corresponding QXRD phase limits was performed to understand these long-standing relationships from a QXRD perspective. **Figs. 20 and 21** are illustrations of special correlations elucidated in ASTM C150.

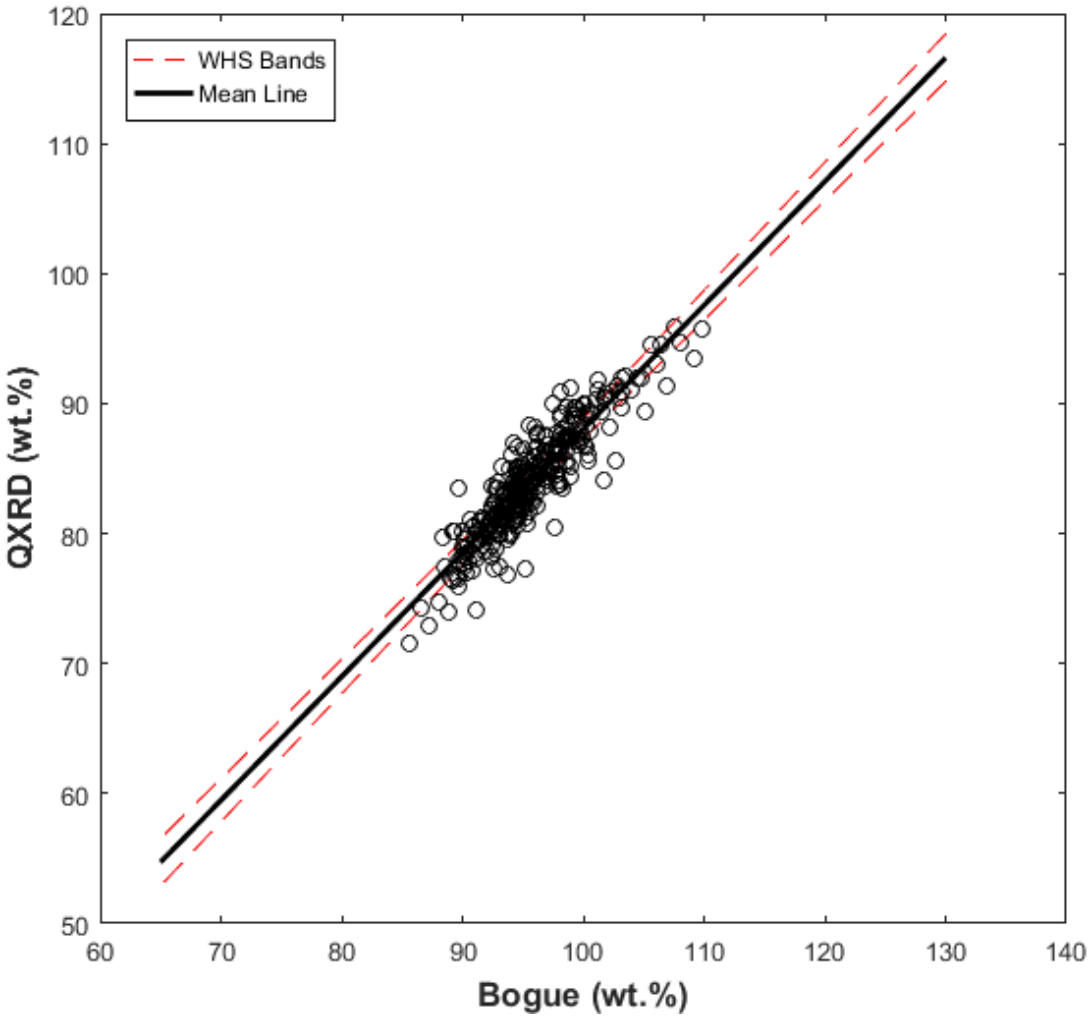

Fig. 20. Plot of C3S + 4.75.C3A correlation

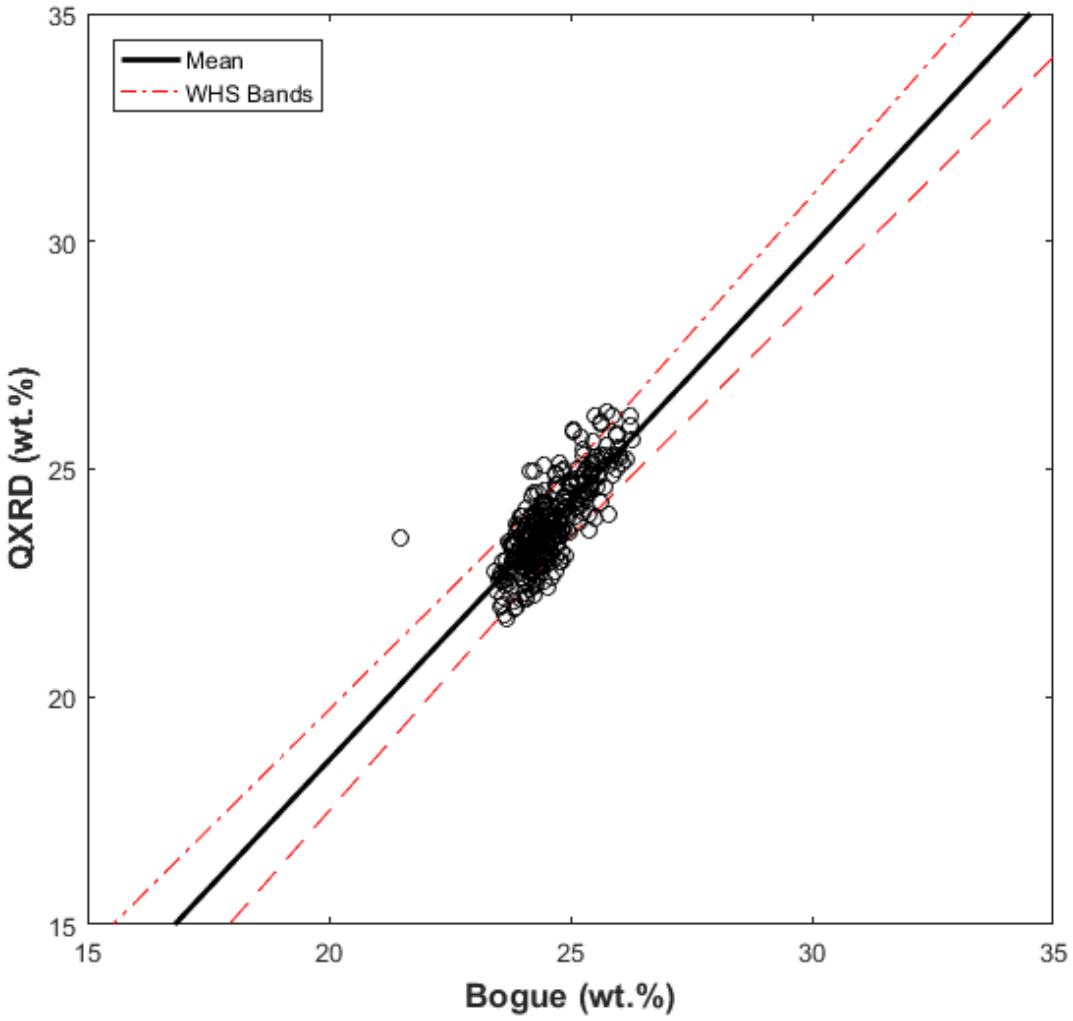

Fig. 21. Plot of C4AF + 2.C3A correlation

4.1.4. Specification limits and discussion

The correlation technique was then applied to obtain the QXRD phase specification limits, and resulted in the following estimates as in **Table 3**. This extrapolation was performed on the Bogue method specific ASTM C150 specifications limits. In general, the Bogue quantification overestimates phases at lower quantities (example, aluminate) and underestimates phases at higher quantities (example, alite) relative to direct determination methods. The same pattern was observed

here in alite and aluminate correlations which are significant in affecting the performance of the cement.

Table 3. QXRD specification ranges for the important phases in cement

Phase	Significant cement type	ASTM C150 limits (max. Bogue wt.%)	QXRD estimations (wt.%)		
			Lower limit	Mean	Upper limit
Alite	Type IV	35	33.4	40.3	45.3
Belite	Type IV	40	28.6	37.3	53
Aluminate	Type II	8	5.1	6	6.9
	Type III	15	12.5	14.4	16.3
	Type IV	7	4	4.8	5.5
	Type V	5	1.7	2.4	3.2
C3S + (4.75 x C3A)	Type II	100	87.5	88	88.6
C4AF + (2 x C3A)	Type IV	25	23.3	24.3	25.2
Aluminate	Type III	8	5.1	6	6.9
	Type III	5	1.6	2.4	3.2

Stutzman [144] designed a similar table for the Bogue to QXRD conversion through statistical processing. Comparison of the tables illustrates that the limits of the QXRD estimations are wider in the current estimations than the one from literature. The mean estimated QXRD from that of the literature data widened by an additional 1.3 wt.% from the mean estimated QXRD of the calculated dataset (**Fig. 17**). Adding the deviation caused by the retention of the Bogue errors into the correlation further increases the divergence of the literature dataset from the given Bogue quantification. The following points need to be considered to fully understand the divergence reduction by the current model.

The volume of the dataset considered in this study was thrice the compatriot volume considered by the literature model. In standard linear regression, increasing the volume of data tends to increase the accuracy of predictions.

The divergence of the dataset considered by the literature model was wider since it incorporated Bogue and QXRD data collected over several decades (1960-2006) from various sources around the world. The quantification wasn't adjusted for technological advancements to the oxide quantification by XRF, which can now determine oxide compositions to an accuracy of ±0.2 wt.%. Moreover, the considered QXRD data was sourced from different quantification methods namely, single-peak fitting, internal standard method, RIR method, and Rietveld refinement.

The data considered in this study was gleaned from a cement lab that utilized the same XRD and XRF instruments, following the same methodologies, to generate the data. This lack of variation in quantification methodology makes the QXRD estimation more stable and consequentially more reliable. Although the current dataset may not incorporate machine-to-

machine variability between instruments, such differences are minor and the upper and lower limits are sufficiently large to integrate them into the estimation.

4.2. Supplementary enhancements to QXRD-based protocols

4.2.1. Blended cements

4.2.1.1. Caveats in QXRD amorphous quantification

The detection and quantification of amorphous phase by QXRD requires the usage of the internal or external standard techniques. Both techniques are proven to be labor-intensive and have well-known drawbacks. While the internal standard method has a problem with the achievement of homogeneity of the standard material with the cement, the external standard method suffers from X-ray absorption differences between the standard material and cement leading to quantification errors. Westphal et al. [148] identified that for accurate quantification, a properly homogenous internal standard-cement mixture at a ratio of 1:1 is required. Jansen et al. [149] recognized the shortcomings of both standard methods and came up with a remastered external standard method modified from Suhermann et al. [150]. Jansen and co-workers [149, 151] generated the linear absorption coefficients of the cement phases and the standard material phase separately and derived a special relation called as the G-factor. The G-factor is a manifestation of the ZMV method [152] of external standard analysis that is popularly practiced in cement chemistry investigations using QXRD. The G-factor method requires the calibration of the absorption coefficients only once to get the approximate amorphous phase fraction.

The equation for calculating the internal standard phase composition is given by,

$$W_\alpha = \frac{S_\alpha (ZMV)_\alpha}{\sum_{j=1}^{n} S_j (ZMV)_j} \qquad \rightarrow \qquad Eq.(6)$$

Where, S_α = the Rietveld scale factor for phase α,

ZM = the mass of the unit cell contents,

V = the volume of the unit cell,

n = the number of phases in the analysis

Eq. (7) provides the equation for calculating the phase constituent of the external standard using the G-factor calibration,

$$W_\alpha = \frac{S_\alpha (ZMV)_\alpha \mu_m^*}{G} \qquad \rightarrow \qquad Eq.(7)$$

Where, μ_m^* = the mass absorption coefficient of the entire sample, and

G = normalization constant used to calculate the relative weight fraction of the amorphous phase

A recent idea to directly quantify the amorphous phase fraction in blended cements is the PONCKs (Partially or No Known Crystalline structures) or pseudo-phase characterization [40, 152-154]. This technique records information about the mass, volume, and atomic number (ZMV) values of the commonly seen fly ash/slag amorphous phase and stores them into a pseudo crystal structure, called a PONCKs phase. The PONCKs amorphous phase can be refined similar to a crystalline phase to obtain the amorphous weight fraction.

Stetsko in 2016 [155] compared the internal, external, and PONCKs techniques and observed little variation between their amorphous phase fractions. However, there lies a caveat in the PONCKs method with the creation of a proper amorphous pseudo-phase. The composition of the fly ashes and slags produced in the United States vary considerably, and no single ASTM standard classifies the fly ashes or slags based on their chemical nature/mineralogical contents. Hence, the application of a single pseudo-phase for an amorphous fly ash or slag cannot be

generalized over all fly ashes or slags obtained from different sources. Thus, one needs to be cautious when investigating the QXRD-generated amorphous phase fractions and be mindful of these shortcomings.

4.2.1.2. QXRD quantification of fly ash added to blended cement

ASTM C595 specifies that fly ash addition to Type I cement should be between 20-40 wt.% replacement of cement. However, the exact quantity of fly ash addition is known only to the manufacturer. QXRD characterization of fly ash addition to Type I cement can provide an indication of the added fly ash quantity by the back-calculation of the cement and fly ash. Comparison between the determined and back-calculated fly ash can provide a relationship that can be generalized over Type I-P cements.

A source of low calcium fly ash was mixed with negligibly amorphous Portland cement at 5%, 10%, 20%, 30%, and 40% replacement ratios by weight. The phase fractions of the fly ash and the cement were pre-determined through QXRD, where a single PONCKs amorphous phase was used to characterize the amorphous component of fly ash. PONCKs technique is better than the internal standard technique in rapidly quantifying low amorphous contents. An amorphous fraction less than 20 wt.% in the cement is difficult to detect using the internal standard method, unless proper intergrinding without damaging the mineral contents is performed, which is a labor-intensive and low efficiency method [148, 149, 151].

Comparison of the QXRD characterization of the added fly ash composition and the back-calculated fly ash composition yielded very good convergence. The back-calculated fly ash phase fractions were generated by multiplying the original phase fractions in cement and fly ash by their respective replacement ratios. Some of the observations that were made include,

(1) Variation from stoichiometry is least at commercial fly ash addition ranges (20-30 wt.%).

(2) Back-calculation of fly ash was performed using individual QXRD phase contents of fly ash and cement before mixing. This is the reason why the back-calculated estimates aren't equal to stoichiometric fly ash addition.

(3) Amorphous fly ash phase was measurable by QXRD only when the amorphous composition was >5 wt.% and closer to 10 wt.%.

Table 4. Comparison of the added fly ash quantity against the fly ash quantity from QXRD

FLY ASH QUANTITY		
Replacement Levels	QXRD	Back-calculated FA
5	8.86	8.09
10	9.76	10.2
20	20.2	25.27
30	29.27	34.61
40	36.12	43.95
Std. error of estimate (%) =	16.43	6.98

Table 4 illustrates a direct comparison of QXRD versus stoichiometric quantification of fly ash added to cement. A standard uncertainty of ±3 wt.% is added to fly ash QXRD

determinations to account for the approximation contributed by the amorphous phase quantification techniques. The standard errors of estimate signify the errors contributed by the analysis only between two techniques that arrive at the same results [145]. The results suggest that QXRD determination of added fly ash suffers at additions less than 10 wt.% and greater than 40wt.%. However, the determinations are extremely reliable in the mid-range and are better than calculated estimates. This points to the non-linearity of the distributed phase determination by QXRD. **Fig. 22** represents the backcalulation of added fly ash quantity from QXRD.

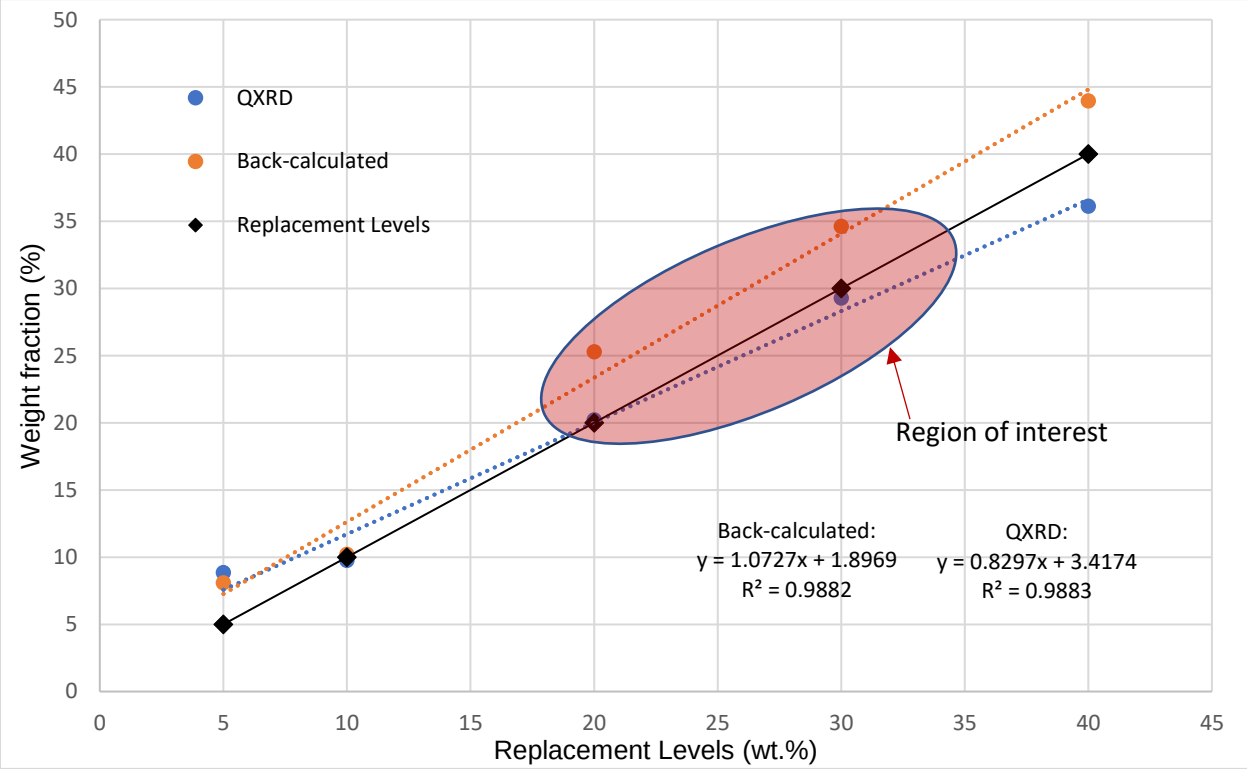

Fig. 22. Comparison between the added fly ash determinations at different replacement ratios generated from QXRD and back-calculation from the original fly ash and cement QXRD phase quantification

4.2.2. Isothermal Calorimetry

The importance of the anhydrite polymorphic presence in cement isn't yet given due deliberation by all industries. The reason behind this fallacy is that the full extent of the reactivity differences between anhydrite and gypsum in cement is not pronounced on cement manufacturers. Following cement hydration through isothermal calorimetry can provide a clear picture. However, cement companies are increasingly in favor of using the ASTM C563 specification to decide on the calcium sulfate addition rather than isothermal calorimetry. The following information can provide some clarity on the usefulness of isothermal calorimetry in differentiating between low reactive anhydrite-based calcium sulfate versus highly reactive gypsum-based calcium sulfate in cement.

Cement hydration can be followed as a five-staged pattern from isothermal calorimetry. The first two stages correspond to the initial heat of dissolution, followed by a dormant period where no reaction occurs. After 2 hours, the hydration of C3S proceeds with the formation of CSH (calcium silicate hydrate) and CH (calcium hydroxide/Portlandite) phases. This is followed by the onset of a sulfate depletion point where all sulfates are consumed to form ettringite at around 10 hours. If any residual aluminate is present, the C3A reacts back with the ettringite converting it into monosulfate or calcium sulfoaluminate. This is followed by a rate of gradual hydration in the last stage (deceleration stage). Within an almost constant particle size distribution, the presence of anhydrite can be detected by the absence of a sulfate depletion point during the third stage of cement hydration [107] whereas with the hemihydrate the sulfate depletion is accelerated [13].

An isothermal calorimeter contains sample and reference cells placed in an isothermal bath. The heat produced by the reaction in the sample cell is logged as a difference in power required to maintain the isothermal condition. Usual reference materials have an inert characteristic and must

have a heat capacity similar to the analyte. Common reference material for cement analysis is sand or quartz (heat capacity approximately 0.75 kJ/(kg.K)). The Omnical SuperCRC micro-calorimeter was first calibrated for evaluating the baseline drift based on ASTM C1702. The calibration coefficient and base heat flow of the calorimeter were derived using KCl thermal standard.

4.2.2.1. Effect of sulfate polymorphs

A mixture of clinkers, with known mineralogy (Table 8), was mixed individually at a ratio of 0.95 clinker to 0.05 gypsum or anhydrite. The sample and reference cells were filled with 4.18 ± 0.5 wt.% of the prepared cement and 2.85 ± 0.5 wt.% of sand (Specific heat = 0.75 J/K) respectively. The method B in ASTM C1702 was followed to record the hydration behavior. Water addition to the cement (ratio of water:cement = 0.5:1) was performed with the help of syringes after making sure that heat flow between both cells was minimal. The experiment was logged for 72 hours at a step of 0.3s per recording. The difference between the anhydrite cement and gypsum cement can be apparent from the following figures (**Figs. 23 and 24**).

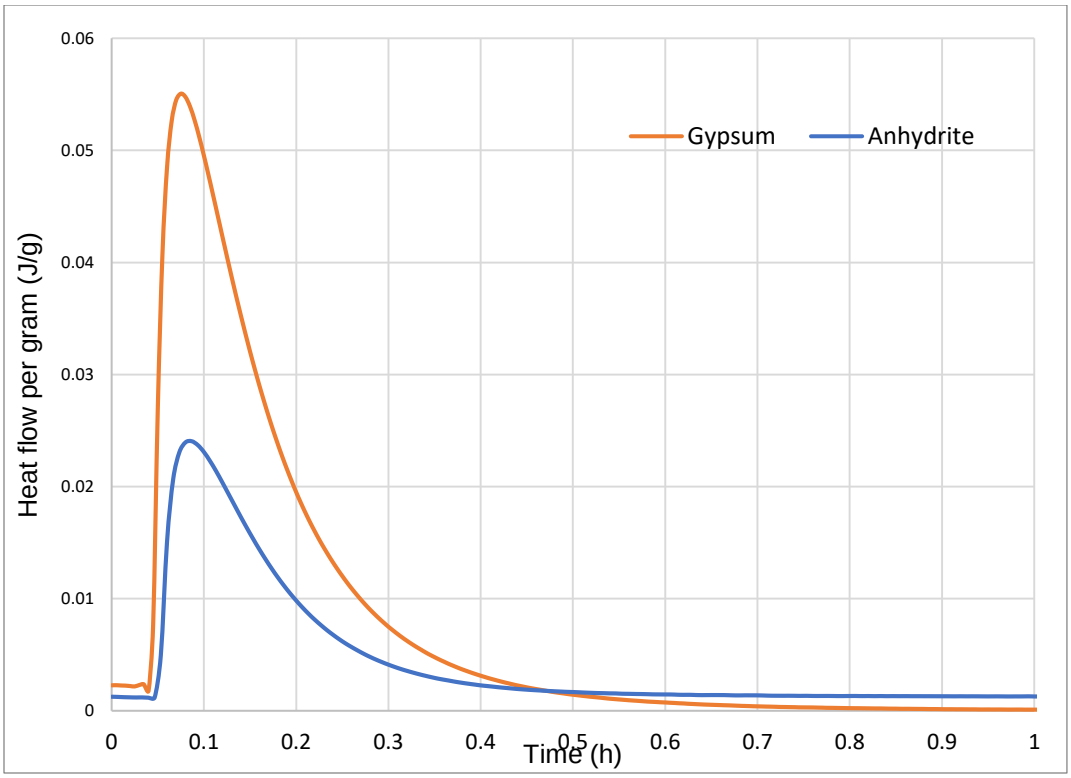

Fig. 23. Initial heat of hydration peak of clinker with gypsum and anhydrite

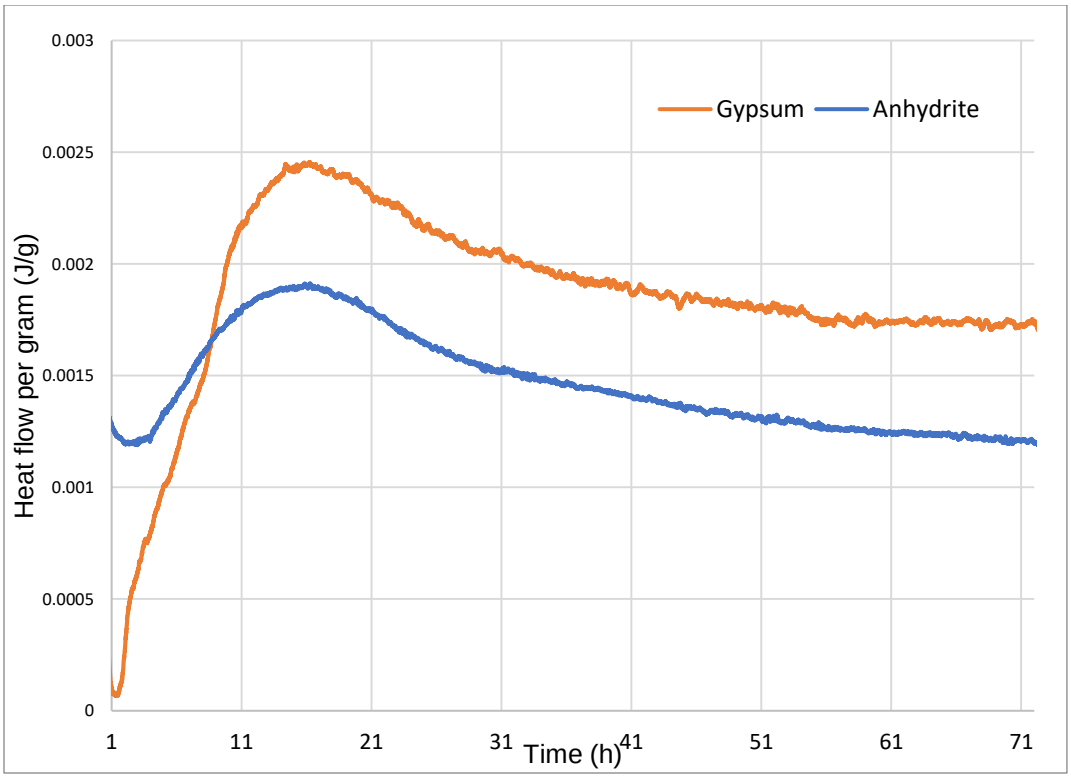

Fig. 24. Hydration peak of clinker with gypsum and anhydrite respectively

The amount of heat produced in the first stage of the gypsum reaction with clinker was greater than the same produced by the anhydrite reaction. Due to anhydrite's lower solubility, the gypsum contains more readily dissolvable sulfate ions than the anhydrite. The ions are released immediately on dissolution which produces a higher first peak than the anhydrite [109].

Moreover, the observed total hydration heat produced due to gypsum reaction was higher than the anhydrite reaction. Since the cubic-C3A particles are suspended in a sulfate-ion rich solution, their reactivity is lower than ideal [13]. Anhydrite does not dissolve as readily as gypsum which can leads to slow formation of longer needles of ettringite [105]. This reaction proceeds slowly and merges along with the CH and CSH formation reactions. Hence, the delayed conversion to monosulfate in anhydrite is a function of both the C3A polymorphic form as well as the calcium sulfate form.

Winnefeld [107] observed that some anhydrite remains in the solution even after 3 full days of hydration. It was also suggested that the heat of hydration of anhydrite-containing cement will be greater than 4-6 times the similar parameter with a gypsum-based cement depending on the anhydrite to gypsum ratio. In this work, the heat of hydration of clinker with pure gypsum was almost 25 times greater than the heat of hydration of clinker with pure anhydrite at working substitution levels for the same time.

The experiment reveals that the presence of calcium sulfate as anhydrite will result in hydration delay as explained in the above discussion. An illustration of this effect is represented by **Fig. 24.**

4.2.3 Thermogravimetric Analysis

Four cements with varying calcite fractions, calculated from QXRD, from 1 to 12.5 wt.% were analyzed from 400 to 1000°C. The amount of TGA calcium carbonate can be calculated by quantifying the gradual weight loss due to CO_2 expulsion from 500 to 900 °C. The CO_2 loss is converted to the amount of calcite lost (in mg) by multiplying with the molecular weight of calcite. Now the TGA calcite wt.% can be calculated based on the original quantity of sample (about 30mg) (for instance, **Table 5**).

Table 5. Calcite quantification from TGA analyses and compared against QXRD

Samples	TGA	SD	QXRD	1σ Uncertainty
Sample 1 - IL cement	7.95	±1.2	7.3	±0.8
Sample 2 - Type I cement	4	±0.6	3.8	±0.2
Sample 3 - IL cement	9.89	±1.5	12.5	±1
Sample 4 - Type I cement	6.94	±1	0.4	±0.3

From the graph (**Fig. 25**), we can see that the TGA and QXRD quantification are highly comparable considering the uncertainties of the QXRD and the TGA. A similar effect can be gauged from the correlation between QXRD and TGA after removing the outlier Sample 4. Since the calcite percentage in cement is not constrained by any limitation (except cost), the QXRD can be considered to be quite an accurate mode of quantifying calcite content in cement. However, the uncertainty of QXRD is a significant factor which can vary from 0-5 wt.% depending on the cement type and additive calcite quantity [156].

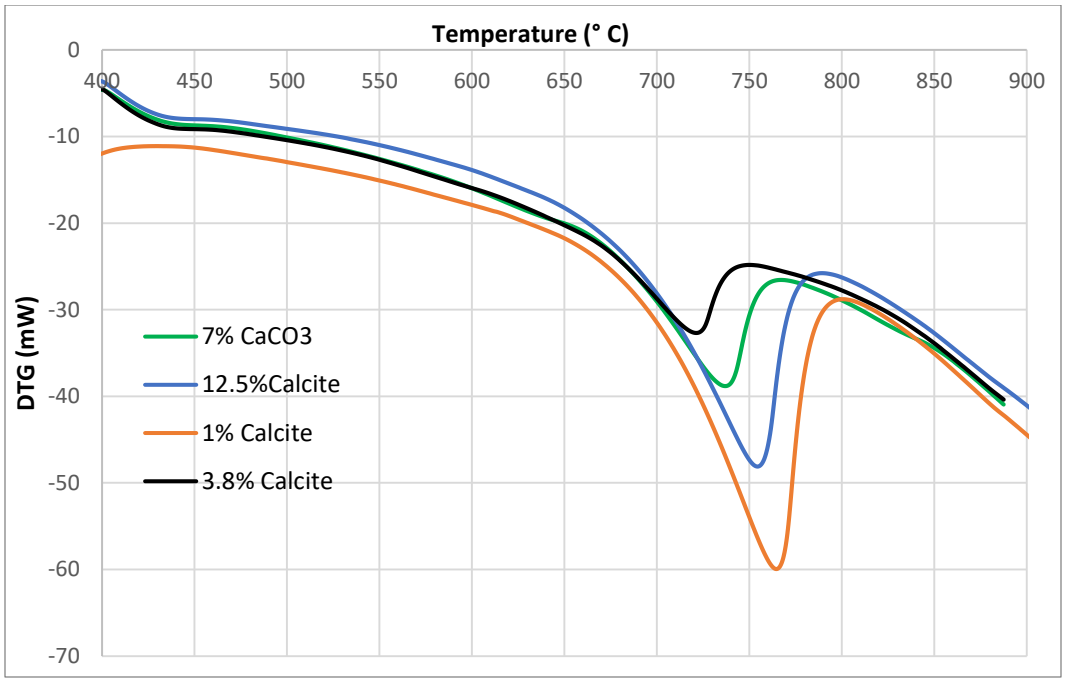

Fig. 25. Representations of the calcite quantities by the TGA peak profile

5. EXPERIMENTAL INVESTIGATIONS

5.1. Stage I: Experiment to improve QXRD precision

The XRD experiment to improve precision involves the utilization of a consistent sample format, such as a pellet, that was extracted from hydraulic pressing. Identification of the optimum pressure and sample quantity was processed by fixing the height of the final specimen and limiting the preferred orientation whenever possible. Several pellet iterations with differences in applied pressure, dwell time, and sample quantity were evaluated before the exact parameters were narrowed down. Other factors related to XRD measurement (such as scan time, scan range, refinement parameters, etc.) were embellished by deciding on the quality of the XRD pattern. Depending on the extent of preferred orientation, the demand for the preferred orientation correction shall be ascertained. The alite phase in the pellet is supposed to present an increased preferred orientation, which can be corrected using the March-Dollase orientation correction and correlated with the accurate alite quantification through microscopy.

5.1.1. Preparation of pellets

Cement pellets were made by pressing the specimen to an optimized pressure of 280 MPa, with a dwell time of 15 seconds. No grinding was performed on the commercial cements and the pellets were pressed without the use of a binder. The pelletization methodology was identical for both the clinker powder and the cement, with the bulk clinker ground to around 30 μm (passing through 400 mesh and retained on 625 mesh US sieve). The particle sizes of the cements were around 15-20 μm. The clinker was obtained from Lehigh Hanson cement plant in Union Bridge, Maryland, and was of the Type I/II variety. The cement samples were provided by the Texas Department of Transportation (TxDOT), and comprised of the most common North-American cement types (Type I/II, III, II/V, and IL). X-ray diffraction measurements were performed on a

Bruker D2 instrument operating at 30kV and 10mA (300W), a Bruker D8 instrument operating at 40kV and 25 mA (1000W), and a PANalytical X'Pert MPD operating at 40kV and 40mA (1600W).

In the Bruker instruments (D2 and D8), the bulk powder samples were loaded onto a 51.5mm diameter PMMA holder with a height of 8.5mm, and a specimen well diameter of 25mm. In the PANalytical instrument (MPD), a similar loading scheme was followed except that the specimen well diameter was around 30mm. However, for the pellets a customized loading technique was followed. In the D2 and D8, the pellet was held tightly in a backloading holder and then height adjusted by pressing the underlying PMMA backing till the pellet was flat with the holder surface. Since the diameter of the pellet (24.5 mm) was equivalent to the well diameter (25 mm), movement of the pellet inside the well was precluded. This movement can cause unwanted signals arising from the empty space in the well to be detected. In the MPD, the pellet was rigidly clamped in the backloading holder and was held without movement.

5.1.2. Cumulative QXRD protocols

The following section comprises the pertinent QXRD protocols that are to be satisfied for an accurate and comprehensive QXRD analysis. The protocols are divided into instrumental and refinement parameters in order to delineate the measurement effects and the analysis effects. Rietveld refinement was performed using DIFFRAC.TOPAS 5.0 (Bruker) and X'Pert Highscore Plus (PANalytical) following similar refinement procedures. **Tables 6 and 7** represent the common instrumental and Rietveld refinement protocols respectively.

5.1.2.1. Instrument parameters

Table 6. Instrumental settings necessary for a good X-ray diffraction pattern generation

Settings	Bruker D2	Bruker D8	PANalytical MPD
Current (mA)	10	25	40
Voltage (kV)	30	40	45
Power (W)	300	1000	1600
Detector Assembly	LynxEye Position Sensitive Detector (PSD)		X'Celerator PSD
Bragg-Brentano geometry	Y-goniometer	θ-2θ	θ-2θ
Source to Detector length (mm)	282	560	560
Soller slits (°)	4	2.5	2.3
Divergence slit (mm)	0.6 (Fixed)	0.3 (Fixed)	1 (Variable)
Anti-air scattering (AAS) module (mm)	2	3	No AAS
PSD opening width (°)	5.8	3	2.2
Scan Range	7 to 70° 2θ		
Step size	0.02° 2θ	0.018° 2θ	0.015° 2θ
Scan time (minutes)	20	20	20
Spin rate (rpm)	15	15	15

5.1.2.2. Refinement parameters

Table 7. Rietveld refinement protocols to be followed for a physically reasonable analysis

	TOPAS 5.0 (and later versions)	**HighScore Plus 4.5 (and later versions)**
1	Chebyshev background function (3^{rd} order), refinement of (1/X) function for blended cements	Chebyshev background function (3^{rd} order), refinement of (1/X) function for blended cements
2	Specimen displacement (mm): refinement limits at ±0.5	Zero position error or specimen displacement: refine any one of the two
3	Lorentz - Polarization factor: set at 0	Fix or uncheck all other parameters. Refine only the background function till a good fit is obtained (increase the polynomials for fit improvement). Fix the fitted background and if used, the (1/X) function.
4	Absorption correction (1/cm): refine between 95 and 105 (optimal value for cement is around 100)	Now refine all lattice parameters (a, b, c), unit cell angles, and other structure parameters. Refinement limits: same as TOPAS.
5	Lattice parameters: refinement limits at ±0.1	Peak shape function: Fix the Pseudo-Voight (PV) mixing parameter, η at 0.6 or refine it if better fitting is desired.

(Table 7 Continued)

	TOPAS 5.0 (and later versions)	**HighScore Plus 4.5 (and later versions)**
6	Unit cell angles (α, β, γ): refinement limits at ±1°	Cagliotti parameters: select u, w, and u; for Pawley or LeBail fitting of amorphous hump in blended cements select PV components $\eta_1 + \eta_2\,(2\theta) + \eta_3\,(2\theta)^2$.
7	Scale factor: refinement without limits	Simultaneously refine the lattice parameter a and peak shape parameter w.
8	Crystallite size L (nm): refinement limits at 50 to 1000 nm	Refine v along with a and w. Perform similar additive refinements with u, and if necessary η_1, η_2 and η_3.
9	Atomic positions and displacement parameters: no refinement	Scale factor, crystallite size, preferred orientation: Refinement limits similar to TOPAS
10	Preferred orientation (March-Dollase correction): refinement for alite, gypsum, anhydrite, calcite, dolomite, and portlandite between 0.5 to 1	
	Refinement format: Fundamental Parameters (automatically selected in TOPAS), refines all parameters together	Refinement format: Hierarchical. Step-by-step refinement is followed, if not results will differ.
Start Refinement		
	No. of cycles for a good fit: 1-2 cycles	No. of steps for a good fit: 20-30 steps

5.1.3. Precision enhancement

A recent analysis of a set of anhydrous cements was carried out by 29 different labs around the world to calculate the precision and bias of the QXRD method **[63]**. However, the successful evaluation of both the precision and bias of the results was based on the assumption that the resulting consensus means would be almost equal to the actual cement composition. The proficiency test served a good purpose to designate the consistency (precision) of QXRD protocols to within a select range (example, ±3 wt.% for alite). But the test shall be fully effective only if the actual phase composition of the cement or clinker is known, for accuracy evaluation of the consensus means. Moreover, a degree of freedom was provided to the sample preparation stage where the sample preparation protocols of the different labs weren't restricted or stabilized.

Here, the QXRD precision was evaluated after making the clinker sample preparation consistent across all instrumentation. The improved precision is apparent from the restriction of the quantification variability to within ±1 wt.% for alite. During pelletization, the alite crystallites can get oriented preferentially and this can cause a slight overestimation in its quantification. Apart from the alite overestimation and corresponding belite underestimation, a slight ferrite underestimation due to absorption contrast effect was the only other anomaly observed from pellet quantification. The mass absorption coefficient of ferrite is very high compared to the other cement phases, which leads to an increased X-ray absorption by the ferrite relatively. The total quantity of sample used for making the pellet (4g) is several times higher than the powder (0.5g). A combination of these two effects lead to an increased X-ray absorption behavior by the ferrite phase in the pellet than the powder, and hence the corresponding underestimation. The repeatability and reproducibility of powder and pellet QXRD is represented in **Fig. 26**.

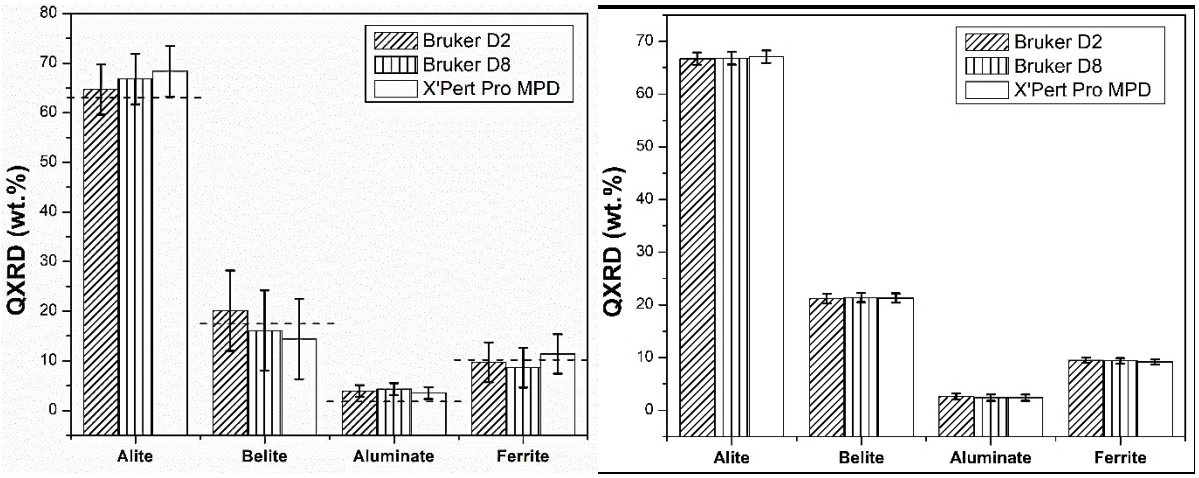

Fig. 26. Comparison between powder (left) and pellet (right) quantification for the major clinker phases across instrumentation. The powder sample utilized here was the NIST SRM 2686a and for the pellet a Type I clinker was used. The dotted lines on the left image indicate the NIST reference values.

Notwithstanding the aforementioned effects, the precision of pellet QXRD was significantly improved from powder QXRD. This observation was extended to cement by the rigorous testing of 9 commercial cement pellets, with varying mineralogy, representing different ASTM C150 cement types. QXRD results of the major cement phases illustrated the overwhelming improvement to the precision in all 9 cements. **Fig. 27** denotes the precision sacrificed during the performance of powder QXRD by comparing the quantification of the powder and the pellet in two different instruments (Bruker D2 Phaser and D8 Advance). The instruments differed heavily in their peak resolution characterization and in the operating power and were at wide variance in the quality of the produced pattern. The precision error (%) is an index of the deviation of the results when the same protocol is reproduced in cements of varying composition in both the instruments. It was calculated by multiplying the %standard deviation of the

quantification performed in different machines by 2.8, as per ASTM E177. **Fig. 28** illustrates the improved precision through pellet QXRD against other methods.

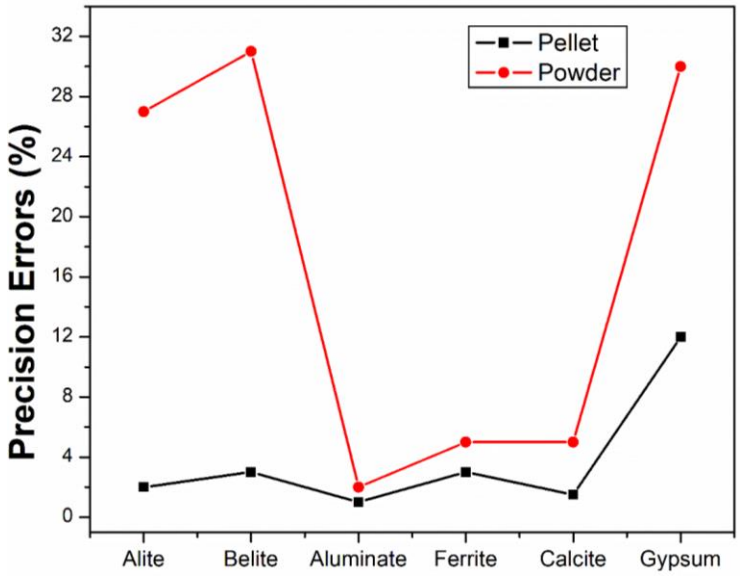

Fig. 27. Plot showing cumulative precision errors in different cement phases in the 9 cements between pellet and powder

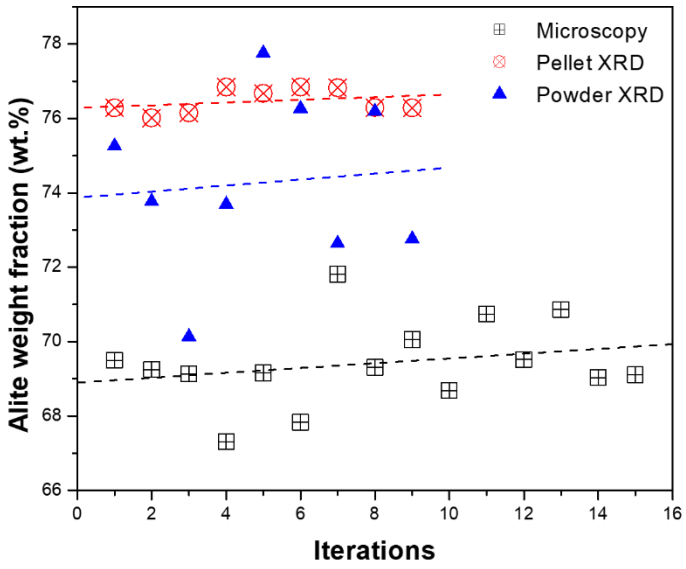

Fig. 28. Graph showcasing the precision and accuracy differences of all the investigated quantification techniques for the alite phase in the Type I/II clinker.

It can be seen from Fig. 28 that pellet XRD generates the most precise results in the clinker between all techniques. The effect of preferred orientation is evident in the alite overestimation after pelletization, and in a few powder samples. The dotted lines represent linear regression curves which reveal the difference in precision between the methods as a function of their increasing slopes (Slopes of, pellet XRD = 0.06, powder XRD = 0.4, microscopy = 0.15). Lower the slope, better the precision.

5.2. Stage II: Experiment to calibrate pellet QXRD accuracy

5.2.1. Powder and Pellet QXRD

Four clinker nodules of varying phase proportions were obtained from a Lehigh Hanson cement plant in Maryland. The clinker nodules were fine ground to size fractions around 30 µm initially for QXRD analysis. After initial size reduction, the clinker powders were pelletized and analyzed using X-ray diffraction at conditions explained previously.

For the analysis of the powder QXRD, the clinker powders at 30 µm were micronized with ethanol. The common practice is to add 5 mL of ethanol per gram of the clinker to minimize heat and maximize powder mobility. Micronizing was performed for 5 minutes after which the 30 µm average-sized clinker particles were reduced to below 10 µm. The wet, finely-divided clinker powders were dried in an oven at 60 °C for 2 hours to completely remove the ethanol. The dried clinker powders can be broken up by grinding at a very light pressure inducement using a mortar and pestle for 30 seconds. Powder QXRD of the micronized and dried clinkers was proceeded by backloading over a well-sanitized, frosted or stained surface to prevent preferred orientation. **Fig. 29** represents the increased preferred orientation in pellet QXRD and **Table 8** illustrates the powder and pellet QXRD comparison between four clinkers.

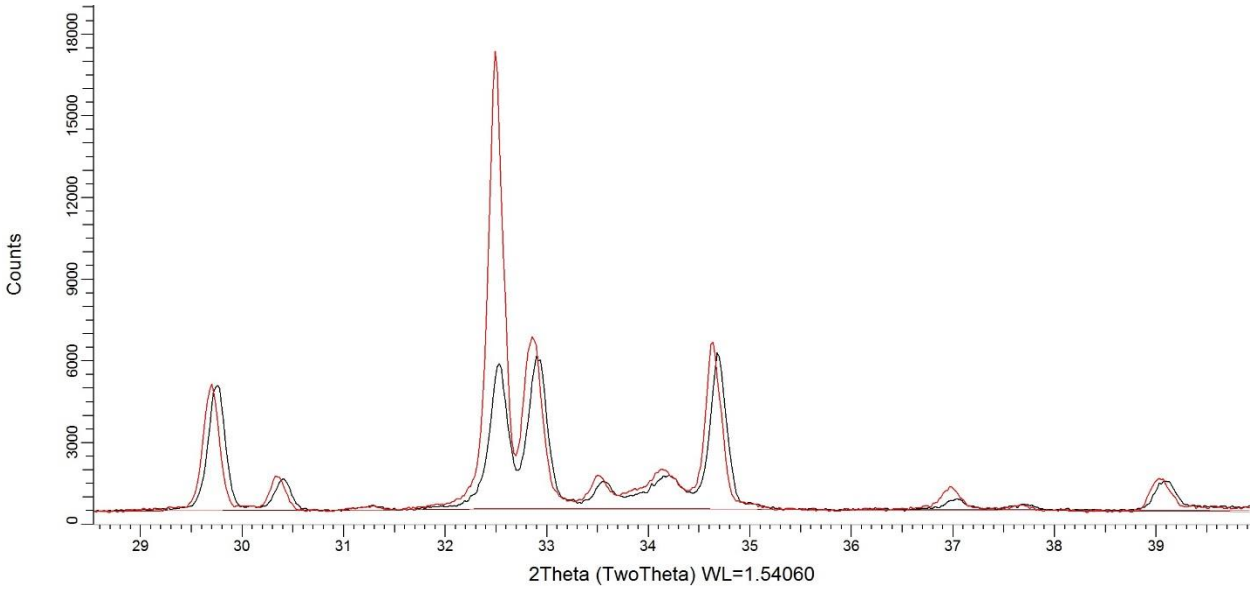

Fig. 29. XRD patterns of the powder (black) and pellet (red). The reduction in preferred orientation is clearly evident in the wet ground, backloaded powder XRD at the peak range 32-33 ° 2θ. Pellet XRD is mildly shifted to the left due to the specimen displacement effect.

Table 8. Powder and pellet QXRD of the clinkers

Phases	Clinker 1		Clinker 2		Clinker 3		Clinker 4	
	Powder	**Pellet**	**Powder**	**Pellet**	**Powder**	**Pellet**	**Powder**	**Pellet**
Alite	71.58	73.19	71.6	71.8	70.44	71.12	61.16	64.85
Belite	9.91	9.23	9.92	9.79	11.33	11.12	16.42	14.8
Interstitial	16.64	14.36	15.135	14.215	16.09	15.295	19.62	17.65

5.2.2. Optical microscopy

The clinker nodules were ground to pass through sieve numbers 40 to 60 mesh to get size fractions between 420 and 250 μm. The size fractioned clinker powders were embedded in epoxy, polished using standard petrographic techniques, and etched in HF vapor for 90 to 120 seconds. Based on the chemical contents, each clinker was subject to different etching times within the range.

The optical microscopic images of the epoxy-mounted clinkers were taken in a Zeiss Axisokop 40 under reflected light at magnifications of 100X, 200X, and 500X. Magnification was altered to generate enough image fields and the specimen was moved such that all areas along its length were captured. 8 images with 3 to 5 fields on each image (24 to 40 image fields per sample) were viewed to complete each specimen imaging. Each image was of 2722 x 2208 pixels^2 resolution with a width of 160 μm. The dimensions of the image field varied based on the location of the regions of interest.

5.2.3. Point-counting (PC)

Point-counting procedure was modified from ASTM C562 and C1356M and applied here. A grid was superimposed on each image and the observed phases were counted with the help of their etching discriminations. The grid dimensions were varied depending on the dimensions of the image field. However, a total of around 200 grid points was maintained on each field with the grid area varying between 2 mm^2 to 15 mm^2. The number of points counted on each specimen was equal to number of image fields multiplied by the number of grid points (40 x 200 = 8000 points). An examples point-counting grid on an original optical microscopic image is represented in **Fig. 30**. The number of grid points was selected based on the minimum number that is required to obtain a relative accuracy of 10%, the best prescribed precision range in ASTM C562. On average, the relative accuracy was maintained around 7 to 9% which indicates high precision. Hence, the counts were increased from a minimum of 4000 points to obtain highly representative and accurate results. A 10% standard deviation should be applied for the results from **Table 9**.

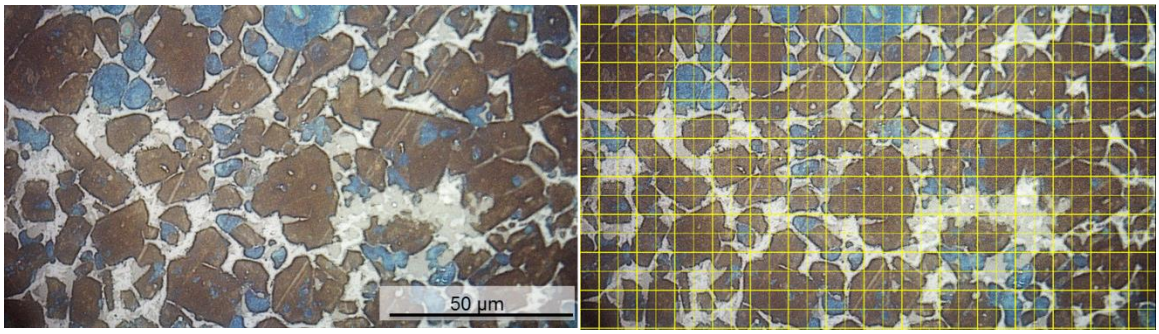

Fig. 30. (Left) Polished, etched clinker with the respective phases, alite (brown), belite (blue), aluminate (light gray), ferrite (white). (Right) Illustration of the grid used for point-counting

Table 9. Point-counting results of the important cement phases from the four clinker samples

Phases	Clinker 1	Clinker 2	Clinker 3	Clinker 4
Alite	72.06	72	70.43	61.6
Belite	11.24	12.3	12.17	18.50
Interstitial	16.7	15.6	17.393	20

5.2.4. Scanning electron microscopy

Similar clinker polished sections, without etching, of the same samples prepared for optical microscopy were prepared for scanning electron microscopic analysis. Carbon coating of the polished section specimens was performed prior to SEM imaging. An FEI Quanta 600 instrument operating at 15 kV and at a working distance of around 12 mm was used to image the specimens in high vaccum. Backscattered electron imaging distinguished the major cement phases based on their gray levels along with the distinction of periclase and epoxy-filled voids. The area of focus or the spot size of the electron beam was maintained at 4 units (2.6 nm^2). The total image acquisition time of an image (one frame) with 2048 x 1887 $pixels^2$ resolution was 1 minute and 20 seconds.

EDS analysis was carried out to obtain images for X-ray microanalysis. The current and voltage were maintained constant while minor adjustments were made to the working distance and spot size to get a large count rate on the detector. Typical count rate values circled around 4500 cps (counts per second) as input counts to yield 4000 cps as output counts. The field width of an

EDS mapped image was 256 µm and the dwell time of the X-ray beam on a single pixel was 16.7 ms. The time taken to complete one frame (cycle) of mapping was varied depending on the number of counts obtainable in different specimens. However, the total mapping time was extended till around 150-200 frames were performed on each sample.

5.2.5. Multispectral image analysis (MSIA)

The image analysis was proceeded by following a series of steps till a clear distinction between all the concerned phases were obtained. The alite and belite can be differentiated based on the Ca and Si ratios from the EDS spectra collected after a period of 45 minutes to 1 hour for different samples. Corresponding Al and Fe maps from the EDS spectra at different points distinguish between the aluminate and ferrite phases. The Fe mapped image also displays locations of ferrite concentration albeit with a minor overlap illustrating the aluminate phase locations. Periclase and voids are both low electron absorption mediums, which makes their grey levels very close together. The quality of the BSE image is highly significant as the grey level contrast between periclase (dark gray) and voids (black) can be directly apparent from the BSE image. Nevertheless, proper spatial distribution of the periclase can be obtained from the Mg elemental map.

The following steps describe the process from processing the raw BSE image towards obtaining a phase segmented image with colored phase distinctions.

1. The elementally mapped images from the EDS should be background subtracted to delineate the actual elemental occurrence from the continuous background. In ImageJ, use Process>Math>Subtract and enter a value from 0-256 depending on the strength of the continuous background. Care should be taken to ensure that the representations of low concentration elements (characterized by low brightness) do not vanish from the mapped

images after background subtraction. The background gray level is not a highly sensitive part of the process and can be neglected altogether for images that display excellent phase distinction and image clarity.

2. Edge discrimination is significant for quantification since the edges control the end of phase quantification for a single crystal. Use Process>Filters>Median Blur and adjust the blurring range to get clear phase distinctions without any discontinuities on the crystals. Although pseudo-coloring or false coloring using an image analysis software (such as ImageJ) can be used to improve the phase distinctions, it wasn't resorted to in this case to preserve the originality of the mapped colorations as much as possible. The EDS images are sharpened using Process>Sharpen for better edge contrast to obtain enhanced EDS maps.
3. Now, the raw BSE image is converted to a processed image using Process>Enhance Contrast. The value of the saturated pixel radius is adjusted till the best contrast is identified. The "Equalize Histogram" option should be checked only for the first contrast adjustment while for the ensuing adjustments it can be left unchecked.
4. Adjust the scale of all the images till they are match exactly. It is better to keep the scale of the EDS mapped images as the scale for the BSE image. All images are converted to grayscale from RGB in steps from 16-bit to 8-bit.
5. Now, the enhanced EDS images are superimposed on the processed BSE image through the Color Merge operation in ImageJ. Use Process>Color>Merge Channels in the order BSE image (red), Al map (blue), and Mg map (green). Sometimes, the Fe map would need to be included as a secondary color when the aluminate phase could not be distinguished. Detection of aluminate phase from the matrix is difficult from a cursory look at the BSE image, as is the case with the belite phase. The background subtracted Al mapped image, in combination with

the BSE image can help illustrate the Al-rich locations in the BSE image. The final image should look similar to the one on the right in **Fig. 31** and the composite image in **Fig. 32**.

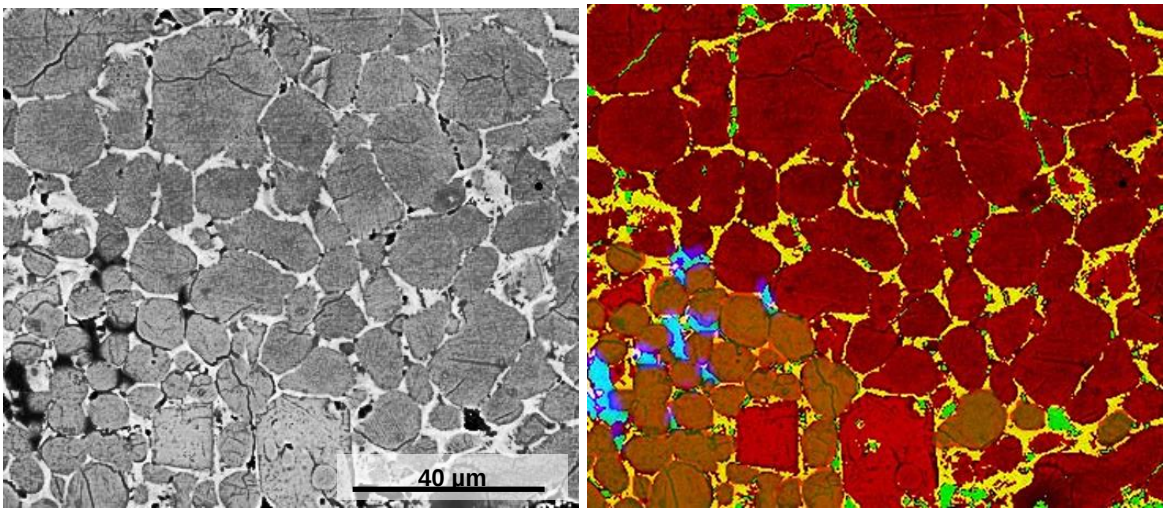

Fig. 31. Composite image delineating all phases with alite (dark red), belite (brown), aluminate (pink), ferrite (yellow), periclase (blue), and voids (green) from a BSE image (red) + Al map (blue) + Mg map (green) combination. Phases were automatically assigned based on the order of the image combinations. Field width is 256 µm.

The Color Merge operation provides the composite image with all phases distinguished for image analysis. The composite image is fed into a free software program called Multispec, which is capable of distinguishing phases corresponding to a specific spectral (RGB) definition through a process of image-training. Firstly, the phases are classified by making rectangles on the image and assigning specific phases to each polygons. Phase classes are trained following image-training algorithms which deduce the fractions of each of the listed phase fields (alite, belite, interstitial phases, and epoxy) to provide the final quantification. The results of the analysis can be determined through a list of available statistical formulations based on sample necessities. Through a simple process of trial-and-error, the “Fisher Linear Likelihood” algorithm was found to work best for the

fine pixelation variations between the clinker phases, in all image-fields. The final area fraction results are converted into mass fractions by multiplying with the densities, according to Delese [79]. **Table 10** represents the multispectral image analysis results of the quantified clinkers.

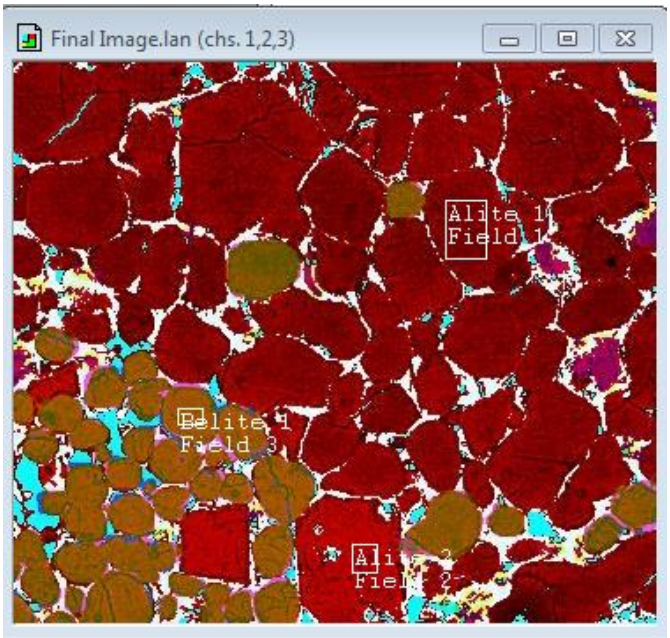

Fig. 32. Screenshot of the multispectral image analysis quantification of the area fractions in a clinker for the same image represented in Fig. 22 (left)

Table 10. Multispectral image analysis results of the important cement phases from the four clinker samples

Phases	Clinker 1	Clinker 2	Clinker 3	Clinker 4
Alite	69.4	71.36	71	61.55
Belite	11.39	10.41	10.31	18.05
Interstitial	19.21	18.24	18.69	20.4

5.3. Comparison of powder & pellet QXRD with PC & MSIA

Since accuracy of the pellet cannot be determined through NIST 2686a due to the lack of reference values, alternative direct determination techniques were resorted to. The significant direct determination techniques for clinker and cement analysis are the optical microscopy-point counting method (PC) and the BSE-EDS image analysis method (MSIA).

Comparison of all 4 direct determination techniques (as in **Table 11**) revealed an acceptable degree of variation between them in the quantification of the major cement phases. Discrepancy between pellet and powder QXRD was around 2% for the alite phase, and 12% for the interstitial phases. The influence of preferred orientation on alite overestimation in pellet and absorption contrast in underestimating ferrite quantification in QXRD were prominent over both pellet and powder QXRD. However, such effects weren't found to affect the accuracy of the quantification in comparison with PC and MSIA.

Table 11. Clinker quantification from powder QXRD, pellet QXRD, point-counting, and multispectral image analysis methods

Phases	Powder	Pellet	MSIA	PC
Clinker 1				
Alite	71.58	73.19	69.4	70.06
Belite	9.91	9.23	11.39	11.24
Interstitial	16.64	14.36	19.21	18.7
Clinker 2				
Alite	71.6	71.8	71.36	71
Belite	9.92	9.79	10.41	11.3
Interstitial	15.135	14.215	18.24	17.6
Clinker 3				
Alite	70.44	71.12	71	70.43
Belite	11.33	11.12	10.31	11.17
Interstitial	16.09	15.295	18.69	18.39
Clinker 4				
Alite	61.16	64.85	61.55	61.6
Belite	16.42	14.80	18.05	18.50
Interstitial	19.62	17.65	20.4	20

Tables 12 and **13** represent the standard deviation differences between point-counting (PC) and multispectral image analysis (MSIA) quantification and compare those with the powder and pellet. It can be observed that the variation of powder and pellet QXRD is not appreciable for the alite and the belite phase. This firmly establishes that preferred orientation is not an issue with pellet QXRD and also the efficiency of the March-Dollase preferred orientation correction. However, the variance with the interstitial phase quantification is quite substantial from the powder QXRD. This is the reason that accuracy calibration is crucial for the pellet QXRD method. The variation is illustrated as column charts in **Figs. 33-35**.

Table 12. Variation of pellet QXRD against the accurate values of the cementitious phases in the four clinkers

Clinkers	Pellet vs. PC-MSIA SD (±wt.%)		
	Alite	**Belite**	**Interstitial**
1	1.95	1.21	2.43
2	0.33	1.31	2.04
3	0.37	0.93	1.71
4	1.89	2.02	1.49

Table 13. Variation of powder QXRD against accurate values of the cementitious phases in the four clinkers

Clinkers	Powder vs. PC-MSIA SD (±wt.%)		
	Alite	Belite	Interstitial
1	1.42	0.81	1.47
2	0.32	1.26	1.67
3	0.33	0.93	1.30
4	0.24	1.09	0.39

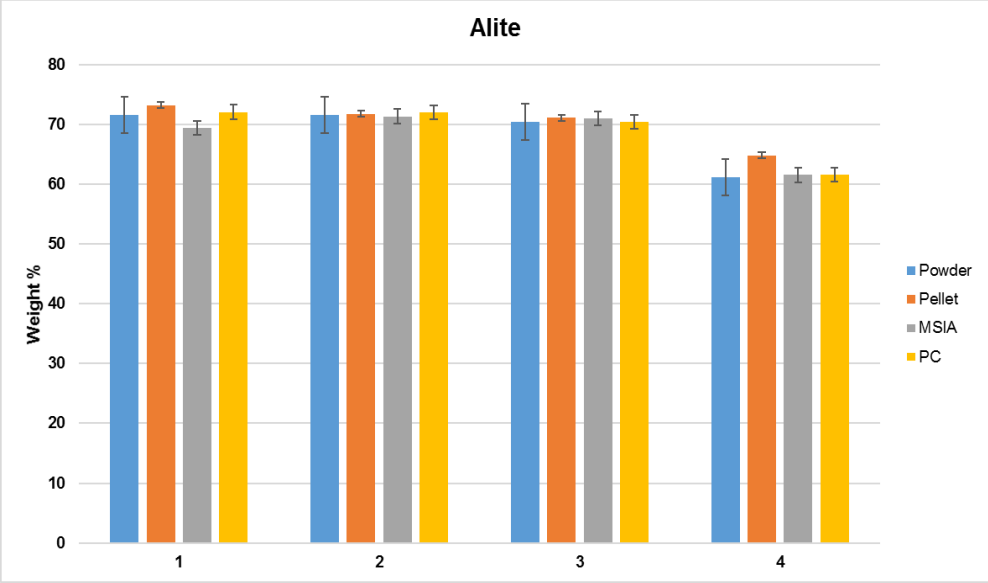

Fig. 33. Alite accuracy variation between the different direct quantification techniques used in this study

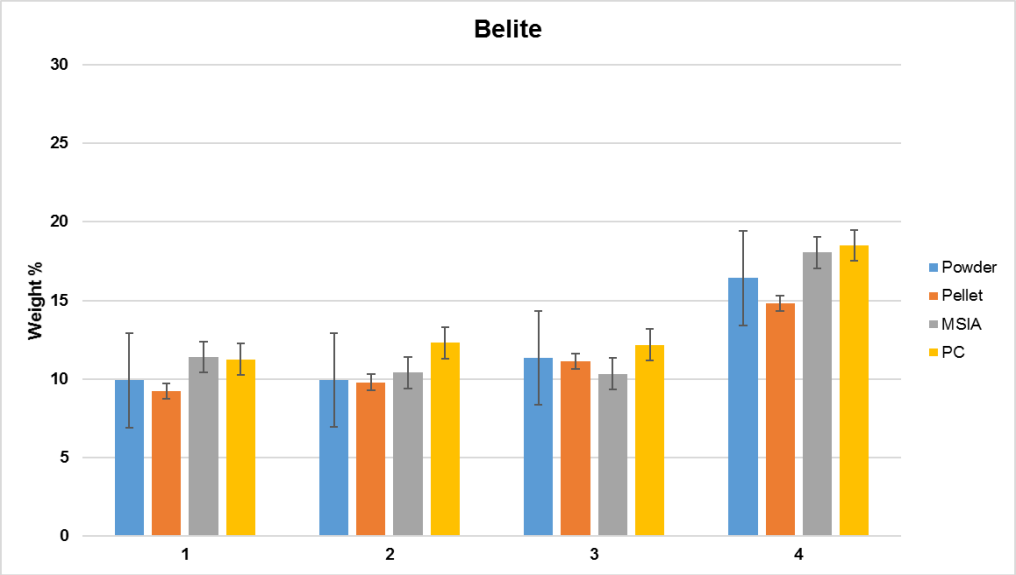

Fig. 34. Belite accuracy variation between the different direct quantification techniques used in this study

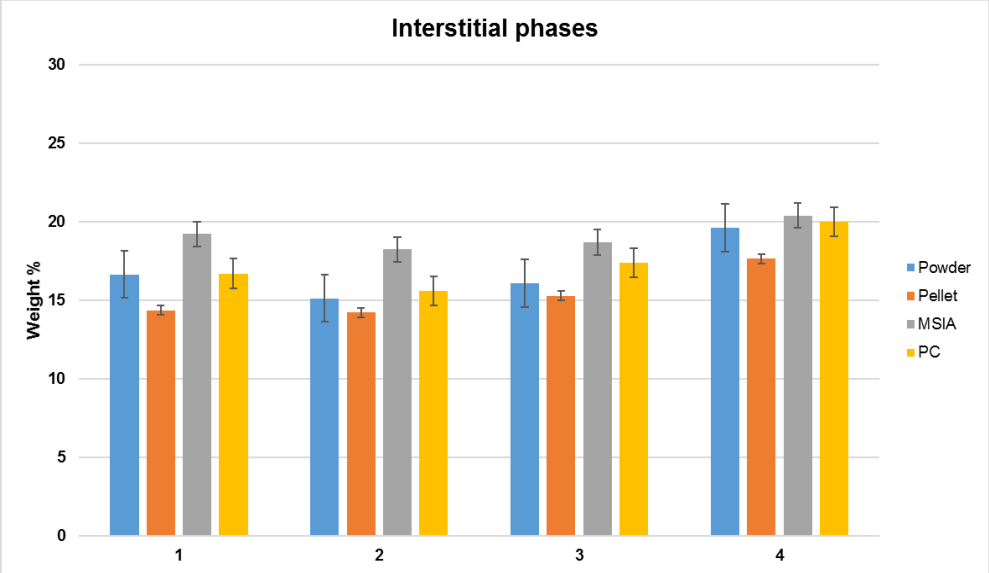

Fig. 35. Interstitial phase accuracy variation between the different direct quantification techniques used in this study

5.4. Precision comparison

The reproducibility was improved significantly from powder QXRD without significantly sacrificing the accuracy. ASTM E177 calculates the reproducibility limit as a multiplier of the standard deviation (1.414 x √2 x standard deviation). The round robin analysis conducted by NIST in 2004 dealt the global repeatability and reproducibility of QXRD to compare against the Bogue method. This was used as a foundation to generate the first ASTM QXRD standard, the C1365.

Table 14. Historical reproducibility limit comparison against QXRD and Bogue

With 95% coverage factor	**Alite (wt.%)**	**Belite (wt.%)**	**Aluminate (wt.%)**	**Ferrite (wt.%)**
QXRD Repeatability[157]	2.9	3.1	2.1	1.7
QXRD Reproducibility[157]	6.3	3.8	4.8	4
QXRD accuracy errors[9]	2.4	2	1	1
Bogue accuracy errors [9]	9.6	9.6	2.2	1.4

Comparison of the ASTM reproducibility limits between the powder and pellet QXRD techniques (**Tables 14-16**) reveals that the pellet QXRD method improves on both aspects of precision: repeatability and reproducibility. An almost negligible variation between different instruments, the Bruker D2, Bruker D8, and, the PANalytical MPD using different Rietveld refinement programs was observed. Hence, the improvement in precision of pellet QXRD was

established here. This can serve as a founding ground on which accuracy calibration can be performed due to the unchanging quantification.

Table 15. Repeatability limit comparison between pellet and powder QXRD

QXRD Repeatability[#]	Alite (wt.%)	Belite (wt.%)	Aluminate (wt.%)	Ferrite (wt.%)
Powder	1	1	1	3
Pellet	0.3	0.5	0.8	1.3

Table 16. Reproducibility limit comparison between pellet and powder QXRD

QXRD Reproducibility[#]	Alite (wt.%)	Belite (wt.%)	Aluminate (wt.%)	Ferrite (wt.%)
Powder	5.1	8.1	1.2	4
Pellet	1.2	0.9	0.6	0.5

5.5. Accuracy calibration

A linear regression correlation of the interstitial phase (**Fig. 36**) and alite (**Fig. 37**) from pellet QXRD was plotted against the corresponding point-counting determinations. The extent of the deviation between the point-counting and multispectral image analysis from the pellet (x-axis) was quantified as the root mean square error between the axes. It was observed that the point-

counting method is closest to the pellet quantification and was finalized as the basis for accuracy calibration. Since the interstitial phases were naturally better separated in the etched clinker than the color-coded clinker image field from MSIA, the point-counting can be considered to be directly representative of the actual clinker contents. The utilization of the MSIA method for accuracy calibration does not provide extremely divergent results as is apparent from the coefficient of variation from the pellet QXRD. Alternatively, if the MSIA method were only to be used for accuracy calibration then the variation from point-counting would be only 4% for the interstitial phases and 0.2% for the alite phase.

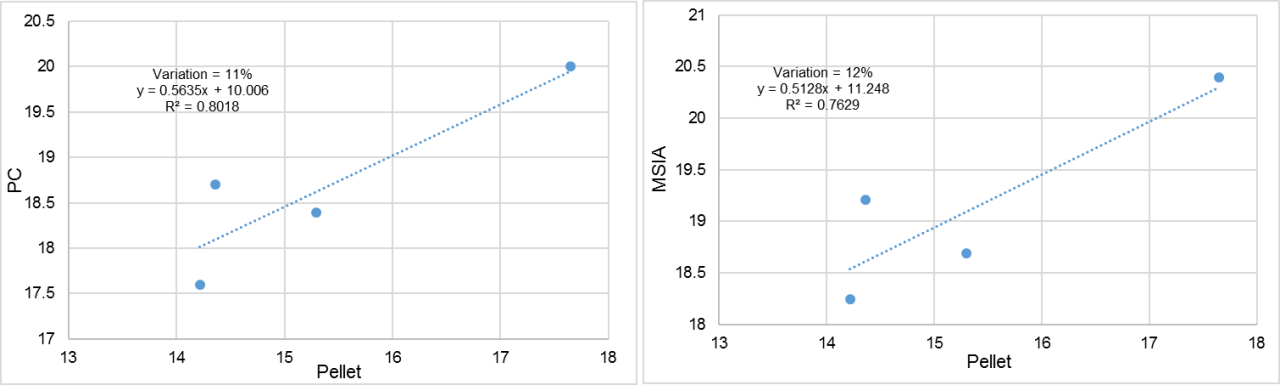

Fig. 36. Regression plot between interstitial phase quantification of pellet QXRD and point-counting (left) and multispectral image analysis (right)

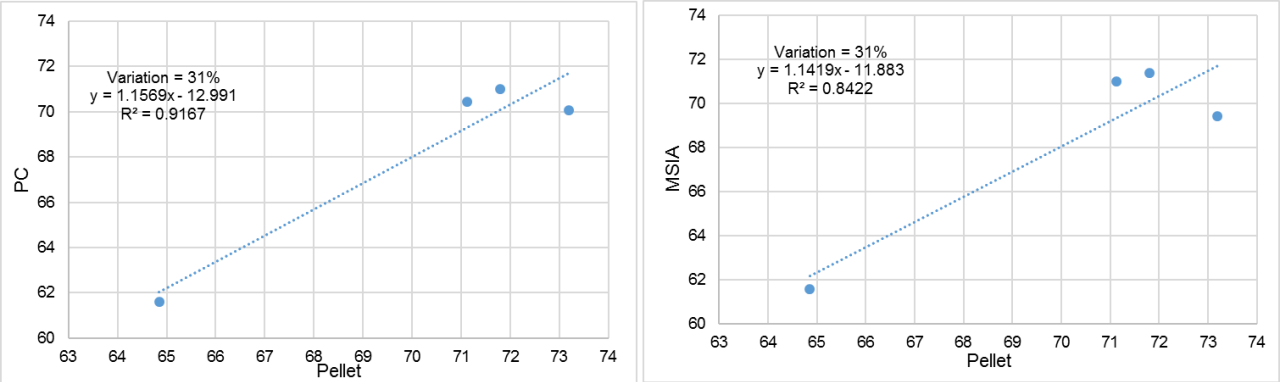

Fig. 37. Regression plot between alite phase quantification of pellet QXRD and point-counting (left) and multispectral image analysis (right)

5.6. Discussion on anhydrous cement analysis

With the questionable accuracy of the Bogue method, the demand for a more accurate quantification scheme was met by QXRD and point-counting techniques. However, the degree of exertion required to analyze cements and clinkers through point-counting made it an undesirable process. The QXRD accompanies with a few systematic and random errors in lieu of its sample preparation protocols. Hence, the cement industry continued with the utilization of the Bogue method which had served well with good precision for quality control.

Since QXRD provides with more information about the morphology and reactivity of the contents than the Bogue method, efforts were made to make QXRD more precise and consistent. But such efforts did not concentrate on sample preparation which was highly divergent owing to a combination of lack of personnel expertise, lab restrictions, and, instrumentation limitations. The idea of making pressed pellets was floated around in industrial circles with some XRD vendors even making automated pelletizing equipments. However, it did not gain much friction in the scientific community owing to inherent problems with preferred orientation correction. There was

a characteristic need to establish pelletization as a workable method by addressing its limitations. Here, a parallel can be drawn from the existing analysis to explain the need for a quantification program that has the accuracy of the direct determination techniques while inheriting the ease of application of the Bogue method.

Hence, the establishment of a direct and automatable X-ray diffraction methodology was realized through the pelletization effort. The pellet QXRD displayed significantly better accuracy than the Bogue method while addressing the inconsistency problem of the QXRD method. With a single validation from either of the microscopy techniques described in this work, the pellet QXRD can be promoted to generate fast and accurate cement phase quantification for routine quality control and quality analysis. For the manufacturer, excellent comparison between instrumentation used by both the supplier and consumer can be realized no matter the hardware or software discrepancies. As a result, cement manufacturers can also be more aggressive to the ASTM phase specification limits with the significantly improved precision.

5.7. Conclusions

An XRD ready pellet was generated and the quantification was shown to have good agreement with the other direct quantification techniques. The following conclusions were obtained from the comparative analysis:

1. Pelletizing the powder was found to improve the precision of QXRD substantially as was seen from the comparison of the reproducibility limits (**Table 15**). This addresses a major shortcoming in QXRD and can be exploited for industrial adoption by following a procedure similar to,

(i) About 4g of the bulk cement powder (without grinding) is pelletized at a pressure around 280 MPa with 15 seconds of dwelling. In order to maintain consistency, the pellet must be strong enough to survive a fall from 3 feet. No cracks, ridges, or, roughness should be observed on the pellet surface directly exposed to X-rays.

(ii) The pellet must be loaded onto an XRD backloading holder and the surface is made to be flat against the sample holder by forcing the pellet onto a closing glass slide on the holder surface.

(iii) After measurement, correction for the preferred orientation must be made using the March-Dollase parameter to monitor the increase or decrease in preferred orientation. Correction for micro-absorption may not be possible owing to the requirement of high-resolution SEM or TEM for calculating ferrite particle size and the high sensitivity of the correction to the calculated particle size.

2. The pellet vs. powder QXRD comparison yielded slightly overestimated alite quantification and slightly underestimated ferrite quantification. However, the difference between pellet and powder QXRD was well-within the ambit of the uncertainty limits of the powder QXRD.
3. To realize high-accuracy, calibration of the pellet QXRD was performed against point-counting and multispectral image analysis (MSIA) techniques. Pellet and powder QXRD results displayed reasonably small variations from the microscopy techniques. This was apparent from the closeness of the standard deviation errors in the comparison between pellet and powder QXRD against the microscopy techniques (**Tables 12 and 13**). The potential of the MSIA technique as a direct quantification method was established with correlation against the point-counting method yielding a variation of 4%.

6. SUMMARY

The conclusions described in this section were congregated from a survey of existing literature and industrial practice aided by on the quantitative X-ray diffraction of anhydrous cement and clinker.

6.1. Summary of the literature survey

- The Bogue method was observed to show large variation in quantification of cement and clinker. Investigations into the formulations of the Bogue and Modified Bogue revealed that the Bogue method contributes to an error of 9.6 wt.%.
- Quantitative X-ray diffraction through Rietveld method is an acceptable alternative to the Bogue method for direct cement phase quantification. Although the Rietveld refinement method for QXRD has been in employment for several decades, the protocols to be followed for an error-free analysis has not yet been comprehensively documented.
- In this effort, the vital protocols that are required for anhydrous cement analysis were tabulated for the most popular XRD instrumentation and software. Some of the significant components of the protocols include the common pitfalls with sample preparation, measurement, and, analysis.
- Extensive fine-grinding along with backloading the cement recognized as the best sample preparation method for powder QXRD with low probability of errors. However, the precision of the QXRD and to some extent the accuracy, were found to be inconsistent and a little dubious respectively.

6.2. Summary of the experimental investigations

- A method was designed to foment increased precision in QXRD of anhydrous cement and clinker. The powder QXRD program was converted to a pellet QXRD by analyzing pressed pellets into a sample holder rather than a randomly oriented powder.
- The streamlined orientation of the crystallites in the pellet can lead to an increased preferred orientation. However, the rest of the powder QXRD random errors that contribute to the eccentricity in precision are mitigated heavily in the pellets. Although precision was increased, the quantification of alite, belite, and ferrite are disturbed in the pellets from their accurate values owing to their characteristic errors. The deficiencies, preferred orientation and micro-absorption, are a combination of the crystal morphological effects and the chemical properties of the phases. Hence their addressal was actively considered for accuracy calibration of pellet QXRD.
- Accuracy calibration of pellet QXRD was performed utilizing generally agreed direct quantification techniques - point-counting and image analysis. An innovative method of image analysis called multispectral image analysis (MSIA) was utilized to perform the accuracy calibration of pellet QXRD. The characteristic programs required for MSIA were assembled and following lengthy image processing and analysis steps, the phase quantification of the clinkers was obtained. Comparison between point-counting and MSIA yielded minute variations which don't effectively disturb clinker analysis performed on an industrial scale.
- Comparison between all the quantification techniques detailed the success of the pellet QXRD in generating a consistently accurate analysis. The accuracy of the pellet QXRD was found to be globally reasonable with the microscopy techniques and the variation was

similar to powder QXRD variation from microscopy. Hence, pellet QXRD was established to provide consistently accurate QXRD analysis all the while inheriting the ease of application of the Bogue method.

6.3. Contributions from this study

The research presented herein has employed analytical techniques which are commonly used in industry to analyze cement and clinker, with the exception of MSIA. As a result, this research has the potential to churn out enhanced tools that can be naturally applied to an industrial setting. Improvements to these tools were performed keeping in mind serving academic and industrial interests alike, and satisfying the technical requirements required for flexibility between manual and automated analysis. Some of the contributions of the study include,

- The protocols for QXRD analysis of cement and clinker were accumulated and ideal sample preparation conventions were laid out. This study differs from similar studies of this type in the scale and specifics of the described QXRD protocols. Almost all parameters were considered, and verdicts were specified with respect to choosing the best parameter.
- This research was meant as a precursor investigation into addressing the precision and accuracy problem directly rather than taking the round robin route. Pelletization to improve precision was not established by any hitherto known study. In addition, the exact steps required to successfully quantify cement and clinker through pelletization applicable to both automated and manual preparation were provided.
- This study is the first full-scale investigation into the potential of MSIA as a workable tool for quantifying several clinkers in quick succession. A step-by-step procedure to perform MSIA was provided to make it easier for replication.

- In reference to existing industrial practice, the conversion of Bogue estimations to QXRD values was performed with a homogenous sample distribution. This assessment provides the flexibility to perform QXRD for quality control without the need of an XRD machine.
- Apart from quality control, the regions where QXRD can influence process control in cement manufacturing was consolidated in this study. This study can help accelerate QXRD employment in online testing since the proper protocols and the regions of improvement are described under one investigation.

6.4. Recommendations for future research

Although the current study involved addressing a significant problem regarding industrial QXRD analysis, it only explores the possibilities for introducing improved analytical tools in common engineering practice. In future, some of these recommendations that can be investigated to augment this study,

- Point-counting is an extremely labor intensive technique with each sample taking 6-8 hours to be quantified. Automation of the point-counting method should be performed using color extraction algorithms written using Python code.
- The MSIA technique must be further promoted as an accurate analysis tool for cement and clinker chemistry research. Further automation of the MSIA method and more clarity with the effect of each quantification algorithm will lead to wide embracement of this method by the cement chemical community.
- Most importantly, there is an urgent need to update the ASTM QXRD standard, C1365 to discredit time intensive protocols such as selective dissolution and fine-grinding plus backloading. The most recent update in April 2018 included selective dissolution as a

crucial step before QXRD analysis. However, this practice is not possible in an industrial setup and will hinder the employment of the C1365 to online quality control and analysis.

REFERENCES

[1] ASTM C150M: Standard Specification for Portland Cement, ASTM International, West Conshohocken, PA, 2017.

[2] H.F.W. Taylor, Cement Chemistry: 2nd Edition, Thomas Telford Publishing, London, UK, 1997.

[3] P.J. Jackson, Portland Cement: Classification and Manufacture, in: P.C. Hewlett (Ed.), Lea's Chemistry of Cement and Concrete, Butterworth-Heinemann, Oxford (UK), 1998, pp. 26-94.

[4] X. Li, W. Zhou, S. Wang, M. Tang, X. Shen, Effect of SO3 and MgO on Portland cement clinker: Formation of clinker phases and alite polymorphism, Constr. Build. Mater. 58 (2014) 182-192.

[5] D.E. Macphee, E.E. Lachowski, Cement Components and Their Phase Relations, in: P.C. Hewlett (Ed.), Lea's Chemistry of Cement and Concrete, Butterworth-Heinemann, Oxford (UK), 1998, pp. 95-129.

[6] S. Midness, J.F. Young, D. Darwin, Concrete: Second Edition, 2003, pp. 15-55.

[7] H.F.W. Taylor, Modification of the Bogue calculation, Adv. Cem. Res. 2(6) (1989) 73-77.

[8] L.P. Aldridge, Accuracy and precision of phase analysis in portland cement by Bogue, microscopic and X-ray diffraction methods, Cem. Concr. Res. 12(3) (1982) 381-398.

[9] P. E. Stutzman, A. Heckert, A. Tebbe, S. Leigh, Uncertainty in Bogue-calculated phase composition of hydraulic cements, Cem. Concr. Res. 61-62 (2014) 40-48.

[10] A.A. Hanhan, Influence of the SO3 Content of Cement on the Durability and Strength of Concrete Exposed to Sodium Sulfate Environment, MS Thesis, University of South Florida, 2004, p. 112.

[11] S. Pourchet, L. Regnaud, J.P. Perez, A. Nonat, Early C3A hydration in the presence of different kinds of calcium sulfate, Cem. Concr. Res. 39 (2009) 989-996.

[12] L.P. Chaignat, F. Winnefeld, B. Lothenbach, G.L. Saout, C.J. Muller, C. Famy, Influence of the calcium sulphate source on the hydration mechanism of Portland cement–calcium sulphoaluminate clinker–calcium sulphate binders, Cem. Concr. Compos. 33 (2011) 551-561.

[13] R.J. Myers, G. Geng, E. Rodriguez, P.d. Rosa, A.P. Kirchheim, P.J.M. Monteiro, Solution chemistry of cubic and orthorhombic tricalcium aluminate hydration, Cem. Concr. Res. 100 (2017) 176-185.

[14] J. Benstead, Effect of clinker-gypsum grinding temperature upon early hydration of Portland cement, Cem. Concr. Res. 12 (1982) 341-348.

[15] R.H. Bogue, Calculation of the compounds in Portland Cement, Ind. Eng. Chem. 1(4) (1929) 192-197.

[16] L.A. Dahl, Estimation of Phase Composition of Clinker: Bulletin 1, Portland Cement Association, 1939, p. 43.

[17] H.M. Rietveld, A profile refinement method for nuclear and magnetic structures, J. Appl. Cryst. (1969) 65-71.

[18] L. Hjorth, K.G. Lauren, "Belite in Portland Cement" Cem. Concr. Res. 1 (1971) 27-40.

[19] L. Aldridge, R.P. Eardley, Effects of Analytical Errors on the Bogue calculation of compound composition, Cem. Tech. 4 (1973) 177-183.

[20] W.A. Gutteridge, "On the dissolution of interstitial phases in Portland cement", Cem. Concr. Res. 9 (1979) 319-324.

[21] C.R. Hubbard, R.L. Snyder, RIR - Measurement and Use in Quantitative XRD, Powder Diffr. 3(2) (1988) 74-77.

[22] J. C. Taylor, C.E. Matulis, Absorption contrast effects in the quantitative XRD analysis of powders by full multiphase profile refinement, J. Appl. Cryst. 24 (1991) 14-17.

[23] J.C. Taylor, Aldridge, L. P., Full-profile Rietveld quantitative XRD analysis of Portland Cement: Standard XRD profiles for the major phase tricalcium silicate, Powd. Diffr. 3(8) (1993) 138-144.

[24] P.E. Stutzman, Guide for X-ray powder diffraction analysis of Portland cement and clinker, NIST Intern. Rep. 5755 (1996) 1-38.

[25] W.A. Klemm, J. Skalny, "Selective dissolution of clinker minerals and its application", Martin Marietta Laboratories MML, 1977, pp. 1-30.

[26] D.L. Bish, R.C. Reynolds, Sample Preparation for X-Ray Diffraction in: D.L. Bish, J.E. Post (Eds.), Modern Powder Diffraction, Washington D. C. (USA), 1989, pp. 73-100.

[27] S.T. Smith, R.L. Snyder, W.E. Brownell, Minimization of Preferred Orientation in Powders by Spray Drying, Adv. X-ray Anal. 22 (1979) 77-88.

[28] R. Jenkins, T.G. Fawcett, D.K. Smith, J.W. Visser, M.C. Morris, L.K. Frevel, JCPDS - International Centre for Diffraction Data Sample Preparation Methods in X-ray Powder Diffraction, Powder Diffr. 1(2) (1986) 51-63.

[29] A.M. Bystrom-Asklund, Sample Cups and a Technique for Sideward Packing of X-ray Diffractometer Specimens, Am. Mineral. 51 (1966) 1233.

[30] L.D. Calvert, A.F. Sirianni, G.J. Gainsford, A Comparison of Methods for Reducing Preferred Orientation, Adv. X-ray Anal. 26 (1983) 105-110.

[31] D.L. Bish, S.A. Howard, Quantitative Phase Analysis Using the Rietveld Method, J. Appl. Cryst. 21 (1987) 86-91.

[32] D.B. Wiles, R.A. Young, A new computer program for Rietveld analysis of X-ray powder diffraction patterns, J. Appl. Cryst. 14 (1981) 149-151.

[33] D.K. Smith, G.G.J. Jr., A. Schieble, A.M. Wims, J.L. Johnson, G. Ullmann, Quantitative X-ray powder diffraction methods using the full diffraction pattern, Powd. Diffr. 2 (1987) 73-77.

[34] H. Motzet, H. Poellmann, U. Koenig, J. Neubauer, Phase quantification and microstructure of a clinker series with lime saturation factors in the range of 100, 10th International Congress on the Chemistry of Cement, Gothenburg, 1997.

[35] T. Westphal, G. Walenta, M. Gimenez, E. Bermejo, T. Fuellmann, K. Scrivener, H. Poellmann, Characterization of cementitious materials, Inter. Cem. Rev., 2001.

[36] G. Walenta, T. Fuellmann, M. Gimenez, I. Leroy, R. Friedle, G. Schnedl, D. Hartung, G. Staupendahl, C. Lauzon, D. Decary, Quantitative Rietveld analysis of cement and clinker, Inter. Cem. Rev., 2001.

[37] G. Walenta, T. Fuellmann, Advances in quantitative XRD for clinkers, cements and cementitious additions, Adv. X-ray Anal. 47 (2004) 287-296.

[38] G.L. Saout, V. Kocaba, K. Scrivener, Application of the Rietveld method to the analysis of anhydrous cement, Cem. Concr. Res. 41 (2011) 133-148.

[39] K.L. Scrivener, T. Fuellaman, G. Walenta, E. Galucci, E. Bermejo, Quantitative study of Portland cement hydration by X-ray diffraction/Rietveld analysis and independent methods, Cem. Concr. Res. 34 (2004) 1541-1547.

[40] R. Snellings, K. Salze, K.L. Scrivener, Use of X-ray diffraction to quantify amorphous supplementary cementitious materials in anhydrous and hydrated blended cements, Cem. Concr. Res. 64 (2006) 89-98.

[41] A. G. de la Torre, M. G. Lopez-Olmo, C. Alvarez-Lua, S. Garcia-Granda, M.A.G. Aranda, Structure and microstructure of gypsum and its relevance to Rietveld quantitative phase analyses, Powd. Diffr. 19 (2004) 200-246.

[42] A.G. de la Torre, A. Cabeza, E. R. Losilla, M.A.G. Aranda, Quantitative Phase Analysis of ordinary Portland cement using synchrotron radiation powder diffraction, Z. Kristallogr. Suppl. 23 (2006) 587-592.

[43] ASTM, C1365: Standard Test Method for Determination of the Proportion of Phases in Portland Cement and Portland-Cement Clinker Using X-Ray Powder Diffraction Analysis, West Conshohocken, PA (USA), 2018.

[44] T. Fuellmann, G. Walenta, M. Gimenez, I. Leroy, R. Friedle, G. Schnedl, D. Hartung, G. Staupendahl, Quantitative Rietveld analysis of Portland cement clinkers for automated quality and process control in industrial production - Part II, Inter. Cem. Rev., 2009.

[45] M. Enders, Quantitative XRD (Rietveld-method) in cement plants: quality control of clinker production, ZKG Int. 60(5) (2007) 50-59.

[46] M. Enders, Sample preparation for quantitative X-ray diffraction in cement plants: sources of errors and solutions, ZKG Int. 58 (2005) 28-37.

[47] M. Enders, Quantitative XRD analysis in automated cement laboratories: requirements for the sample preparation, ZKG Int. 56(5) (2003) 54-62.

[48] C. Manias, D. Retallack, I. Madsen, Plant optimisation and control using continuous online XRD for mineral phase analysis, Zem. Kal. Gips., 2001, p. 14.

[49] A. Clearfield, J.H. Reibenspies, N. Bhuvanesh, Principles and Applications of Powder Diffraction, Blackwell Publishing, London, UK, 2008.

[50] P.E. Stutzman, P. Feng, J.W. Bullard, Phase Analysis of Portland Cement by Combined Quantitative X-Ray Powder Diffraction and Scanning Electron Microscopy, J. Res. NIST 121 (2016) 47-107.

[51] V.K. Pecharsky, P.Y. Zavalij, Fundamentals of Powder Diffraction and Structural Characterization of Materials, 2 ed., Springer, New York, USA, 2009.

[52] T. Moderl, Improved backloading for better results, Mat. Sci. Forum, Transtech Publications, Switzerland, 2001, pp. 240-247.

[53] McCrone Micronising Mill: User Manual, Glen Creston Ltd., London (UK).

[54] P.E. Stutzman, G. Lespinasse, S. Leigh, *"Compositional analysis & certification of NIST Reference Material Clinker 2686a"*, NIST Technical Note 1602, US Department of Commerce, 2008, p. 48 pages.

[55] V. Kocaba, Development and Evaluation of Methods to Follow Microstructural Development of Cementitious Systems Including Slags, PhD Thesis, EPFL, Switzerland, 2009, p. 263.

[56] M.A.G. Aranda, A.G. de la Torre, L. Leon-Reina, Rietveld Quantitative Phase Analysis of OPC Clinkers, Cements and Hydration Products, Rev. Min. Geochem. 74(1) (2012).

[57] L. Leon-Reina, A.G. de la Torre, J.M. Porras-Vasquez, M. Cruz, Alcobe, X., , M. Ordonez, F. Gispert-Guirado, A. Larranage-Varga, M. Paul, T. Fuelman, R. Schmidt, M.A.G. Aranda, Round robin on Rietveld quantitative phase analysis of Portland cements, J. Appl. Cryst. 42 (2009) 906-916.

[58] E.P. Bertin, Principles and Practice of X-ray Spectrometric Analysis, Springer US, New York (USA), 1975.

[59] ASTM E177: Standard Practice for Use of the Terms Precision and Bias in ASTM Test Methods, ASTM International, West Conshohocken, PA (USA), 1986.

[60] L.P. Aldridge, Accuracy and Precision of an X-ray diffraction method for analyzing Portland cements, Cem. Concr. Res. 12 (1982) 437-446.

[61] J.R. Crandall, R.L. Blaine, Statistical Evaluation of Interlaboratory Cement Tests, Proc. Am. Soc. Test. Mater. 59 (1959) 1129-1154.

[62] W.J. Youden, Statistical Aspects of the Cement Testing Program, Soc. Test. Mater. 59 (1959) 1120-1128.

[63] P.E. Stutzman, Quantitative X-ray Powder Diffraction of Portland Cements: Proficiency Tests for Laboratory Assessment, Adv. Civ. Eng. 3(1) (2014) 122-141.

[64] I. C. Madsen, N. V. Y. Scarlett, L. M. D. Cranswick, T. Lwin, Outcomes of the international union of crystallography comission on powder diffraction round robin on quantitative phase analysis: samples 1a to 1h, J. Appl. Cryst. 34 (2001) 409-426.

[65] ASTM E691: Standard Practice for Conducting an Interlaboratory Study to Determine the Precision of a Test Method,, ASTM International, West Conshohocken, PA (USA).

[66] ASTM C670: Standard Practice for Preparing Precision and Bias Statements for Test Methods for Construction Materials, ASTM International, West Conshohocken, PA (USA).

[67] S.T. Petersen, B. Weber-Wisman, X-ray Powder Sample Preparation, World Cem. (5) (1997) 34-40.

[68] R.L. Gordon, G.W. Harris, Effect of Particle-Size on the Quantitative Determination of Quartz by X-ray Diffraction, Nature 175 (1955) 1135.

[69] H.P. Klug, L.E. Alexander, X-Ray Diffraction Procedures for Polycrystalline and Amorphous Materials, Wiley, New York (USA), 1974.

[70] D.K. Smith, Particle statistics and whole-pattern methods in quantitative X-ray powder diffraction analysis, Powd. Diffr. 16(4) (2001) 186-188.

[71] P.S. Whitfield, L.D. Mitchell, The effects of particle statistics on Rietveld analysis of cement, Z. Kristallogr. Suppl. 30 (2009) 53-59.

[72] K. Luke, F.P. Glasser, Selective dissolution of hydrated blast furnace slag cements, Cem. Concr. Res. 17 (1986) 273-282.

[73] B.A. Supernant, G. Papadopoulous, Selective Dissolution of Portland Fly Ash Cements, J. Mater. Civil. Eng. 3(1) (1991) 48-59.

[74] K. Scrivener, P.L. Pratt, Backscattered electron images of polished sections in the scanning electron microscope, 1984.

[75] H.L. Ch'atelier, Experimental Researches on the Constitution of Hydraulic Mortars (English Translation), McGraw-Hill, New York, 1905.

[76] P.H. Bates, A.A. Klein, Properties of calcium silicates and calcium aluminates occurring in natural Portland cement, Technological Papers of the Bureau of Standards, US Bureau of Standards, 1917.

[77] D. Campbell, Microscopical examination and interpretation of Portland cement and clinker, Second ed., Portland Cement Association, Illinois, 1999.

[78] F. Hofmánner., Microstructure of Portland Cement Clinker, Holderbank Management and Consulting, Ltd., Switzerland, 1975.

[79] M.A. Delesse, Mechanical Methods for Determining the Composition of Rocks (in French), Annales des Mines1866.

[80] ASTM, E562: Standard test method for determining the volume fraction by systematic manual point counting, 2011.

[81] ASTM, C1356: Standard test method for quantitative determination of phases in Portland Cement clinker by microscopical point-count procedure, 2012.

[82] K.O. Kjellsen, R.J. Detweiler, O.E. Gjorv, Backscattered electron imaging of cement pastes hydrated at different temperatures, Cem. Concr. Res. 20 (1990) 308-311.

[83] K.L. Scrivener, Backscattered electron imaging of cementitious microstructures: understanding and quantification, Cem. Concr. Compos. 26 (2004) 935-945.

[84] M. Mouret, E. Ringot, A. Bascoul, Image analysis: A tool for the characterisation of cement in concrete - metrological aspects of magnification, Cem. Concr. Compos. 23 (2001) 201-206.

[85] P.T. Durdzinski, C.F. Dunant, M.B. Haha, K.L. Scrivener, A new quantification method based on SEM-EDS to assess fly ash composition and study the reaction of its individual components in hydrating cement paste, Cem. Concr. Res. 73 (2015) 111-122.

[86] R.T. Chancey, P.E. Stutzman, M.C.G. Juenger, D.W. Fowler, Comprehensive phase characterization of crystalline and amorphous phases of a Class F fly ash, Cem. Concr. Res. 40 (2010) 146-156.

[87] P.E. Stutzman, J.W. Bullard, P. Feng, Quantitative Imaging of Clinker and Cement Microstructure, NIST Technical Note 1877, Gaithesburg, Maryland, 2015.

[88] J.I.G.e. al., Scanning electron microscopy and X-ray microanalysis, 2 ed., Plenum Press, New York, USA, 1981.

[89] MultiSpec: A Freeware Multispectral Image Data Analysis System, URL: https://engineering.purdue.edu/~biehl/MultiSpec/.

[90] ImageJ: Image Processing and Analysis in Java, URL: http://imagej.nih.gov/ij/.

[91] J. Lee, T.C. Keener, M. Knoderer, S. Khang, Thermal decomposition of limestone in a large-scale thermogravimetric analyzer, Thermo. Acta 213 (1993) 223-240.

[92] G. Villain, M. Thiery, G. Platret, Measurement methods of carbonation profiles in concrete: Thermogravimetry, chemical analysis and gammadensimetry, Cem. Concr. Res. 37 (2007) 1182-1192.

[93] A. Morandeau, M. Theiry, P. Dangla, Investigation of the carbonation mechanism of CH and C-S-H in terms of kinetics, microstructure changes and moisture properties, Cem. Concr. Res. 56 (2014) 153-170.

[94] G. Platret, F.X. Deloye, Thermogravimetry and carbonation of cements and concretes, Actes des Journées des Sciences de l'Ingénieur du réseau des Laboratoires des Ponts et Chaussées, Publication LCPC,, Paris, 1994, pp. 237-243.

[95] G. Ye, X.L.G.D. Schutter, A.M. Poppe, L. Taerwe, Influence of limestone powder used as filler in SCC on hydration and microstructure of cement pastes, Cem. Concr. Compos. 29 (2007) 94-102.

[96] Z. Tu, M. Guo, C.S. Poon, C. Shi, Effects of limestone powder on CaCO3 precipitation in CO2 cured cement pastes, Cem. Concr. Compos. 72 (2016) 9-16.

[97] H. El-Hassan, Y. Shao, Z. Ghouleh, Reaction Products in Carbonation-Cured Lightweight Concrete, Journal of Materials in Civil Engineering 25(6) (2013) 799-809.

[98] M. Castellote, C. Andrade, X. Turrillas, J. Campo, G.J. Cuello, Accelerated carbonation of cement pastes in situ monitored by neutron diffraction, Cement and Concrete Research 38(12) (2008) 1365-1373.

[99] V. Rostami, Y. Shao, A.J. Boyd, Z. He, Microstructure of cement paste subject to early carbonation curing, Cement and Concrete Research 42(1) (2012) 186-193.

[100] J. Dweck, E.I.P. Lasota, Quality control of commercial plasters by thermogravimetry, Thermo. Acta 318 (1998) 137-142.

[101] J. Dweck, P.M. Buchler, A.C.V. Coelho, F.K. Cartledge, Hydration of a Portland cement blended with calcium carbonate, Thermo. Acta 346 (2000) 105-113.

[102] G. Kakali, S. Tsivilis, A. Tsialitas, Hydration of ordinary portland cements made from raw mix containing transition element oxides, Cem. Concr. Res. 28 (1998) 335-340.

[103] Z.P. Bazant, M.G. Kaplan, Concrete at High Temperatures: Material Properties and Mathematical Models, Longman-Addison-Wesley, London, 1996.

[104] F.J. Tang, E.M. Gartner, Influence of sulfate source on Portland cement hydration, Adv. Cem. Res. 1(2) (1988) 67-74.

[105] J.P. Bayoux, A. Bonin, S. Marcdargent, A. Mathieu, M. Verscaeve, Study of the hydration properties of aluminous cement and calcium sulphate mixes, in: R.J. Mangabhai (Ed.), Calcium aluminate cements, SPON Press, London, 1990.

[106] D. Torrens-Martin, L. Fernandez-Carrasco, Effect of sulfate content on cement mixtures, Constr. Build. Mater. 48 (2013) 144-150.

[107] F. Winnefeld, B. Lothenbach, M. Plotze, The influence of different calcium sulfates on the hydration of Portland cement - A practical study, ZKG Int. 58(3) (2005) 62-70.

[108] M. Zajac, A. Rossberg, G.L. Saout, B. Lothenbach, Influence of limestone and anhydrite on the hydration of Portland cements, Cem. Concr. Compos. 46 (2014) 99-108.

[109] A. Quennoz, K.L. Scrivener, Hydration of C3A-gypsum systems, Cem. Concr. Res. 42 (2012) 1032-1041.

[110] A. Quennoz, K.L. Scrivener, Interactions between alite and C3A-gypsum hydrations in model cements, Cem. Concr. Res. 44 (2013) 46-54.

[111] M. Bigare, A. Guinier, C. Maizieres, M. Regourd, N. Yannquis, W. Eysel, T.H. Hahn, E. Woermann, Polymorphism of Tricalcium Silicate and Its Solid Solutions, J. Am. Cer. Soc. 50(11) (1967) 609-619.

[112] I. Maki, K. Goto, Factors influencing the phase constitution of alite in Portland cement clinkers, Cem. Concr. Res. 12(3) (1982) 301-308.

[113] I. Maki, K. Kato, Phase Identification of Alite in Portland Cement Clinker, Cem. Concr. Res. 12 (1981) 93-100.

[114] L. Gobbo, L. Sant' Agostino, L. Garcez, C3A polymorphs related to industrial clinker alkalies content, Cem. Concr. Res. 34 (2004) 657-664.

[115] A.C. Jupe, X. Turrillas, P. Barnes, S.L. Colston, C. Hall, D. Häusermann, M. Hanfland, Fast in situ X-ray-diffraction studies of chemical reactions: a synchrotron view of the hydration of tricalcium aluminate, Phys. Rev. B 53 (1996) R14697-R14700.

[116] L. Black, C. Breen, J. Yarwood, C.S. Deng, J. Philips, G. Maitland, Hydration of tricalcium aluminate (C3A) in the presence and absence of gypsum-studied by Raman spectroscopy and X-ray diffraction, J. Mater. Chem. 16 (2006) 1263-1272.

[117] A.N. Christensen, T.R. Jensen, N.V.Y. Scarlett, I.C. Madsen, J.C. Hanson, Hydrolysis of pure and sodium substituted calcium aluminates and cement clinker components investigated by in situ synchrotron X-ray powder diffraction, J. Am. Cer. Soc. 87 (2004) 1488-1493.

[118] L.G. Baquerizo, T. Matschei, K.L. Scrivener, M. Saiedpour, L. Wadso, Hydration states of AFm cement phases, Cem. Concr. Res. 73 (2015) 143-157.

[119] H.W.W. Pollitt, A.N. Brown, The Distribution of Alkalis in Portland Cement Clinker, Proceedings of the Proceedings of the 5th International Symposium on the Chemistry of Cement, Tokyo (Japan), 1968.

[120] I. Maki, Nature of the prismatic dark interstitial material in Portland cement clinker, Cem. Concr. Res. (1973) 295-313.

[121] M. Regourd, A. Guinier, The Crystal Chemistry of the Constituents of Portland Cement Clinker, Proceedings of the 6th International Congress on the Chemistry of Cement, Moscow (Russia), 1974.

[122] F.C. Lee, H.M. Banda, F.P. Glasser, Substitution of Na, Fe and Si in tricalcium aluminate and the polymorphism of solid solutions, Cem. Concr. Res. 12 (1982) 237-246.

[123] A.K. Chatterjee, Raw Materials Selection, in: F.M.M. J.I. Bhatty, S.H. Kosmatka (Ed.), Innovations in Portland Cement Manufacturing, Portland Cement Association, Skokie, Illinois (USA), 2004.

[124] D. Lechtenberg, Dried sewage sludge as an alternative fuel, Glob. Cem. Mag. (2011) 36-39.

[125] S. Puntke, Auswirkungen des Phosphateintrages in Drehofenanlagen der Zementindustrie auf Klinkermineralogie und Zementeigenschaften, TU ClausthalZellerfeld, 2005.

[126] P.S. D. Rapson, Improving control and quality, World Cem. (2006) 67-71.

[127] H. Moeller, Control of product quality during the use of secondary materials, VDZ Congress 2009: Process Technology of Cement Manufacturing, Verlag Bau + Technik GmbH Düsseldorf, Düsseldorf (Germany), 2009.

[128] Z. Wang, W. Wang, Influence of sewage sludge on the formation and microstructure of Portland cement clinker, 8th International Symposium on Cement & Concrete (ISCC2013), Nanjing (China), 2013.

[129] N. Husillos Rodríguez, S. Martínez-Ramírez, M.T. Blanco-Varela, S. Donatello, M. Guillem, J. Puig, C. Fos, E. Larrotcha, J. Flores, The effect of using thermally dried sewage sludge as an alternative fuel on Portland cement clinker production, J. Clean. Prod 52 (2013) 94-102.

[130] N. Gineys, G. Aouad, F. Sorrentino, D. Damidot, Incorporation of trace elements in Portland cement clinker: thresholds limits for Cu, Ni, Sn or Zn, Cem. Concr. Res. 41 (2011) 1177-1184.

[131] N. Gineys, G. Aouad, D. Damidot, Managing trace elements in Portland cement - Part II: Comparison of two methods to incorporate Zn in a cement, Cem. Concr. Compos. 33 (2011) 629-636.

[132] A. Stumm, K.Garbev, G. Beuchle, L. Black, P. Stemmermann, R.Nüesch, Incorporation of zinc into calcium silicate hydrates, Part I: formation of C-S-H(I) with C/S = 2/3 and its isochemical counterpart gyrolite, Cem. Concr. Res. 35 (2005) 1665-1675.

[133] N. Saikia, S. Kato, T. Kojima, Influence of Sn on the hydration of tricalcium aluminate Ca3Al2O6, J. Therm. Anal. Calorim. 109 (2012) 273-286.

[134] P.-H. Shih, J.-E. Chang, H.-C. Lu, L.-C. Chiang, Reuse of heavy metal-containing sludges in cement production, Cem. Concr. Res. 35 (2005) 2110-2115.

[135] W. Huang, H. Kazemi-Kamyab, W. Sun, K. Scrivener, Effect of cement substitution by limestone on the hydration and microstructural development of ultra-high performance concrete (UHPC), Cement and Concrete Composites 77 (2017) 86-101.

[136] D.P. Bentz, Activation energies of high-volume fly ash ternary blends: hydration and setting, Cem. Concr. Compos. 53 (2014) 214-223.

[137] D. P. Bentz, J. Tanesi, A. Ardani, Ternary blends for controlling cost and carbon content: high-volume fly ash mixtures can be enhanced with additions of limestone powder, Concr. Int. 35(8) (2013) 51-59.

[138] K. Song, W. Kim, J. Bang, S. Park, C.W. Jeon, Polymorphs of pure calcium carbonate prepared by the mineral carbonation of flue gas desulfurization gypsum, Mater. Des. 83 (2015) 308-313.

[139] V. T. Cost, T. Matschei, J. Shannon, I.L. Howard, Extending the use of fly ash and slag cement in concrete through the use of Portland-limestone cement, Proceedings NRMCA international concrete sustainability conference, 2014.

[140] B.L. T. Matscehi, F. P. Glasser, The role of calcium carbonate in cement hydration, Cem. Concr. Res. 37 (2007) 551-558.

[141] K. De. waardt, M. Ben Haha, G. Le Saout, K. O. Kjellsen, H. Justnes, B. Lothenbach, Hydration mechanisms of ternary Portland cements containing limestone powder and fly ash, Cem. Concr. Res. 41 (2011) 279-291.

[142] J. Moon, J. E. Oh, M. Balonis, F. P. Glasser, S. M. Clark, P.J.M. Monteiro, High pressure study of low compressibility tetracalcium aluminum carbonate hydrates 3CaO Al2O3 CaCO3 11H2O, Cem. Concr. Res. 42 (2012) 105-110.

[143] I. Dreizler, D. Knoefel, Effect of magnesium oxide on the properties of cement, ZKG B. 35(12) (1982) 293-301.

[144] P. Stutzman, NIST Technical Note 1692: Direct determination of phases in Portland cements by Quantitative X-ray Powder Diffraction, US Department of Commerce, Washington D.C, 2010.

[145] J. Mandel, F. Linnig, Study of Accuracy in Chemical Analysis Using Linear Calibration Curves, Anal. Chem. 29(5) (1957) 743-749.

[146] J. Sieber, D. Broton, C. Fales, S. Leigh, B. MacDonald, A. Marlow, S. Nettles, J. Yen, Standard reference materials for cements, Cem. Concr. Res. 32 (2002) 1899-1906.

[147] J. Mandel, Evaluation and Control of Measurements, Marcel Dekker, New York, 1991.

[148] T. Westphal, T. Fullmann, H. Pollmann, Rietveld quantification of amorphous portions with an internal standard-mathematical consequences of the experimental approach, Powd. Diffr. 24 (2009) 239-243.

[149] D. Jansen, Ch. Stabler, F. Goetz-Neunhoeffer, S. Dittrich, J. Neubauer, Does Ordinary Portland Cement contain amorphous phase? A quantitative study using an external standard method, Powd. Diffr. 26(1) (2011) 31-38.

[150] P.M. Suherman, A.v. Riessen, B. O'Connor, D. Li, D. Bolton, H. Fairhurst, Determination of amorphous phase levels in Portland cement clinker, Powd. Diffr. 17(3) (2002) 178-186.

[151] D. Jansen, F. Goetz-Neunhoeffer, C. Stabler, J. Neubauer, A remastered external standard method applied to the quantification of early OPC hydration, Cement and Concrete Research 41(6) (2011) 602-608.

[152] A.B. R. Snellings, K. Scrivener, The existence of amorphous phase in Portland cements: Physical factors affecting Rietveld quantitative phase analysis, Cem. Concr. Res. 59 (2014) 139-146.

[153] G.V.P.B. Singh, K.V.L. Subramaniam, Quantitative XRD study of amorphous phase in alkali activated low calcium siliceous fly ash, Constr. Build. Mater. 124 (2014) 139-147.

[154] I.C.Madsen, N.V.Y. Scarlett, A. Kern, Description and survey of methodologies for the determination of amorphous content via X-ray powder diffraction, Z. Kristallogr. 226 (2011) 944-955.

[155] Y. P. Stesko, N. Shanahan, H. Deford, A. Zayed, Quantification of supplementary cementitious content in blended Portland cement using an iterative Rietveld–PONKCS technique, J. Appl. Cryst. 50 (2017) 498-507.

[156] A. Kumar, T. Oey, G.P. Falla, R. Henkensiefken, N. Neithalath, G. Sant, A comparison of intergrinding and blending limestone on reaction and strength evolution in cementitious materials, Construction and Building Materials 43 (2013) 428-435.

[157] P.E. Stutzman, Development of an ASTM standard test method on X-ray powder diffraction analysis of hydraulic cements, Adv. X-ray Anal. 47 (2004) 206-211.

APPENDIX

I. MATLAB Code used to generate the WHS bands

```
n = length(x);

[p,stats] = polyfit(x,y,1);

slope = p(1);

intercept = p(2);



for i = 1:n

    slopemat = slope.*x;

end



ycap = intercept + slopemat;



%ycap was obtained as a matrix.



[nullh, fcoeff, ci, stats] = vartest2(x,y);

lowerf = ci(1);

upperf = ci(2);



wupper = sqrt (2.*upperf);

wlower = sqrt(2.*upperf);
```

```
%Obtained 2 values of W


for j = 1:n

    b5 = sqrt(sum((x-mean(x)).^2));

end

%b5 is a scalar


for j = 1:n

    num5 = abs((x - mean(x))/b5);

end

%num5 is a vector


b4 = num5 + (1/(sqrt(n)));

%b4 is a vector


%Calculate the deviations of y

newdyupper = wupper.*b4;

newdylower = wlower.*b4;


%Calculate the upper and lower bands

UpperLinear = ycap + newdyupper
```

```
Mean = ycap

LowerLinear = ycap - newdylower


%Calculate the standard errors of estimation

for j = 1:n

    upperdev2 = (UpperLinear - Mean)./(Mean);

end

upperdeviation2 = sum(upperdev2)


for j=1:n

    lowerdev2 = (Mean - LowerLinear)./(LowerLinear);

end

lowerdeviation2 = sum(lowerdev2)


%Find the means in each limit

LowerMean = mean(LowerLinear)

MeanofMeans = mean(Mean)

UpperMean = mean(UpperLinear)


%Now plot the curves

plot(x,Mean,'r','LineWidth',2);

hold on;
```

```
plot(x,UpperLinear,'b-.');

plot(x,LowerLinear,'b--');

xlabel('Bogue');ylabel('QXRD');

legend('Mean','WHS Bands','Location','NorthWest');

hold off;

end
```

II. MATLAB Code used to compute the standard error of estimate

```
n=length(x);

isequal(length(x),length(y));

del = (n.*sum(x.^2))-(sum(x));

ysq = sum(y.^2);

ssq = (1/(n-2).*(ysq - (ysq/n) - (del/n)));



Square_of_errors = abs(ssq)

Error_percentage_or_Std_Err_Est = sqrt(abs(ssq))

end
```